MEMS BASED MULTI – CHANNEL PIEZOELECTRIC ACOUSTIC TRANSDUCER FOR FULLY IMPLANTABLE COCHLEAR IMPLANTS

A THESIS SUBMITTED TO
THE GRADUATE SCHOOL OF NATURAL AND APPLIED SCIENCES
OF
MIDDLE EAST TECHNICAL UNIVERSITY

BY

MUHAMMED BERAT YÜKSEL

IN PARTIAL FULFILLMENT OF THE REQUIREMENTS
FOR
THE DEGREE OF MASTER OF SCIENCE
IN
ELECTRICAL AND ELECTRONICS ENGINEERING

JULY 2020

Approval of the thesis:

MEMS BASED MULTI – CHANNEL PIEZOELECTRIC ACOUSTIC TRANSDUCER FOR FULLY IMPLANTABLE COCHLEAR IMPLANTS

submitted by **MUHAMMED BERAT YÜKSEL** in partial fulfillment of the requirements for the degree of **Master of Science in Electrical and Electronics Engineering Department, Middle East Technical University** by,

Prof. Dr. Halil Kalıpçılar
Dean, Graduate School of **Natural and Applied Sciences**

Prof. Dr. İlkay Ulusoy
Head of Department, **Electrical and Electronics Eng.**

Prof. Dr. Haluk Külah
Supervisor, **Electrical and Electronics Eng., METU**

Examining Committee Members:

Prof. Dr. Tayfun Akın
Electrical and Electronics Eng., METU

Prof. Dr. Haluk Külah
Electrical and Electronics Eng., METU

Prof. Dr. Barış Bayram
Electrical and Electronics Eng., METU

Assist. Prof. Dr. Kıvanç Azgın
Mechanical Eng., METU

Assist. Prof. Dr. Dinçer Gökcen
Electrical and Electronics Eng., Hacettepe University

Date: 23.07.2020

I hereby declare that all information in this document has been obtained and presented in accordance with academic rules and ethical conduct. I also declare that, as required by these rules and conduct, I have fully cited and referenced all material and results that are not original to this work.

Name, Surname: Muhammed Berat Yüksel

Signature:

ABSTRACT

MEMS BASED MULTI – CHANNEL PIEZOELECTRIC ACOUSTIC TRANSDUCER FOR FULLY IMPLANTABLE COCHLEAR IMPLANTS

Yüksel, Muhammed Berat
Master of Science, Electrical and Electronics Engineering
Supervisor: Prof. Dr. Haluk Külah

July 2020, 96 pages

This thesis presents multi-channel acoustic MEMS transducer that is able to work within the audible frequency range (250-5500 Hz) and mimic the operation of a cochlea by filtering incoming sound. This transducer is composed of eight thin film piezoelectric cantilever beams possessing different resonance frequencies. The transducer is well suited to be implanted in a middle ear cavity with an active volume of $5\times5\times0.6$ mm^3 and 4.8 mg. Resonance frequencies and piezoelectric outputs of the beams are modeled by using Finite Element Method (FEM). Vibration experiments showed that the transducer was capable of generating up to 139.36 mV$_{pp}$ under 0.1 g excitation. Test results are consistent with FEM model on frequency (97%) and output voltage (89%) values. It was also tested with acoustical excitation in a test setup including artificial tympanic membrane and flexible connection equipment. In that case, it generated up to 50.7 mV$_{pp}$ under 100 dB Sound Pressure Level (SPL). Output voltages observed in acoustical and mechanical characterizations are the highest reported ones to the best of my knowledge. For the first time in the literature, acoustical transducer was excited with speech sound and recovered by using software. Spectrograms of recorded and recovered signals showed close patterns. Moreover, recovered sound was recognizable. Beside stand-alone tests, *in-vivo* and *in-vitro* tests have been conducted with stimulation circuits. This stimulation system can operate in

50 dB dynamic range. Finally, a new beam structure is proposed to improve hearing quality by expanding the covered bands as a future work

Keywords: Acoustic Transducer, MEMS, Fully Implantable Cochlear Implant, Thin Film Piezoelectric

ÖZ

TAMAMEN İMPLANTE KOKLEAR IMPLANTLAR İÇİN MEMS TABANLI ÇOK KANALLI PİZEOELEKTRİK AKUSTİK DÖNÜŞTÜRÜCÜ

Yüksel, Muhammed Berat
Yüksek Lisans, Elektrik ve Elektronik Mühendisliği
Tez Danışmanı: Prof. Dr. Haluk Külah

Temmuz 2020, 96 sayfa

Bu tezde, duyulabilir frekans aralığında çalışan kokleanın çalışmasını taklit edebilen MEMS tabanlı ince piezoelektrik katmanlara sahip çok kanallı tramplen dönüştürücü sunmaktadır. Bu yapı gelen ses dalgasını farklı frekanslarda sallanabilen sekiz adet tramplen yapıyla mekaniksel olarak filtreler. Dönüştürücü 5×5×0.6 mm^3 ve 4.8 mg aktif boyutları ile orta kulak boşluğuna implante edilmek için uygundur. Tramplen yapıların rezonans frekansları ve çıkış voltajları Sonlu Elemanlar Yöntemi kullanılarak modellenmiştir. Mekanik uyarma deneyleri, bu dönüştürücünün 0.1 g ivme uygulandığında 139.36 mV_{pp}'a kadar çıkabildiğini göstermiştir. Bu test sonuçları frekans (% 97) ve çıkış gerilimi (% 89) açışından model ile tutarlıdır. Bu dönüştürücü ayrıca, yapay timpanik membran ve esnek bağlantı yapıları içeren bir test ortamında, üzerine 100 dB ses basıncı uygulandığında 50.7 mV_{pp}'a kadar voltaj oluşturabilmektedir. Bu akustik ve mekanik çıkış voltajları, literatürde kaydedilen en yüksek çıkış değerleridir. Ayrıca, literatürde ilk kez bir akustik dönüştürücü konuşma sinyali ile uyarıldı ve oluşturulan sinyaller yazılım aracılığıyla yeniden birleştirildi. Bu sinyallerin spektrogramı gerçek ses ile benzer salınımlar gösterdi ve yeniden çalınan ses anlaşılabilirdi. Bağımsız testlerin yanı sıra dönüştürücü stimülasyon devreleri ile yapay ve canlı ortam üzerinde test edildi. Bu sistem 50 dB dinamik aralıkta gerekli uyarma sinyallerini oluşturabildi. Son olarak kapsanan frekans bantlarını genişletebilecek ve bu sayede işitme kalitesini arttırabilecek bir tramplen yapı önerilmektedir.

Anahtar Kelimeler: Akustik Dönüştürücü, MEMS, Tamamen İmplante Koklear İmplant, İnce Film Piezoelektrik

To My Family

ACKNOWLEDGEMENTS

I would like to express my sincere gratitude to my supervisor Prof. Dr. Haluk Külah for his support and guidance he gave me during my graduate study and also for giving me the opportunity to be involved in such an exciting project.

I want to thank Aziz Koyuncuoğlu, Bedirhan İlik, Hasan Uluşan and Salar Chamanian for their supports and guidance during this research. They accompanied me in our challenging project.

I especially thank Berkay Çiftci for his help, supports and friendship in my undergraduate and graduate projects. I would also like to thank Andaç Yiğit, Akın Mert Yılmaz, Yasemin Engür, Mert Koç and all members of BioMEMS research group for their collaborations and their friendship. I am honored and enjoyed sharing the same office while creating beautiful memories.

My special thanks to METU-MEMS Center and Orhan Akar for sharing his deep knowledge on microfabrication and for his help in the cleanroom.

I am deeply thankful to my friends especially Derya İrem Karabacak, Mahmut Sinan Yayla, Şükrü Sinan Aydoğdu, Nazlıcan Yamankurt and Kubilay Yılmaz for their encouragements and supports.

This author is financially supported by TUBITAK BIDEB 2210-A 2017-2 Scholarship during this study.

This work has received funding from the European Research Council (ERC) under the European Union's Horizon 2020 research and innovation programme (Grant No:682756).

TABLE OF CONTENTS

CHAPTERS

LIST OF TABLES

TABLES

LIST OF FIGURES

FIGURES

LIST OF ABBREVIATIONS

ABBREVATIONS

CI: Cochlear Implant

MEMS: Microelectromechanical Systems

FEM: Finite Element Method

FICI: Fully Implantable Cochlear Implant

PLD: Pulsed Laser Deposited

PZT: Lead Zirconate Titanate

SPL: Sound Pressure Level

CHAPTER 1

INTRODUCTION

1.1. Motivation

Hearing is the sense that can make you perceive ambient sounds from flapping of an insect to the launching of spacecraft with the help of eardrum, ossicles, and cochlea. This chain makes ear to be the best acoustic sensor by providing wide frequency selectivity (20 Hz – 20 kHz) and dynamic range (0- 140 dB SPL). Unfortunately, World Health Organization (WHO) reports that around 466 million people suffer from hearing loss around worldwide, and 34 million of them are children. It is estimated that around 900 million people will be experiencing hearing loss in year 2050. Hearing loss can be classified as mild, moderate, severe or profound with respect to hearing threshold [1]. Hearing aids can recover mild to moderate hearing loss by amplifying the sound. For more than 90 dB sound pressure level hearing loss (severe to profound), cochlear implants (CIs) are needed [2]. Cochlear Implant (CI) is a surgically implanted device to recover the hearing function of the patient with severe to profound hearing loss caused by irreversibly damaged hair cells. Today's conventional CIs use electrical signals to stimulate auditory nerves bypassing the healthy part of the natural hearing mechanism.

Current state-of-the-art conventional CI users can achieve up to 100 % correct scores on the difficult speech tests [3] and CIs target to obtain music perception in high quality [4]. However, they have some major drawbacks affecting users` life quality: Risk of damaging CIs' outer components especially when exposed to water, aesthetic concerns particularly in children and young patients, daily battery replacement/recharging, and high cost [2], [5]. To overcome the aforementioned problems, a new concept called fully implantable cochlear implants (FICIs) is required. In this concept, implantable sensors and low power interface circuits are utilized along with the natural hearing mechanism to recover hearing.

This thesis aims to present an implantable transducer for the FICI concept. The transducer can mimic the operation of the cochlea by using mechanical filtering to stimulate the auditory nerves via stimulation circuit and conventional cochlear electrode. During that process, natural hearing mechanism is preserved. Therefore, this transducer concept provides an opportunity to eliminate outer parts of the standard CIs and reduce the power consumption of the system.

In this chapter, ear anatomy and hearing mechanism are explained to clarify the operation of the sensor provided in the next chapters. Then, conventional and fully implantable CI introduced in the literature are investigated. Finally, the requirement of FICI systems and previously reported implantable transducers are given.

1.2. Ear Anatomy and Hearing

Ear is the best natural acoustic sensor which provides wide frequency selectivity (20 Hz – 20 kHz) and dynamic range (0- 140 dB SPL) with the help of eardrum, ossicles, and cochlea. This primary sense (hearing) converts acoustic sound pressures to electrical signals. Ear anatomy consists of several small parts that have specific purpose and function for hearing.

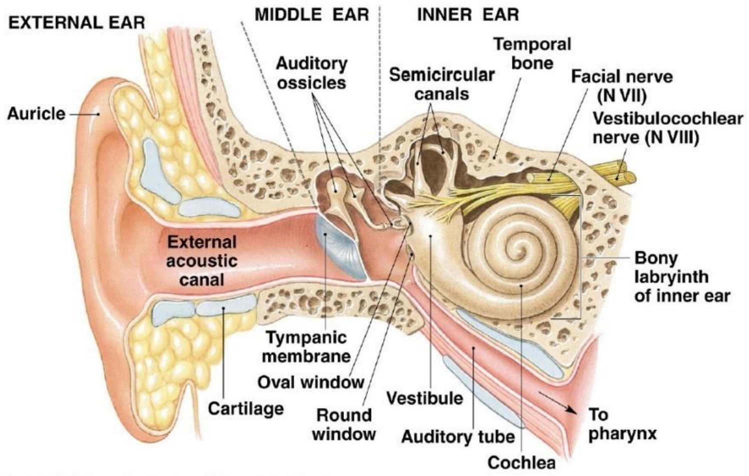

Figure 1.1. Anatomy of the ear [6].

Figure 1.1 shows the anatomy of the ear. As shown in the illustration, it is separated into three parts as the external ear, the middle ear, and the inner ear. Acoustic canal and auricle are found in the external part of the ear. This part collects sound signals, directs them to the middle ear, and protects the remaining parts of the ear. Besides, the ear canal amplifies the sound level (10-12 dB around 2500 Hz) while sound passes from 2.5 cm long 5 to 7 mm diameter tube before reaching the middle ear [7]. The middle ear part consists of the eardrum and ossicles (malleus, incus, and stapes). They convert the acoustic signals to mechanical vibrations and transfer these vibrations to the oval window. Therefore, the middle ear is the link between the air pressure in the outer ear and fluid pressure in the inner ear. While eardrum area is approximately 17 times of oval window. The inner ear includes semicircular canals, oval window, round window, and cochlea. The semicircular canal is responsible for an equilibrium of the body while cochlea and the others are responsible for hearing. Figure 1.2 shows the cochlea which is a 2.5 turns spiral-shaped structure. It contains thousands of sensory receptors to convert fluidic pressure into electrical stimulation. This organ provides frequency selectivity in the range between 20 Hz to 20 kHz [6].

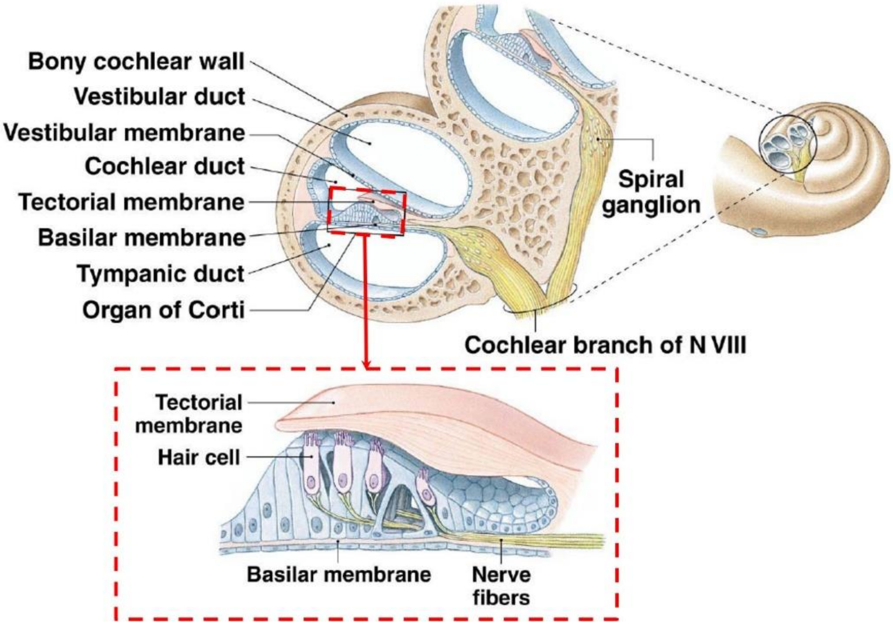

Figure 1.2. The cochlea, organ of corti [6].

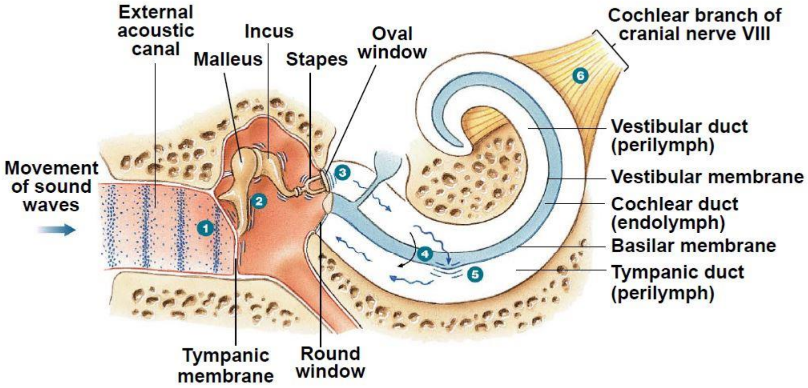

Figure 1.3. Illustration of hearing mechanism [6].

In Figure 1.3, the hearing mechanism is illustrated. Incoming sound waves excite the tympanic membrane (1). Then, movement of the membrane causes displacement of the ossicles, as a result, sound signals are converted to mechanical vibrations (2). Vibrations of ossicles at the oval window turn into pressure waves in the inner ear (3). These pressure waves cause vibration on hair cells and the cells convert them into electrical signals (4-5). Finally, the frequency and the intensity of the stimulus are transmitted to the central nervous system over the cochlear branch of the cranial nerve as electrical signals [6], [7].

1.3. Hearing Loss

There are several reasons for hearing loss. They are investigated in two main groups as conductive hearing loss and sensorineural hearing loss. Type of hearing loss changes treatment methods.

Conductive hearing loss occurs due to the problems in transferring the sound waves on the hearing chain. This problem causes reduction of sound intensity and can be recovered by traditional hearing aids or middle ear implants. Hearing aids basically amplify the incoming sound to retrieve the operational vibration on the hearing chain [8]. On the other hand, middle ear implants are used when there is a complete distortion on the hearing chain. These devices detect the incoming sound and vibrate the healthy part of the hearing chain [9].

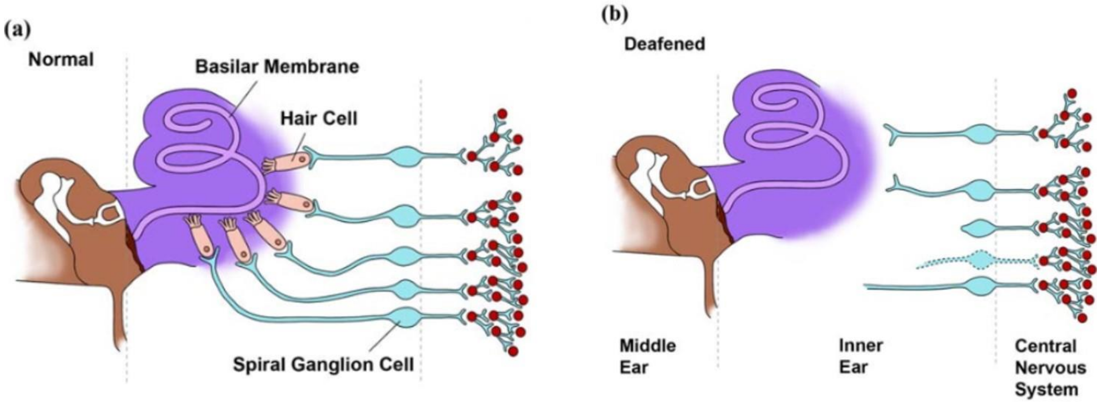

Figure 1.4. Anatomy of sensorineural hearing loss: (a) healthy hair cell connection and (b) deafened ear [10].

Sensorineural hearing loss is caused by irreversible damage to hair cells in the cochlea. In this hearing loss type, acoustic waves in the inner ear cannot be converted to electrical signals. Figure 1.4 shows the anatomical reason for sensorineural hearing loss and illustration of hair cell connections.

Cochlear implants (CIs) are used to recover the hearing loss caused by hair cell distortions. These implants take sound signals and stimulate healthy auditory neurons [2], [10]. If auditory neurons are damaged, auditory brain stem implants must be used to recover the hearing [11].

1.4. Cochlear Implants (CIs)

Hearing loss treatments change with hearing loss level and disordered part of the hearing system as explained in Section 1.3. In the concept of this thesis, conventional CI systems are investigated to understand reasons behind major drawbacks of current systems.

For over 50 years, cochlear implants have been used to recover severe to profound hearing loss inside healthy nerve system. In CI systems, sound signals are converted to electrical signals and these signals stimulate the auditory nerves in the cochlea. Figure 1.5 shows the parts of the conventional cochlear implants [12].

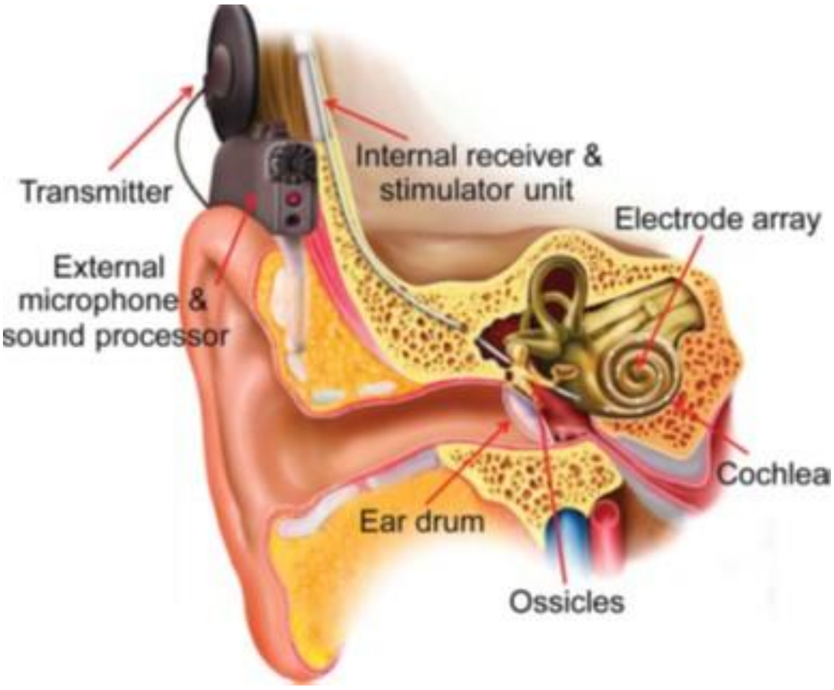

Figure 1.5. Illustration of conventional cochlear implant [12].

Conventional cochlear implants have two main parts as shown in Figure 1.5: External and internal units. The external unit includes an external microphone, sound processor, battery, and RF transmitter, while internal unit contains RF receiver, stimulation unit, and cochlear electrode. Figure 1.6 shows functional diagram of this operation [2], [13].

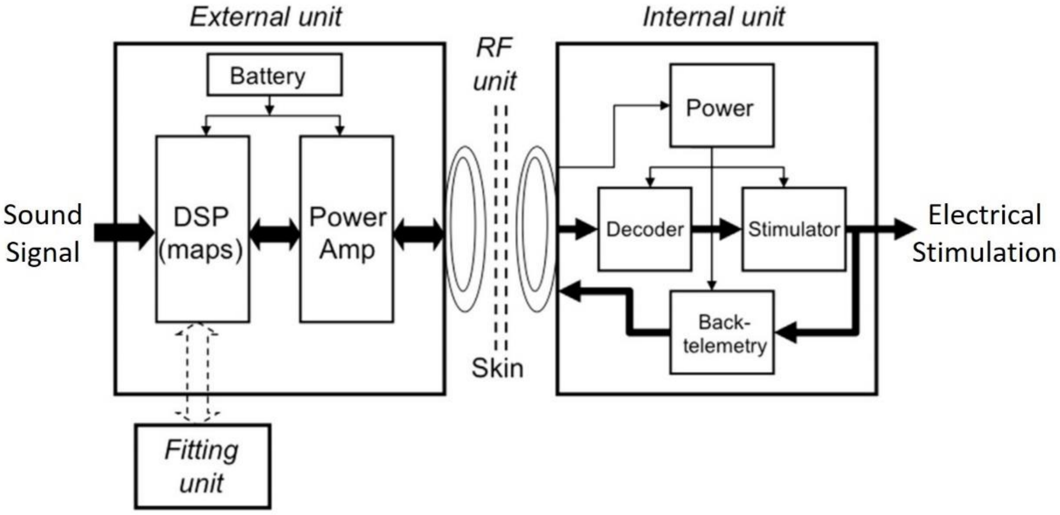

Figure 1.6. Functional block diagram of conventional cochlear implant [13].

External microphone and sound processor (DSP) are employed to sense the sound signals and turn them into electrical signals. The external battery unit provides the required energy for the cochlear implant, including the inner part. Power and processed signals are transmitted into the skin via RF transmitter and emitter units. The power transmitted to inner unit drives the electronic circuit in this part of the CI. The signal carrying the information about the sound wave is transformed into biphasic pulses in the stimulation circuit. Then, generated pulses are transmitted to stimulate nerves via electrode array. Finally, back telemetry units are utilized to send stimulation information to the external side for patient fitting [2], [13], [14].

Conventional cochlear implants have been used over 50 years as in the explained method [15] and can recover daily hearing up to 100% correction. They can even provide high-quality music perception to patients [3], [4]. However, the current state-of-the-art conventional CIs have major drawbacks. They recover the hearing by bypassing not only the damaged hair cells but also the healthy parts of the hearing chain to stimulate the nerve cells directly. They require daily battery recharge/replacement, have high cost and risk of damaging outer components, especially when exposed to water. In addition to these, there are aesthetic concerns, particularly for children and young patients [2], [5]. Therefore, a new concept is required to eliminate these problems.

1.5. Fully Implantable Cochlear Implants (FICIs)

Drawbacks of cochlear implants can be removed by Fully Implantable Cochlear Implant (FICI) systems. FICI concepts exclude external components of CI, such as active microphone, transmitter, and external battery. Instead of these components, FICI systems make use of internal acoustic sensor, low power stimulation circuits, harvesting unit or internal battery [12], [16]–[20].

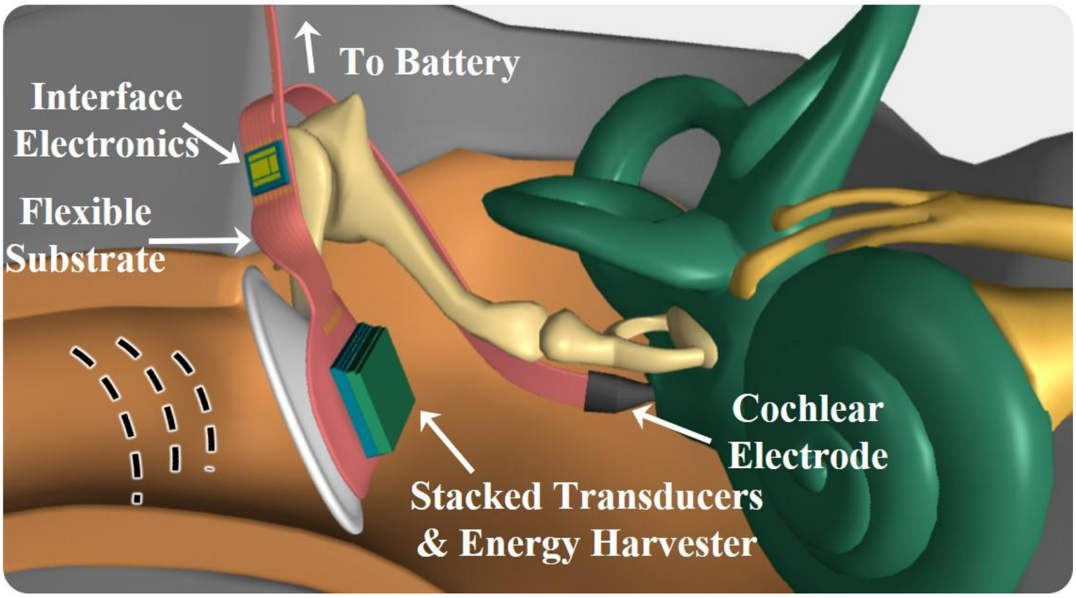

Figure 1.7. FLAMENCO concept illustration for FICI applications [16], [21].

Our research group has proposed a new concept called FLAMENCO in FICI solutions [16]. It combines multi-channel acoustic transducers [22]–[24], piezoelectric energy harvester [25], [26], ultra-low power stimulation interface circuit [27]–[30], energy harvesting interface unit [31]–[33] and commercial CI electrode. All parts of the system are implanted inside the middle ear cavity to meet FICI requirements. Figure 1.7 shows the overall diagram of the concept.

This thesis is solely on implementing the acoustic transducer. This transducer can utilize vibration of natural hearing mechanism instead of an active microphone as shown in Figure 1.7. In addition, it can provide opportunity to eliminate outer parts of the standard CIs and reduce the power consumption of the overall system.

1.6. Implantable Sensors

Sound detection and processing parts are placed in the outer part of the conventional CI systems. However, the implantable sensor is required for fully implantable cochlear systems. This concept provides an opportunity to overcome the aforementioned problems of conventional CIs in terms of sound detection.

Implantable transducers for the hearing devices have been studied in the literature considering different approaches. They can be classified in terms of sensing methods: Piezoelectric, piezoresistive, capacitive, electromagnetic, and optical. Placement is another classification method for implantable devices. They can be implanted on to the middle ear, or it is possible to make them intracochlear. In this section, examples of these methods are investigated.

Udvardi et al. [34] proposed an array of spirally shaped piezoelectric cantilevers to sense incoming sound for middle ear implants which can be seen in Figure 1.8. This transducer can cover the lower part hearing band (300-700 Hz) with 16 spiral cantilevers. Each cantilever covers a 2×2 mm^2 area and they utilize AlN as a piezoelectric material. These Archimedean spiral shaped beams can generate up to 9.6 mV$_{pp}$ under 1g acceleration. This system can work without any driver unit and it has no power consumption.

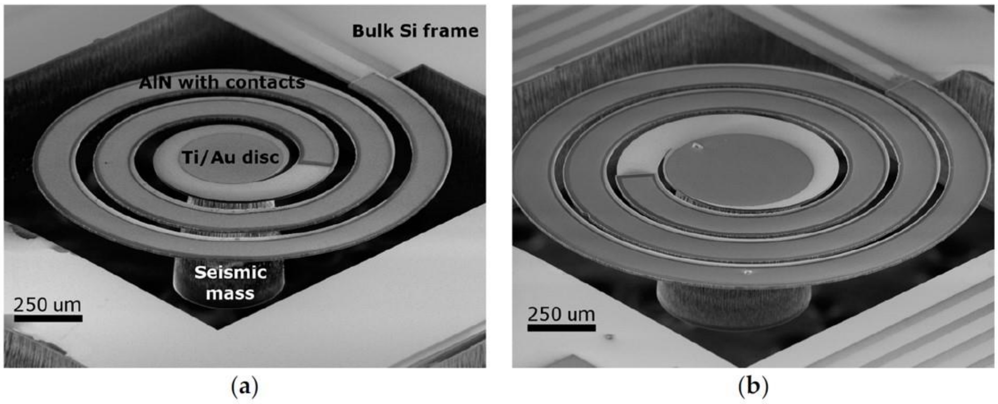

Figure 1.8. SEM Image of spiral-shaped piezoelectric cantilever array [34].

Zhao et al. [17] designed a multichannel piezoelectric transducer for intracochlear applications. The proposed structure includes four cantilever beams that utilize AlN as a structural and piezoelectric layer with varying lengths between 355 and 450 µm as shown in Figure 1.9. These beams vibrate between 19.0 to 40.3 kHz in air actuation and the maximum sensitivity of the beams is 860 µV/Pa. Inside of the cochlea is filled with fluid; therefore, they tested the device in water to mimic the environment. In this case, the device senses the upper part of the hearing band between 4.2 and 10.9 kHz.

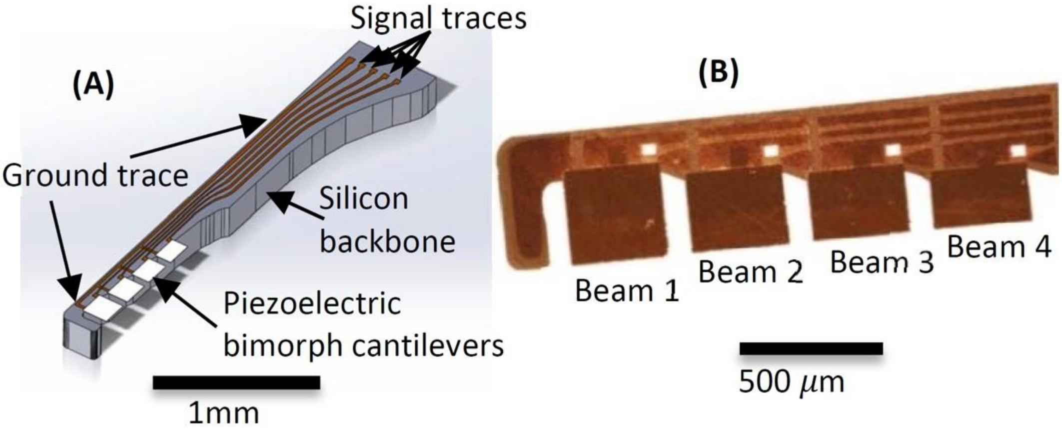

Figure 1.9. AlN transducer for intracochlear implants [17].

Two years later, Zhao et al. [35] presented a modified version of the transducer with *in-vivo* test results. They covered the top and bottom of the cantilevers with parylene and change the range of the length between 300 and 443 µm. This modified version was tested on living guinea pig. Results showed that piezoelectric intracochlear acoustic transducer could give responses between 80-95 dB SPL, in a frequency range of 1-14 kHz with sinusoidal acoustic excitation.

Jia and Gao et al. [36], [37] designed a floating piezoelectric microphone for middle ear implants. Figure 1.10 shows the structure, which includes piezoelectric ceramic bimorph element with a preamplifier circuit.

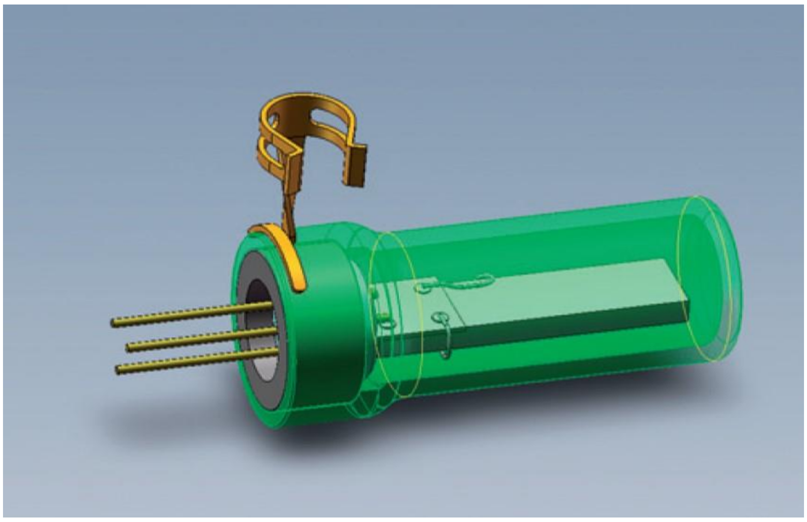

Figure 1.10. Floating piezoelectric microphone model with Titanium clips [36].

This implant was enclosed with a biocompatible capsule structure which can be fixed on the ossicles with its titanium clip to seal the front part of the sensor. Dimension and mass of this microphone are 5.91×2.4×2.02 mm3 and 67 mg which was implanted to the middle ear of a fresh cadaveric head. This transducer could work between 0.5 and 2.5 kHz and consumed 0.12 mW power.

Jang et al. [38] presented a piezoelectric artificial basilar membrane, shown in Figure 1.11. This structure includes 10 channels. The width of each channel is 400 μm while lengths are in the range 1140-3300 μm. These channels filter incoming sounds into the frequency in the range of 10-37 kHz. Maximum output of this structure is 3.55 mV at 9.7 kHz under 112.4 dB excitation and their sensitivity range changes in the range of 0.114-0.48 mV/Pa.

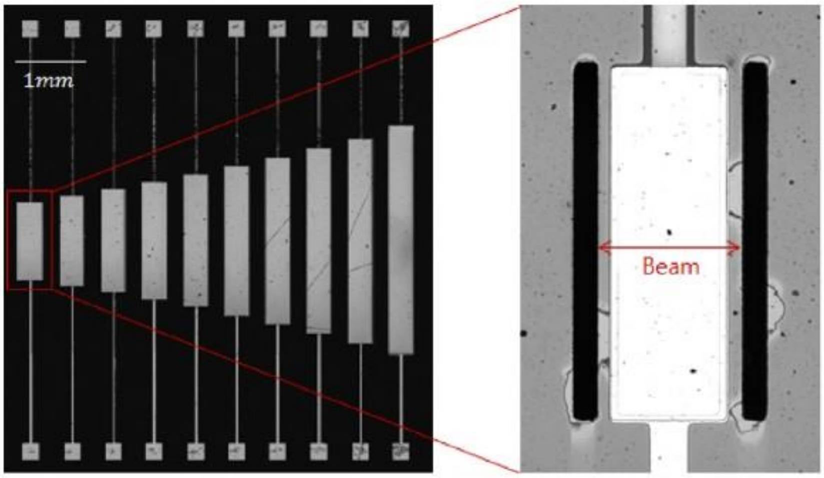

Figure 1.11. Insert figure caption here [38].

Two years later, the same group published a new article with a different structure, shown in Figure 1.12 [39]. This structure is composed of AlN piezoelectric cantilever arrays, which includes eight cantilevers with different lengths to obtain desired frequency range. Lengths of these cantilevers change in the range of 600-1350 μm to obtain frequency selective channels in the range of 2.92-12.6 kHz. The maximum measured voltage of this structure was obtained as 4.06 mV at the resonance frequency (7.04 kHz) of 4th channel under 101.7 dB SPL excitation. They obtained a higher sensitivity range of 0.354-1.67 mV/Pa from their previous study with this structure.

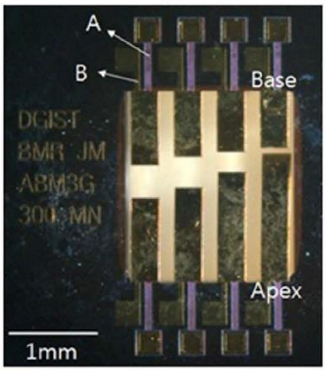

Figure 1.12. Optical image of artificial basilar membrane [39].

They also tested this transducer on an animal model, Hartley guinea pig, with a charge balanced biphasic square wave generator to stimulate the auditory nerves of the animal. They were able to observe evoked auditory brainstem response (EABR) from deafened guinea pig with acoustic stimuli from 75 to 95 dB SPL.

Ko et al. [19] contributed the literature in terms of the implantable acoustic transducer with their designs and *in-vivo* tests to investigate middle ear implantations. They proposed two methods for MEMS capacitive accelerometer-based microphone for middle ear and fully implantable cochlear implants. These methods are shown in Figure 1.13. In the first method (a), the sensor is attached to the bone and spring is employed to transmit the vibration of the hearing mechanism to the sensor. In the second method (b), they planned to attach the sensor to eardrum with bonding glue directly. After temporal bone experiments, they showed direct bonding the sensor, provides higher sensitivity to the system.

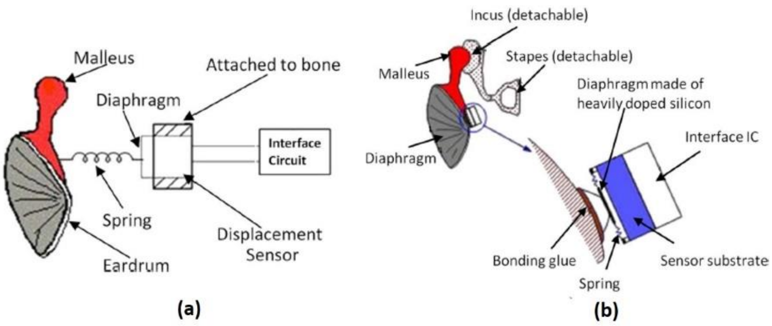

Figure 1.13. Proposed methods for piezoelectric accelerometer based microphones [19].

The same group published a new article on the accelerometer based capacitive MEMS accelerometer with placing the sensor directly on the eardrum [18]. Figure 1.14 shows the structure of the accelerometer, which occupies only 1×1 mm^2 sensing area. However, a low noise interface circuit is required to read out the accelerometer output and it consumes 4.5 mW.

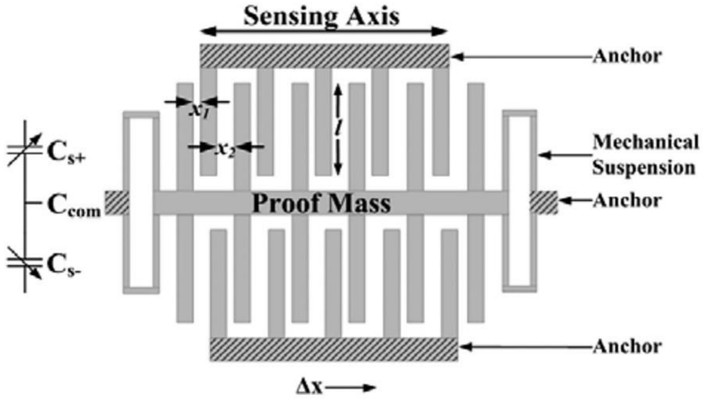

Figure 1.14. Capacitive accelerometer based implantable microphone [18].

Djinovic et al. [40] benefited from a different approach to measure the middle ear acoustical response. They proposed a miniature fiber optic vibrometer based on a modified Michelson interferometer for FICI applications. They were capable of measuring the frequency response of the incus while cadaver and living sheep were exposed to the sinusoidal acoustical excitation from 40 to 90 dB SPL in the range between 100 Hz to 10 kHz (Figure 1.15).

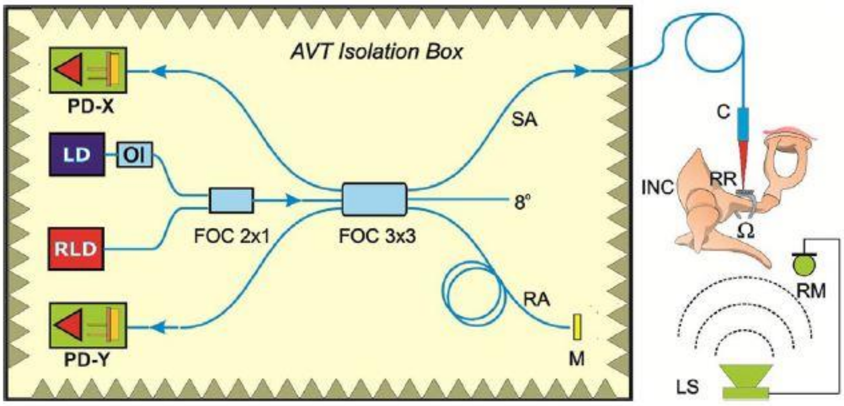

Figure 1.15. Schematic of optical sensing configuration [40].

These methods have several bottlenecks as an implantable sound detector. The size of the device must be compatible with placement in the ear. Mass tolerance of the hearing chain is critical for the vibration level. Therefore, the mass of the transducer must be minimized. Output of the transducer needs to be high to cover a wide dynamic range. Audible frequency range should be covered by the sensor spectrum. Finally, the structure is required to be biocompatible, and it should not consume power during sensing or driving the sensor. Reported sensing methods are investigated below with these considerations.

Electromagnetic sensors reported in the literature [41], are based on Faraday`s law of electromagnetic induction. Due to the nature of the electromagnetic sensor, generated signals depend on changing the magnetic field through a conductor. Therefore, magnet and coil structures are needed for this type of sensing. However, using magnets in an implantable device is not preferable methods because of MRI incompatibility. Therefore, the same group changed the direction of their research to accelerometer based capacitive microphones [18], [19].

Electrostatic (capacitive) sensing methods utilize capacitance change between two charged plates. Displacement between the plates causes capacitance change; thus, the system generates a voltage or current output. Their dimensions and structures can be arranged in the desired frequency range by changing inertial mass and crab legs. However, this method needs a driver voltage to charge plates and consumes power due to inevitable interfacing readout circuit. Presented capacitive acoustic microphones consume 4.5 mW power, which is much higher than the low power stimulation interface circuit for cochlear implants (less than 500 µW, [28]).

Piezoelectric sensing methods do not require a drive voltage or readout circuits for output measurements. It can be implemented with different structures with MEMS fabrication and its parameters can be arranged for proper dimension and output voltage in the limitations. Therefore, in this thesis, the piezoelectric sensing method is used for acoustic sensing.

1.7. Objective of the Thesis and Organization

The main objective of this thesis is to design a multi-channel piezoelectric acoustic transducer to sense sound for fully implantable cochlear implants and prove the feasibility of this method. Thus, bottlenecks of the conventional cochlear implants can be surpassed in terms of sensing sound. In the view of this main objective, the following milestones and deliverables are aimed in the scope of this thesis:

1. Designing a functional transducer in the limitations of middle ear implantable transducer. These limitations are described in the design chapter in detail. Therefore:
    - Vibrations originating from natural hearing mechanism must be utilized by the transducer,
    - These vibrations must be divided into the frequency bands by channels of the transducer. The frequency bands must be distributed in the hearing band with a required number of channels. Recent studies show that 8-channel shows optimal performance.
    - Dimensions of the channels and the transducer must be arranged to make the system implantable in the middle ear. Middle ear volume is around 1 cm^3.
    - Total mass of the implanted device should be below 25 mg. Therefore, the mass of the transducer must be minimized.
    - Output voltages of the channels should be large enough to be sensed by the low power stimulation interface circuits. Therefore, the minimum input level of the circuit (100 μV) must be generated by each channel at daily sound levels (~60 dB).
2. Modeling the structure with finite element analysis to design the transducer in the given restrictions.
3. Fabricating the transducer with a well-defined fabrication process to obtain repeatable and consistent results.
4. Characterization of the transducer with a systematical approach:

- Designing and implementing auxiliary test equipment to establish test environments that mimic the operation of simulation model and the vibration of the middle ear,
- Composing systematical test approach to investigate and detect the reasons for problems,
- Testing transducer with excitation types that are used in the simulation model and existed in the middle ear,
- Comparing the test results which are obtained with the same excitation type with the finite element analysis model,
- Supporting test results with electrical filter outputs in software,
- Interconnecting the transducer with the stimulation interface circuit and characterizing the whole stimulation system in *in-vitro* and *in-vivo* environment.

The remaining parts of the thesis are organized as follows:

Chapter 2 presents the design and modeling of the proposed multi-channel acoustic transducer. First, the requirements of middle ear implantable transducer are explained in detail with discussions from the literature. Then, used structure and material properties are given, and design consideration of the structure is developed. Later, a mathematical model of the structure in the literature is presented. Finally, the developed finite element analysis module on COMSOL Multiphysics is explained and, by using these modules, parameters of the final structure are calculated.

Chapter 3 explains the fabrication flow of the multi-channel acoustic transducer on a Silicon-on-Insulator (SOI) wafer with a 6-mask process. The chapter starts with a general explanation of the process. Then, each step is explained in detail with applied and possible MEMS fabrication methods. Finally, the quality of the fabrication process is discussed, and fabricated dies are presented.

Chapter 4 provides the characterizations of the multi-channel transducer and stimulation system of the fully implantable cochlear implant concept. In the beginning, test procedure is explained with applied and measured quantities. Then, auxiliary test equipment and their characterization are given to show the created test environment to mimic the middle ear environment during tests. Later, each test step is explained, and their results are presented. They are also compared with simulation results if applicable. After stand-alone tests, transducer and stimulation circuits are interconnected and the stimulation system of the fully implantable concept is tested *in-vitro* and *in-vivo* environment. Finally, the design is discussed in terms of limitations with obtained results, and these results are compared with the acoustic transducers in the literature.

Chapter 5 explains the proposed structure to improve the filtering quality of the acoustic transducers for the development of middle ear implantable transducers. At first, reasons for the bandwidth extension is explained, and bandwidth improvement methods are discussed. Then, properties of the proposed structure are explained, and finite element analysis results are shared. Finally, developed fabrication flow is given while explaining differences with multi-channel transducer fabrication in Chapter 3.

At the end, achieved research tasks through this thesis are summarized and possible future works on middle ear implantable multi-channel acoustic sensors are discussed in Chapter 6.

CHAPTER 2

MODELING AND DESIGN OF THE MULTI-CHANNEL PIEZOELECTIC ACOUSTIC TRANSDUCER

2.1. Introduction

The hearing chain continues to vibrate even after profound hearing loss. This situation makes it possible to sense ambient sound with an implantable transducer by using the natural hearing mechanism. This concept has been studied in the literature with different methods that were presented in the previous chapter. They demonstrated the opportunity of piezoelectric devices to generate voltage by using the vibration of ossicles and tympanic membrane. However, none of these structures can satisfy the requirements for a fully implantable CI system. These requirements introduce output level, dynamic range, frequency range, and size limitations. In this chapter, a multi-channel acoustic transducer is proposed that can meet the requirements. Figure 2.1 shows the structure of the transducer.

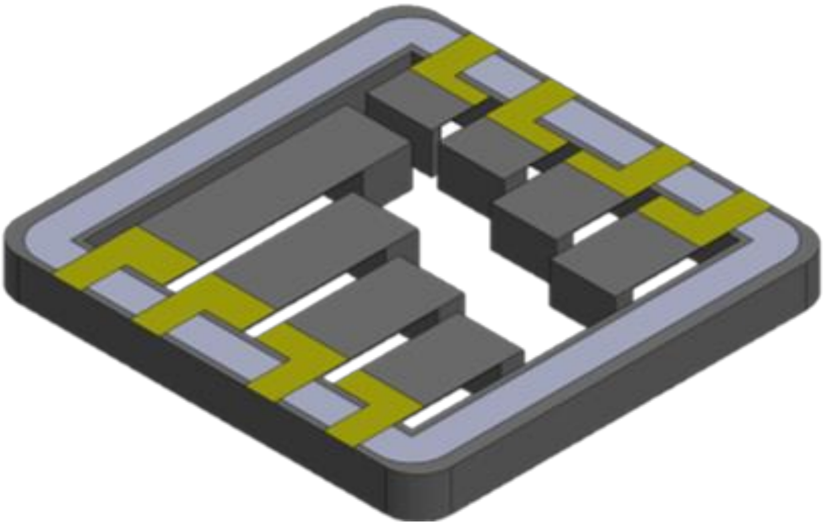

Figure 2.1. MEMS based multi-channel acoustic transducer.

In the first section of the chapter, requirements of the system are explained in detail to emphasize design parameters. Then, proposed structure properties are given with used materials and methods. In the modeling part of the chapter, the mathematical model of this structure and established finite element model in COMSOL Multiphysics are described. Finally, properties and requirements of the designed system are compared.

2.2. Requirements of Multi-Channel Acoustic Transducer

Implantable acoustic transducer needs to meet some invariable limits and critical requirements. The first consideration of the implantable device is about its dimensions since it is placed into a middle ear. This dimension restriction gets in the way of overcoming other problems. Secondly, adding mass or force loading on the hearing mechanism affects the vibration characteristics of the natural hearing mechanism. Besides these physical restrictions, the transducer must cover the daily acoustic band with sufficient number of channels to recover the incoming sound. Finally, stimulation interface circuits between the transducer and auditory neurons are used for neural stimulation. These circuits have minimum input voltage levels at which they function properly to generate the required stimulation signals. Therefore, the transducer should be able to generate this output level at daily sound pressure levels. These restrictions are explained in the following sections.

2.2.1. Dimensions

The transducer is placed on eardrum or ossicles to use natural vibration of the middle ear. The limited volume of the middle ear (1 cm^3) [42] and the area of the eardrum (9×10 mm^2) [43] restrict the dimensions of the transducer. Figure 2.2 illustrates the middle ear cavity to visualize the dimensions. This restriction is the main obstacle which inherently modifies other requirements such as frequency range and output voltage. The frequency range can be broadened by using more channels. Wider structures can also be used to increase the output level of the piezoelectric voltage generator. However, the size of the middle ear restricts the structure dimensions. This cycle shows that restrictions of the implantable transducer depend on each other.

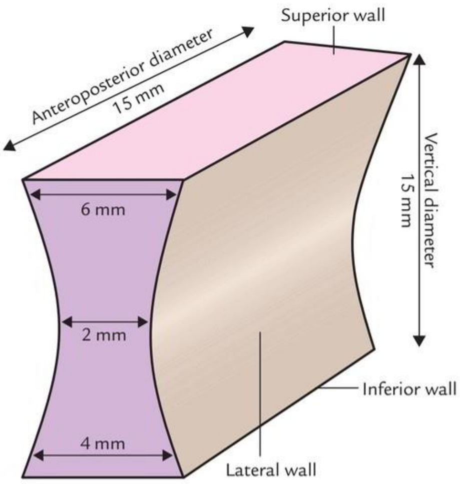

Figure 2.2. Middle ear cavity and its dimensions [44].

2.2.2. Total Mass

Besides the physical dimensions of the middle ear cavity and eardrum, additional mass or force loading on the hearing mechanism affects the natural vibration characteristics. This effect has been studied in the literature, and *in-vivo* studies show that adding 25 mg mass on the eardrum causes 3 dB reduction on the amplitude of the vibration [45]. This mass includes packaging and energy harvester proposed in the system [16]. As a result of this decline in the vibration, the total mass is limited as 25 mg for the implanted package in the concept of the FLAMENCO project.

The mass restriction affects the output voltage level and, thus, the dynamic range of the transducer because increasing the mass on the tip of the beams increases the stress on the piezoelectric layer. This stress level is directly proportional to the output voltage of the structure as it will be shown in the modeling part. Therefore, mass is a critical parameter for middle ear implants and must be considered not only in terms of a single part but also as complete system implementation.

2.2.3. Frequency Range

The human ear has sound perception on a wide frequency selectivity (20 Hz – 20 kHz) and a very high dynamic range (0- 140 dB SPL). However, this sensor properties cannot be achieved with today’s technology. Only daily sound perception can be recovered. The human voice mostly includes 250 Hz to 4kHz [46]. Below this limit is not feasible for hearing devices because of vibrations produced by body movements [47]. On the other hand, the upper frequency range between 4 and 8 kHz is important for speech understanding in noisy situations. In conventional cochlear implants, frequencies are placed between 250 Hz to 6 kHz, and they are distributed linearly below 1200 Hz and logarithmically above 1200 Hz [48]. In the proposed system, the same frequency distribution is applied.

Channels of the transducer must cover the daily acoustic band with an adequate number of channels because sound perception quality depends on the channel numbers, frequency distribution, and filtered frequency band of each channel. Conventional cochlear implants include 4 to 22 channels to filter the incoming sound and to stimulate the neurons. Recent studies show that up to 8 channels, sound perception increases significantly. However, more than 8 channels do not show a major increase [49]–[51]. Figure 2.3 shows speech reception test results of cochlear implant users as a function of stimulated electrode numbers.

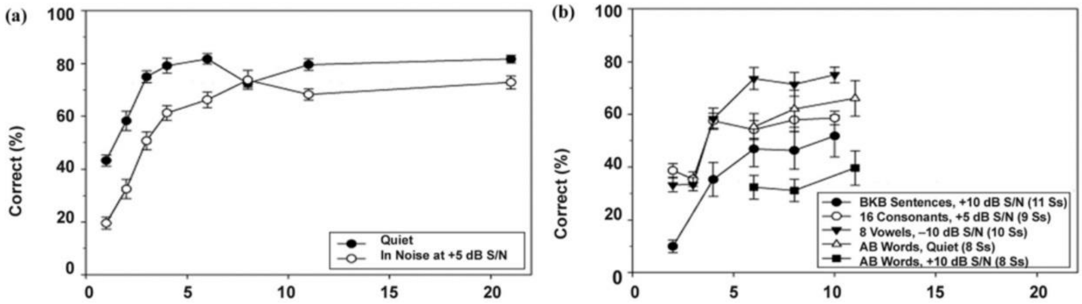

Figure 2.3. Speech reception scores as a function of stimulated electrodes (a) [50] and (b) [51].

Each channel consumes power levels independent from one another while stimulating the nerves. Therefore, increasing the number of channels raises total power consumption proportionally. Limited volume and the loading of the additional mass on the hearing system also restrict the channel number. Because of these reasons, 8-channel is the most appropriate type, and using more than 8 channels is not worth the effort for FICI applications.

2.2.4. Output Voltage

Generated output voltage by the piezoelectric effect is used by an interface circuit to stimulate auditory nerves. This circuit converts filtered signals generated by the transducer into biphasic pulses. Power consumption of the circuit must be minimized to expand the battery life of a cochlear implant. This power consumption requirement limits the minimum input level of the circuit. The limit is 100 µV for an ultra-low-power stimulation interface circuit designed in our group by Hasan Uluşan [27], [28]. Therefore, output voltage levels of each channel must exceed this input limitation to obtain a wide dynamic range.

The piezoelectric output voltage depends on the material properties and stress level on the piezoelectric layer. Accordingly, the structure of the transducer and properties of piezoelectric layer are essential parameters for stimulating the nerves and operating in a wide dynamic range.

2.3. Structure and Material Selection

The previous section shows that requirements of an implantable transducer are related to each other. This leads to an iterative design process. Besides these restrictions, the structure must continue to work for a long time and should be durable for sudden impacts like falling and hitting. These problems can be solved by using an array of cantilever beam structures that deflects more, and that can be easily manufactured. Their resonance frequencies can be arranged in the hearing band by adding a mass on the tip. Moreover, it is beneficial to keep the structure reliable and simple in this meticulous design.

Cantilevers can vibrate at their resonance frequencies with incoming sound. This vibration causes stress on the clamped side of the cantilever. Cantilevers benefit from induced stress to sense the sound by using the piezoelectric effect. The generated voltage from the piezoelectric effect depends on the stress level and the piezoelectric constant of the used material.

In our group, this concept has been studied and developed previously. Beker et al. [26] proposed a structure that includes an array of a cantilever beam with PZT-5A (bulk) for energy harvesting and sensing the ambient sound. He demonstrated this study on a single channel cantilever with a utilized wafer level fabrication of bulk PZT. However, it is not feasible with the aforementioned limitations because a channel of this structure covers $4.25\times4\times0.6$ mm^3, and the fabrication method is hard to complete for smaller beams. Then, İlik et al. [23] demonstrated the feasibility of using thin film piezoelectric on a single channel cantilever beam by using 1 µm PLD-PZT and generated 114 mVpp at 110 dB SPL.

In this study, an array of cantilever beams is used with a thin film PLD-PZT layer. Among other most available piezoelectric materials like AlN and ZnO, PLD-PZT is chosen. ZnO has a strong reactivity, especially when it is exposed to moisture and water. Therefore it is not suitable for biomedical applications [52]. Furthermore, PLD-PZT`s performance values in terms of vibrational energy conversions are superior compared to other materials. A quantified figure of merit (FOM) expressed in (2.1) is employed to show this superiority. In this equation, $e_{31,f}$ represents the piezoelectric coefficient value, ε_{33} is the dielectric permittivity, and ε_0 is the permittivity of free space [53], [54]. Properties of the deposited PLD-PZT can be seen in Table 2.1.

$$FOM = \frac{2e_{31,f}^2}{\varepsilon_0 \varepsilon_{33,f}} \tag{2.1}$$

Table 2.1. *PLD-PZT film properties* [53].

ε_{33} (@1 kHz, 0V)	*tanδ* (@1 kHz, 0V)	*Polarization* *Pr(µC/cm^2)*	$-e_{31,f}$ *(C/m^2)*
2000	0.01-0.02	20	7.7

This structure and selected piezoelectric properties can meet the requirement of the implantable transducer. Using thin film piezoelectric layer enables the fabrication of tightened beams and contributes to lowering the mass of the structure while giving an opportunity to use more beams in a limited area. Furthermore, a large piezoelectric coefficient generates higher output voltage and broadens the dynamic range of the acoustic transducer.

2.4. Modeling of Multi-Channel Transducer

Typical cantilever beam structure with tip mass is shown in Figure 2.4. In this structure, tip mass is used in order to tune the natural frequency of the structure, and the piezoelectric layer is placed onto the fixed part of the beam to utilize stress. While the beam is vibrating, it starts to bend, and this results in alternating compressive and tensile stress on the piezoelectric layer. Finally, the output voltage is generated depending on the stress level.

Three main methods have been used for modeling the structure in Figure 2.4. These methods are lumped parameters [55], distributed parameters [56], and finite element method (FEM).

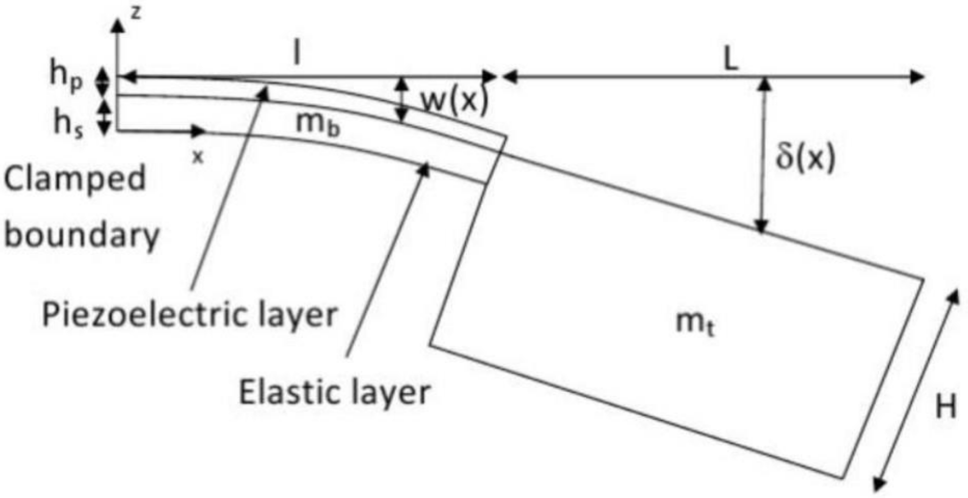

Figure 2.4. Cantilever beam structure with tip mass [55].

Flynn et al. [57] modeled the piezoelectric coupling as a transformer. This transformer links the stress on the piezoelectric layer to an electric field. Using this method, the equivalent model of the structure is established as two ports electrical network which is shown in Figure 2.5 [55]. In this model, the structural part is shown on the right side of the transformer. This ideal transformer presents electromechanical conversion and Γ is the piezoelectric coupling factor. F shows the applied force on the structure. M_{eff}, K_{eff}, and D stand for effective beam mass, mechanical stiffness, and mechanical damping, respectively. In the electrical part, C_P is used to present piezoelectric capacitance.

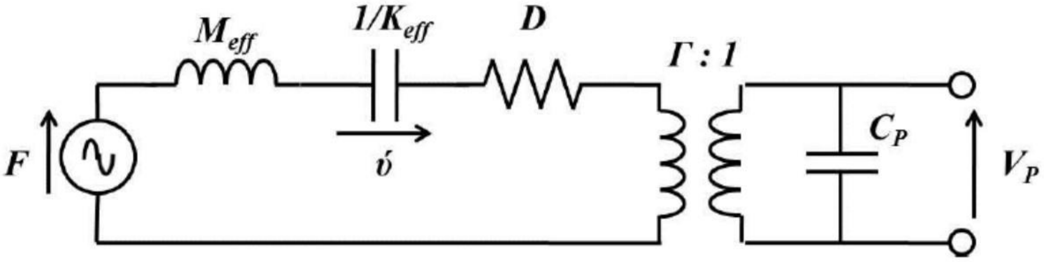

Figure 2.5. Equivalent network model for piezoelectric cantilever beam [55].

Left side of the model represents the mechanical part of the structure. In this model, steady state vibration is applied to the transducer as shown in (2.2), where a_0 is the excitation amplitude, and f is the excitation frequency.

$$F = M_{eff} a_0 \sin(2\pi f\, t) \tag{2.2}$$

Equation (2.3) expresses the effective mass M_{eff} in the model. In this expression, m_{beam} and m_t stand for the mass of the beam and tip mass, respectively.

$$M_{eff} = \frac{33}{140} m_{beam} + m_t \tag{2.3}$$

Equation (2.4) depicts the stiffness of the beam (K_{eff}) in terms of some parameters. In the expression, EI_{eq} provides the equivalent of area moment of inertia over the tensile compliance.

$$K_{eff} = \frac{3EI_{eq}}{l^3(1 + \frac{3L}{2l} + \frac{3L^2}{4l^2})} \tag{2.4}$$

Performance of the transducer structure, i.e. piezoelectric cantilever beam, depends on the generalized electromechanical coupling factor (*K*) and it can be expressed by model parameters as in (2.5):

$$K^2 = \frac{\Gamma^2}{K_{eff}C_p} \tag{2.5}$$

Finally, the resonance frequency of the piezoelectric cantilever beam is expressed as in (2.6):

$$f_r = \frac{1}{2\pi}\sqrt{\frac{k_{eff}}{m_{eff}}}\left(\sqrt{1 + K^2}\right) \tag{2.6}$$

In the electrical side of the model, the piezoelectric capacitance can be calculated making use of physical properties and dielectric permittivity as shown in (2.7):

$$C_P = \varepsilon_{33}\frac{Wl_p}{h_p} \tag{2.7}$$

Lumped model provides an overview of the problem. This model can be utilized as the electrical representation of the system. It is possible to implement this lumped model inside circuit simulation programs with given parameters. However, developed model consists of only one vibration mode of the structure. Because of that, strain distribution, dynamic mode shapes of structures, and their effects on the output characteristic cannot be considered [58].

Finite element method is a numerical method utilizing variational methods to find approximate solutions to boundary value problems where the structure is represented by an assembly of its subdivisions called finite elements. It converts partial differential equation problems into linear equation sets. This method provides several advantages. Structures can be modeled without any assumptions as in the lumped parameter model.

Tip mass effect can be calculated without any special consideration, such as the ratio of the beam to mass length. Anisotropic material properties of the used materials like PLD-PZT can be integrated into the model.

FEM can be solved by various CAD simulation programs. COMSOL Multiphysics was used in this thesis. COMSOL provides tutorials among different structures and applications. Its interface has systematical built-in modules, and hence, it is suitable for parametric studies to arrange resonance frequency and output voltage. Finally, it can be integrated with other structures after separate simulations. This could provide opportunities for further analysis.

Single cantilever beam structure with tip mass and a piezoelectric layer is shown in Figure 2.4. All these parameters must be defined with meticulous design to construct the structure which can meet the requirements of the middle ear implantable transducer. These parameters are:

- h_p = thickness of the piezoelectric material,
- h_s = thickness of the cantilever beam,
- l = length of the piezoelectric material,
- L=Length of the tip mass,
- H= Thickness of the tip mass,
- W= width of the beam.

Before starting to construct the module, some of these parameters such as material properties and commercially available thicknesses are defined. Then, the remaining parameters are characterized using the FEM module.

Selection of the piezoelectric material was given in Section 2.3. Pulsed Laser Deposited (PLD) PZT was chosen because of its properties given in Table 2.1. Thickness of the material is also critical for generated output characteristics. These properties have been studied by Solmates BV [54] where the wafers were deposited with PLD-PZT. Their study shows that using 1 µm PLD-PZT is suitable for beam structure. Therefore, 1 μm PLD-PZT is selected for the proof of concept design. In further studies, this can be optimized with its ingredient ratio and thickness after investigating stress distribution.

Thickness of the beam and tip mass are key parameters for applicable resonance frequencies in the cantilever beam structures. The resonance frequency of the cantilever beam was defined in equation (2.6). This formula and available space in the middle ear show that in order to reach lower frequencies with this structure, thicknesses must be selected properly. Furthermore, mathematical models show that in order to use the maximum effect of the tip mass, it must be applied as a point load on the tip. Effect of the mass decreases while it gets closer to the clamped side of the beam. Therefore, the thickness of the cantilever and mass were selected as 15 μm and 600 μm, respectively. This was a conventional Silicon-on-Insulator (SOI) wafer variant. Using SOI wafers provided well defined thickness parameters after fabrication.

Other parameters were calculated with FEM analysis in COMSOL. In this simulation module, material properties, the orientation of silicon and properties of PLD-PZT with predetermined structural parameters, were inserted. Then, parametric sweeps were applied to define resonance frequencies and obtain a higher output voltage. Figure 2.6 shows created simulation structure in COMSOL to obtain characteristics of the beam with applied parameters.

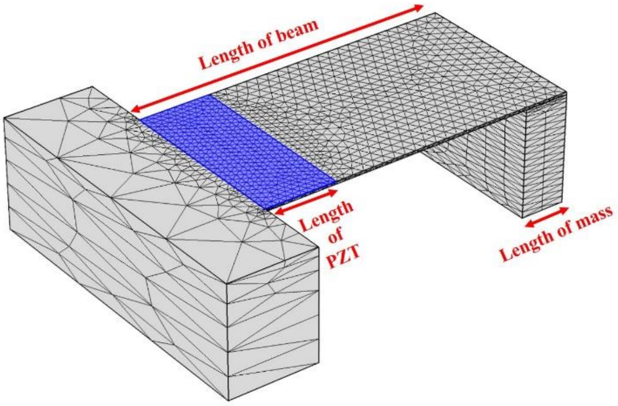

Figure 2.6. *Created simulation structure in COMSOL.*

Computational time and accuracy of the results depend on the meshing of the structure. Decrease in the mesh size improves accuracy. However, this approach expands the computational time, especially when there is a thin layer in the structure. Thin layers cannot mesh with free meshes that form only two elements through the layer. This pattern reduces the accuracy due to the lack of stress level calculation on the material. Therefore, the mesh size of the simulation module was arranged manually until it converges. Figure 2.7 shows the meshed beam structure.

Before creating the simulation module and investigating outputs, several assumptions were made:

- Simulation module run under vacuum condition. Therefore, air drag damping was excluded.
- Ideal load was connected ($R_{LOAD} = \infty$).
- Electrical damping due to input characteristic of interface circuit was excluded.

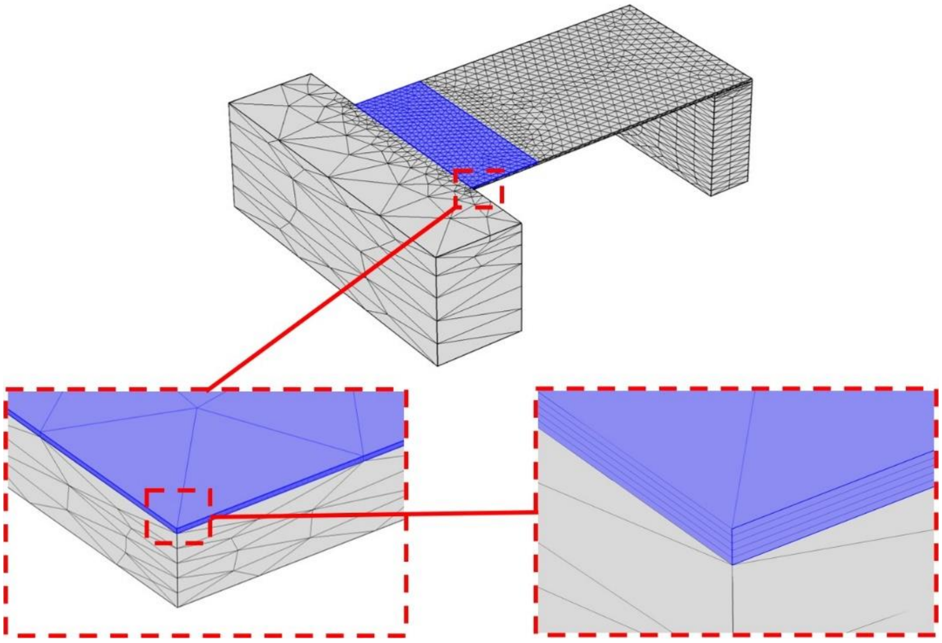

Figure 2.7. Meshing of the structure, blue layer shows piezoelectric layer. Note, base is hidden in focused images.

Furthermore, only the first vibrational modes of the beams were investigated during simulations, even resonance frequencies of these modes were in the audible hearing band (250 Hz – 5.5 kHz). The piezoelectric layer does not cover the area where these vibration modes create stress. Figure 2.8 shows first three modes of beam structure. It is unnecessary to investigate other vibration modes. Note that, fourth and higher modes of beams are not shown because they are not in the audible frequency range.

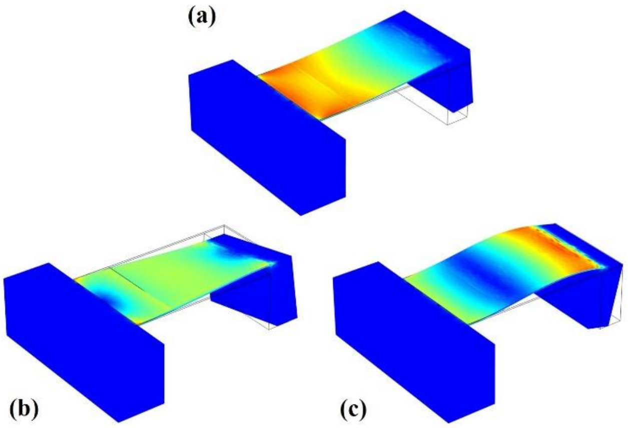

Figure 2.8. First three modes of beam structure with their stress levels (red shows highest and blue shows lowest).

Heretofore, restrictions of the transducer were defined. Material and structure properties were inserted into the module. Then, necessary assumptions were made. Hereupon, the simulation module was run with the flow shown in Figure 2.9.As illustrated in the flow, lengths of the beams, mass, and PZT were determined in the simulations. At each step, restrictions on the middle ear implantable transducer were checked, and mass was tried to be minimized. These simulations calculated the resonance frequency and output voltage of the piezoelectric cantilever beam structure. Resonance frequencies of the beams were tried to be arranged in conventional cochlear implants and parameters were swept with this matter. Output voltage also was tried to be maximized to exceed the minimum input level of the stimulation interface circuit. Output voltage depends on the stress level that is boosted by tip mass and used by active piezoelectric layer. Therefore, the piezoelectric layer is covered on maximum stress levels.

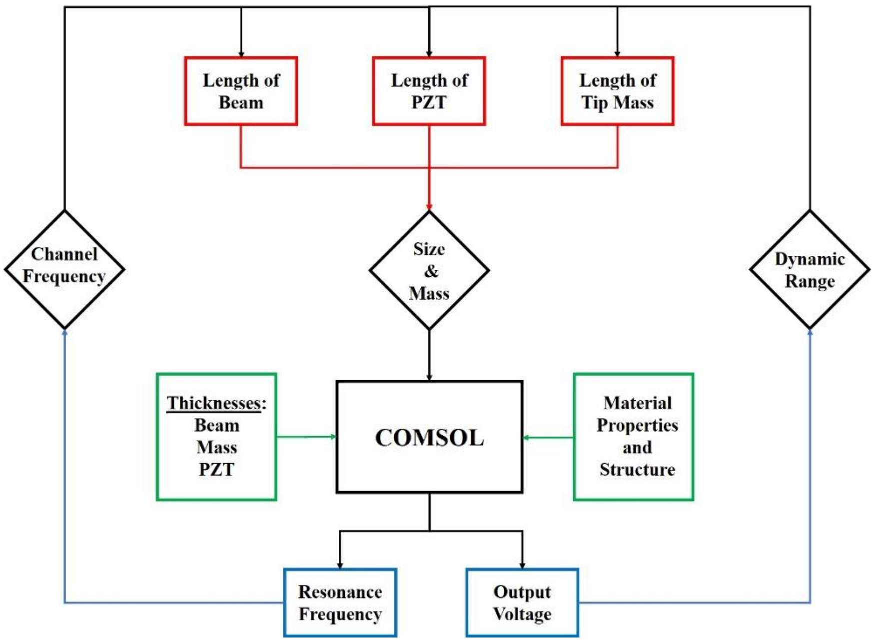

Figure 2.9. Simulation flow of multi-channel acoustic transducer. Red, blue, black, and green indicate simulation parameters, outputs, control systems and predetermined parameters, respectively.

In models and simulations, excitation type was defined as constant acceleration (0.1 g). However, this level corresponds to different sound pressure levels at different frequencies. Also, the structure of the middle ear affects the incoming sound level by amplifying it up to 12 dB with respect to frequency range as described in the ear anatomy section. Therefore, results of the experiments on the human cadaver were taken as a reference during design. In these experiments, vibrations of the umbo are observed by Laser Doppler Vibrometer (LDV) [18], [20]. Measurement place of the ear is illustrated in Figure 2.10.

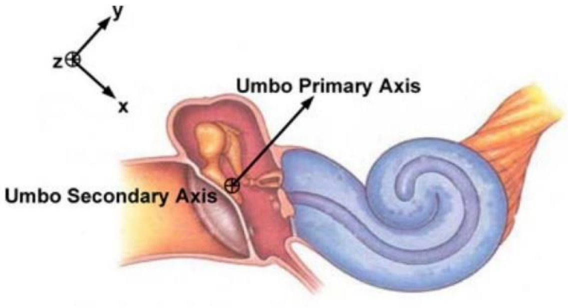

Figure 2.10. Illustration of the measurement place and its axis [18].

Figure 2.11 depicts the vibration characteristics of the human cadaver ear measured by using LDV. Excitation levels correspond to different sound pressure levels with changing excitation frequencies.

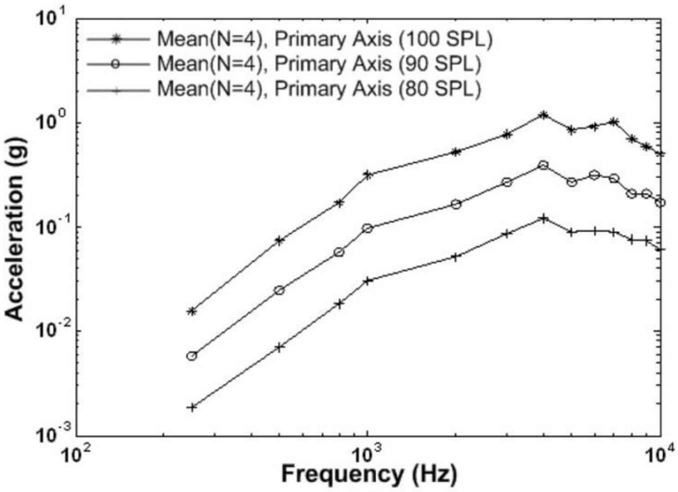

Figure 2.11. Acceleration response curves of umbo along the primary axis of human ear cadaver [18].

In the light of simulation results and these experiments, parameters of the multi-channel acoustic transducer were determined. Furthermore, Zurcher et al. [20] suggest that incus can be removed from the hearing chain to increase the vibration amplitude of eardrum. Figure 2.12 shows the vibration characteristic of the ear before and after the incus removal process. This characteristic can be used for further discussions on output level.

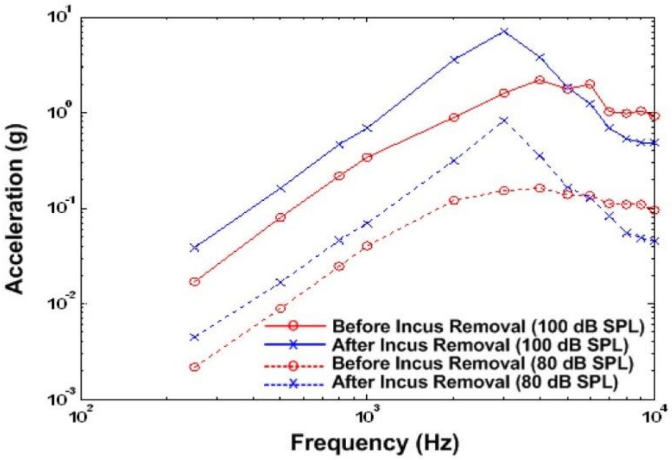

Figure 2.12. Vibration characteristic of umbo before and after incus removal [20].

2.5. Design Parameters

As a result of FEM simulations, the final structure of the transducer was defined. This structure contains eight silicon-based cantilever beams with silicon tip masses to reach the required frequency range. 8-channel system resonance frequencies are placed at 300, 600, 900, 1200, 1600, 2200, 3200, and 4800 Hz as in conventional cochlear implants. Determined parameters of the structure are shown in Table 2.2.

Table 2.2 *Design parameters.*

Channel Number	*Planned Frequency (Hz)*	*Length of Beam (μm)*	*Length of Mass (μm)*	*Length of PZT (μm)*
1	300	3800	750	600
2	600	2700	500	550
3	900	2200	400	450
4	1200	1900	350	400
5	1600	1700	250	400
6	2200	1400	250	300
7	3200	1000	300	300
8	4800	900	150	300

Channels of the transducer were placed with their conjugates to reduce the footprint of the device. In this way, the structure can fit into 5×5×0.6 mm^3 volume and the weight of the transducer without the test frame is only 4.8 mg. These dimensions are well below the limitations and give flexibility to other parts of the fully implantable system i.e., acoustic energy harvester and 3D packaging.

Besides the functional part of the transducer, the structure has some niceties. Structure has two frames, outer one can be separated easily for different test environments. Also, reference nodes of the channels are connected to each other to reduce unnecessary wiring on the structure. Final view of the structure can be seen in Figure 2.13.

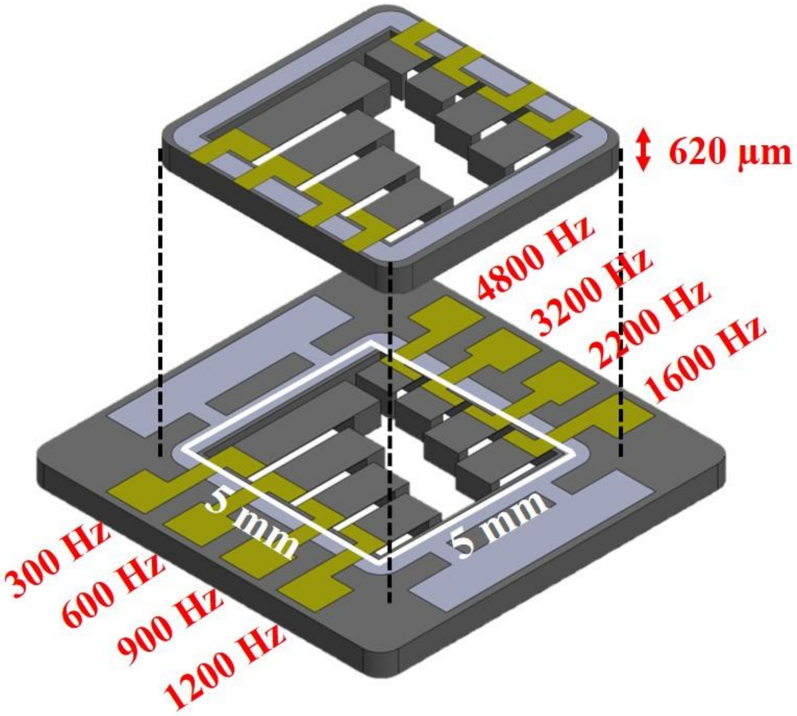

Figure 2.13. MEMS based multi-channel acoustic transducer with and without outer test frame.

2.6. Summary

In this chapter, the design process of the multi-channel acoustic transducer was presented. At first, requirements of the middle ear implantable transducer were given. They were dimensions of the middle ear, mass and force loading on the hearing chain, frequency range, and output voltage of the channels. Then, structure and material selection were explained with their reasoning. Mathematical and simulation models were shared with design considerations. Finally, calculated parameters by using COMSOL Multiphysics and final implantable structure properties were presented.

CHAPTER 3

FABRICATION PROCESS OF TRANSDUCER

3.1. Introduction

In the previous chapter, multi-channel thin film piezoelectric transducer structure is designed, and related parameters are described. Fabrication of the acoustic transducer is a challenging process and it has a critical impact on the performance of the devices. Therefore, error margins of the fabrication must be minimized to provide durable structure and reliable output characteristics for an implantable device. Even a small deviation in the parameters or defects on the structure may cause an unpredictable change in the performance of the transducer.

In this chapter, the fabrication process of the transducer is presented. MEMS based piezoelectric transducers and harvesters have been studied earlier in BioMEMS group, but there were some problems in the previous fabrication flow and margins of the structures for thin film application. Modifications and differences are described in each step.

3.2. Fabrication Process

Transducers were fabricated on 4-inch Silicon-on-Insulator (SOI) wafers by using six photolithographic masks. Figure 3.1 exhibits the general fabrication flow of the transducers. Details of each step, material properties, fabrication concerns are explained in the relevant parts.

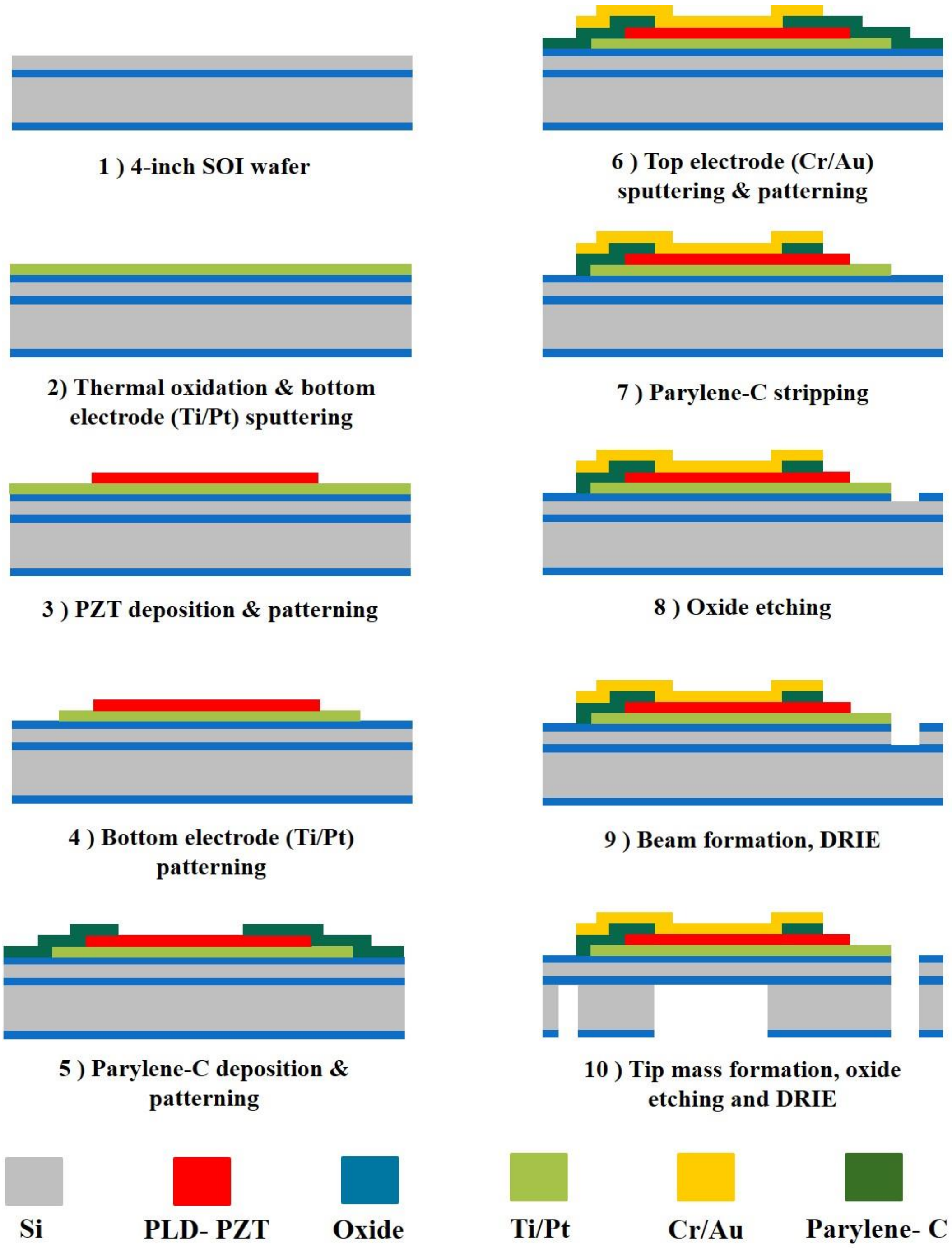

1) 4-inch SOI wafer

2) Thermal oxidation & bottom electrode (Ti/Pt) sputtering

3) PZT deposition & patterning

4) Bottom electrode (Ti/Pt) patterning

5) Parylene-C deposition & patterning

6) Top electrode (Cr/Au) sputtering & patterning

7) Parylene-C stripping

8) Oxide etching

9) Beam formation, DRIE

10) Tip mass formation, oxide etching and DRIE

Figure 3.1. Fabrication flow of MEMS based multi-channel acoustic transducer.

3.2.1. Wafer Selection

For this fabrication, 4-inch SOI wafers (100 oriented) with 15 µm device, 2 µm insulation layer, and 600 µm handle thicknesses were utilized. Using SOI wafer contributes to obtaining high structural accuracy. Stiffness of the cantilever beam and mass of the structure are the crucial parameters for resonance frequency. They were determined by the device layer thickness and handle layer thickness of the wafer. In addition to these, the buried oxide layer was used as a stop layer for the DRIE process in cantilever formation part (Figure 3.1 (1)). This layer prevented over etching and provided a controllable beam release. For these reasons, SOI wafers were preferred to fabricate transducers.

3.2.2. Isolation Layer Coating

The device layer of the SOI wafer was needed isolation layer to prevent lateral leakages between electrodes. Consequently, a 500 nm thermal oxide (SiO_2) layer was deposited. This process last 3 hours at 1000 °C in thermal ovens. The thermal oxide was preferred because of high-temperature process in the fabrication flow. Other oxides were not suitable for this application. Before deposition, wafers were cleaned in Piranha solution to clean any organic residual for 30 minutes. However, this solution causes oxidation on the silicon. Undesired oxidation was removed in buffered HF (BHF) solution (1:7) in 3 minutes.

3.2.3. Bottom Electrode Patterning

Titanium (Ti) and Platinum (Pt) metals were employed as a bottom electrode layer of the transducer. Pt was chosen due to its high thermal conductivity and good stability in an oxygen environment. Ti promotes adhesion for Pt layer. Also, Ti atoms can diffuse out the Pt layers` grain boundaries onto Pt surface, and these Ti atoms enhance the formation of perovskite PZT [59]. Therefore 10/100 nm Ti/Pt layers were sputtered as the bottom electrode of the transducer.

3.2.4. PLD-PZT Deposition and Patterning

Among piezoelectric materials, Pulsed Laser Deposited Lead Zirconate Titanate (PLD-PZT) was chosen because of its piezoelectric properties and suitability to the application. Deposition of 1 μm PLD – PZT layer was processed at Solmates BV by using the SMP-700 PLD device.

The piezoelectric layer was patterned by using an etch and clean solution whose ingredients and ratios are provided by Solmates BV. For this patterning, a clear field photolithographic mask was used to pattern SPR220-3 photoresist which was coated at 3000 rpm and soft baked 15+180 seconds at 115 °C. Then, it was exposed 3.5 seconds, developed 50 seconds in MF24A solution, and hard-baked 30 minutes at 110 °C. Figure 3.2 shows the patterned piezoelectric layer.

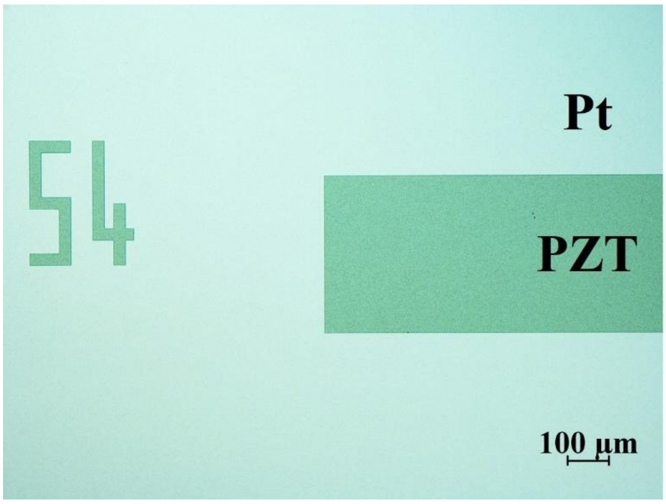

Figure 3.2. Microscopic image after PLD-PZT etch.

3.2.5. Bottom Electrode Patterning

10/100 nm Ti/Pt layers were deposited as a seed layer of PZT and the bottom electrode for the transducer. For patterning, photoresist SPR220-7 was coated on the wafer at 3000 rpm and soft baked 240 seconds. Then, it was exposed 30 seconds, developed 75 seconds in MF24A solution, and hard-baked 40 minutes at 110 °C. Thick resist is important for protecting the PZT layer because Pt etchant harms the PZT layer.

Platinum is a noble metal and this limits our etchant choices. The most practical way to etch Pt is using Hot Aqua Regia solution. It is a mixture of hydrochloric acid (HCl) and nitric acid (NH_4) with a 3:1 ratio at 60 °C. In this fabrication, Pt was patterned by using above-mentioned severe solution.

Below the Pt layer, thin (10nm) Ti was employed as an adhesion layer. This layer was patterned with H_2O_2:HF:DI water solution. Figure 3.3 shows the microscope image of the bottom electrode and the piezoelectric layer.

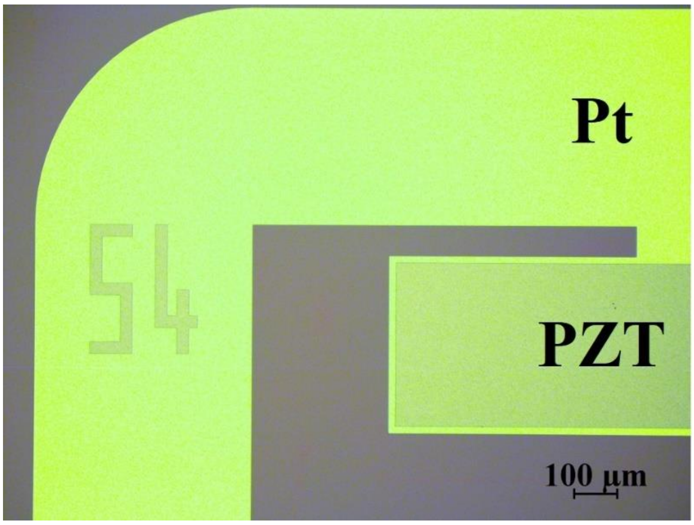

Figure 3.3. Microscope image of the transducer after bottom electrode patterning

3.2.6. Insulation Layer Deposition and Patterning

After the bottom electrode patterning, the Parylene-C layer was deposited on the wafer by using the SCS PDS2010 parylene deposition system. This layer prevents vertical electrical isolation between the top and bottom electrodes. For this purpose, 2.1 mg Parylene-C was used to deposit a 1 µm insulation layer. Dielectric strength of the Parylene-C is 220 V/micron, which means 220 V is the maximum required voltage to produce a dielectric breakdown. Therefore, the deposited layer thickness is suitable for the application. Note that, insulation layer effects are ignored during the design, therefore covering a thicker layer can increase the discrepancies between the designed and fabricated devices.

For parylene etching, the principal etch agent is oxygen plasma, but it must be applied perpendicular to the wafer surface to avoid excessive undercut. Unfortunately, applying oxygen plasma harms the photoresist. Therefore, to increase the thickness of SPR220-3, it was covered at 1500 rpm, and soft-baked 10 minutes. Then, it was exposed 4.5 seconds (with darkfield mask), developed 55 seconds in MF24A solution, and hard-baked 40 minutes at 95 °C. Etching of the 1 μm parylene layer was completed in 1 minute under 100 W directional oxygen plasma. Previous studies show using Fluorine based chemicals like CF_4 enhances etching of parylene [60]. However, during fabrication there was a problem in the Reactive Ion Etching (RIE) device which has CF_4 feeding. Thus, this etch is completed without CF_4.

During this first parylene etching step, only the top of the piezoelectric layer was opened as illustrated in Figure 3.1.(5). Remaining part of the wafer was protected with parylene layer during top electrode deposition and patterning.

3.2.7. Top Electrode Deposition and Patterning

After removing parylene from top of the PLD-PZT layer, 30/400 nm Chromium/Gold layer was sputtered. Au layer provided top electrode connections for the piezoelectric layer, and Cr was used as an adhesion layer for Au. This deposition was processed at 100 W to protect the parylene layer. In previous fabrications, metal particles were observed in the parylene layer when the deposition was carried with 300 W power. Therefore, the top electrode was deposited with 100 W to prevent possible short circuits.

This Cr/Au layer was patterned by using SPR220-3 photoresist. It was covered at 1500 rpm, soft-baked 10 minutes. Then, it was exposed 4.5 seconds (with clear field mask) under UV light, developed 55 seconds in MF24A solution and, hard-baked 40 minutes at 95 °C. Then, commercial Transene etchants were used to remove metal layers apart from the top electrodes, as illustrated in Figure 3.1.(6).

3.2.8. Isolation Layer Stripping

The insulation layer of the transducer was etched partially for the top electrode openings in previous steps. After patterning top electrode layer, the remaining Parylene-C layer was stripped in a minute by using oxygen plasma, as explained in the "Insulation Layer Deposition and Patterning" part. During this process, top electrode patterns were used as a mask. Figure 3.4 shows the microscope view of the transducer after stripping.

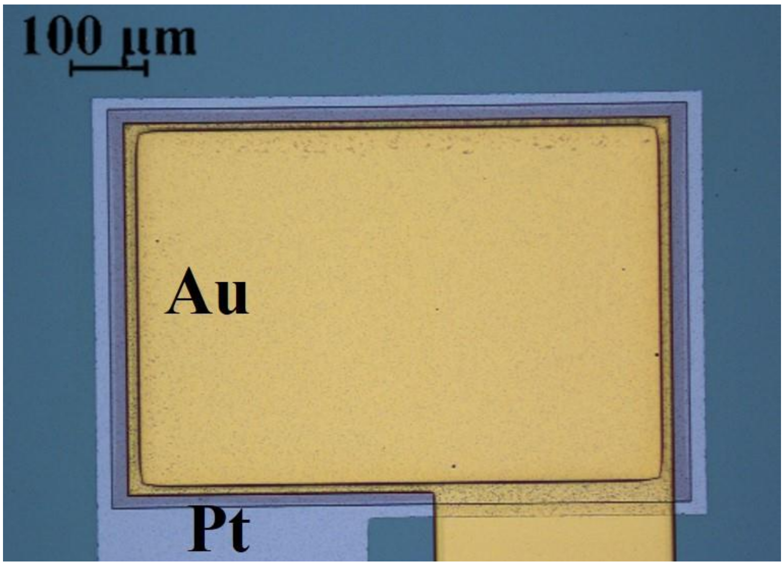

Figure 3.4. Microscope image of transducer after parylene stripping step.

3.2.9. Beam Formation

The electrical part of the structure was completed with the parylene stripping step. In order to build a beam structure, the device layer of the SOI wafer is needed to be shaped. This device layer is sandwiched between two oxide layers as illustrated in Figure 3.1. (9). The oxide layer on the top side can be patterned by using wet and dry chemical etching techniques. RIE can be utilized for oxide etching as a dry etching technique. On the other hand, Buffered HF (BHF) solution is an etchant for oxide. In this batch, due to technical problems, wet etch was used. In order to pattern structure, SPR220-3 photoresist was spun at 1500 rpm for 30 seconds. Then, it was exposed 4.5 seconds (with clear field mask), developed 55 seconds in MF24A solution, and hard-baked 40 minutes at 95 °C. By this lithography, the front side of the wafer was patterned. There was an oxide layer on the backside of the SOI wafer, and wet etch technique could harm this layer. Therefore, the backside of the wafer was covered with S-1813 photoresist by using a spray coating tool. After patterning and protection cautions, the thermal oxide layer was etched by using a BHF (1:5) solution. Microscope view of the transducer at this step can be seen in Figure 3.5.

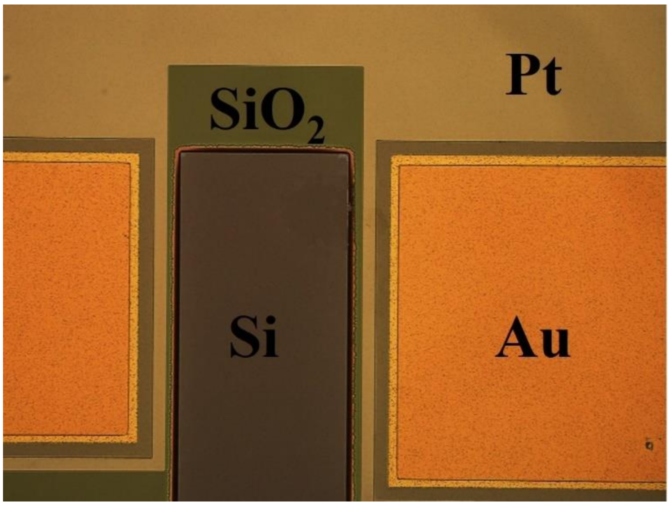

Figure 3.5. Microscope image of the transducer after patterning insulation layer.

The device layer became processable after oxide etching. In order to obtain sharp edges, Deep Reactive Ion Etching (DRIE) tools were used for etching the device layer of the wafer. As mentioned previously, the buried oxide layer was used as a stop layer of the DRIE process. Therefore, the structure could be formed without any residuals at the walls of the transducer.

3.2.10. Tip Mass Formation

Forming tip masses and backside of the transducer were the final parts of the fabrication of the transducer. In these parts, oxide on the backside of the wafer was patterned. Then, it was used as a mask under the photoresist. This is because the photoresist layer by itself could not tolerate DRIE process through the 600 µm etch which was the handle layer thicknesses of the SOI wafer. In order to obtain sharp structures, DRIE was applied for silicon etching.

Micromachined layers on the front side were needed to be protected before processing backside of the wafer. To achieve this, frontside of the wafer was covered with S-1813 photoresist by using spray coating and it was hard-baked 60 minutes at 95 °C.

After getting the necessary precautions to protect frontside, SPR220-3 photoresist was used for patterning the oxide layer, and it was spun at 1500 rpm for 30 seconds. Then, it was exposed 4.5 seconds (with clear field mask), developed 55 seconds in MF24A solution, and hard-baked 40 minutes at 95 °C. During this lithography, the oxide layer was patterned and etched by using BHF (1:5) solution. This etching can also be carried out with a RIE process. Due to technical problems in the RIE tool, this could not be applied in the batch.

Patterned oxide enabled silicon micromachining with through etching of the silicon from the backside of the wafer. The buried oxide layer of the SOI wafer was used as a stop layer in this step. However, cooling gas flows and clamps/chucks to hold the wafer in the DRIE tools could cause damage to beams. In addition, these openings could lead to gas leakage in the device. Therefore, prior to this etching, the wafer should be bonded to protection wafer for the DRIE process. For this function, the best option is to bond alumina wafer. That is because of the fact that its thermal conductivity is higher than silicon wafer and DRIE could not etch alumina wafer. Process and alumina wafers were bonded with the crystal bond. Final view of the layers is illustrated in Figure 3.6 at this step.

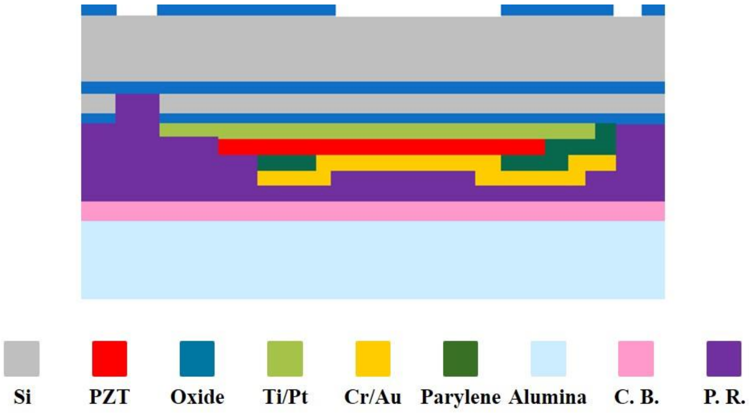

Figure 3.6. Layers of the bonded wafers before tip mass formation.

Etched areas of the structure have different width so, 600 µm silicon etching could not be completed simultaneously. While the parts below beams were etched quickly, parts between the tip masses and frames took a longer time to complete. This situation also showed the importance of using an SOI wafer. At the end of the DRIE process, the structure was in the most fragile condition and position. Because of that, the separation process of the transducers from the crystal bond and alumina wafer should be carried out carefully. As a property of the crystal bond, it could be resolved in the water at 80 °C and residuals of the crystal bond and resist can be removed by using acetone and methanol. This cleaning completed the wafer level fabrication of the transducer. Transducers are connected to wafer with only small silicon layer (thickness: 15 µm, width: 300 µm and length: 200 µm) which can be separated with a razor easily. In this way, they can be removed without the dicing of the wafer. The isotropic view of the fabricate transducer can be seen in Figure 3.7. Moreover, front and back views are shown in Figure 3.8.

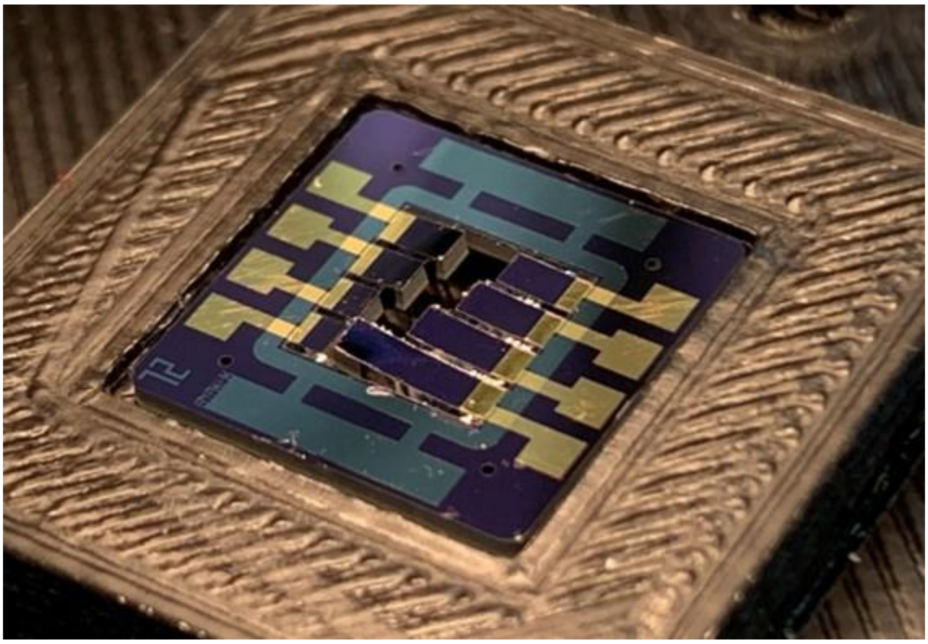

Figure 3.7. Isotropic view of the fabricated transducer.

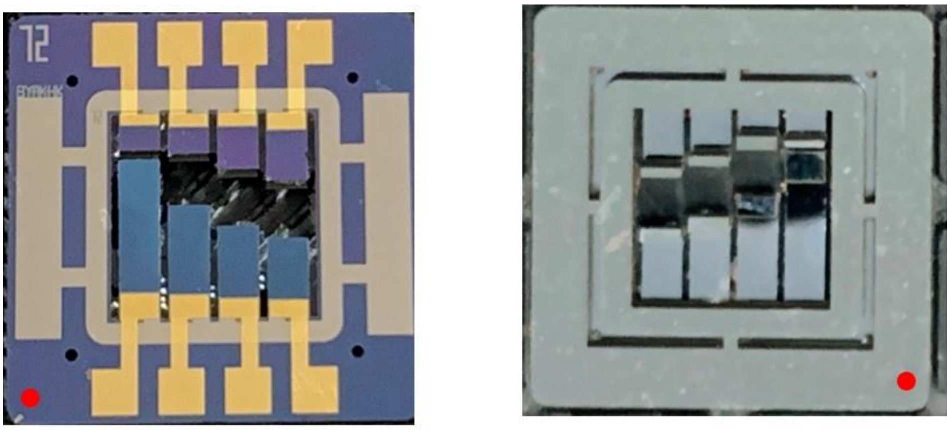

(a) (b)

Figure 3.8. Front (a) and back (b) view of the transducer, red dots show the orientation.

As seen in Figure 3.8 (b), the transducer structure includes two frame layers. Outer frame is made up of pogo pin pads to make easier testing transducer on shaker table tests. This outer frame can be removed easily, and the remaining part`s dimensions are suitable for implementing to the middle ear. The outer frame is connected to the device with four main bridges (615 µm thickness) and a thin silicon layer (15 µm thickness) for contact pad wiring. In order to remove test frame, the thin silicon layer is removed with razor and bridges can be separated by using a diamond cutter. The final structure is depicted in Figure 3.9.

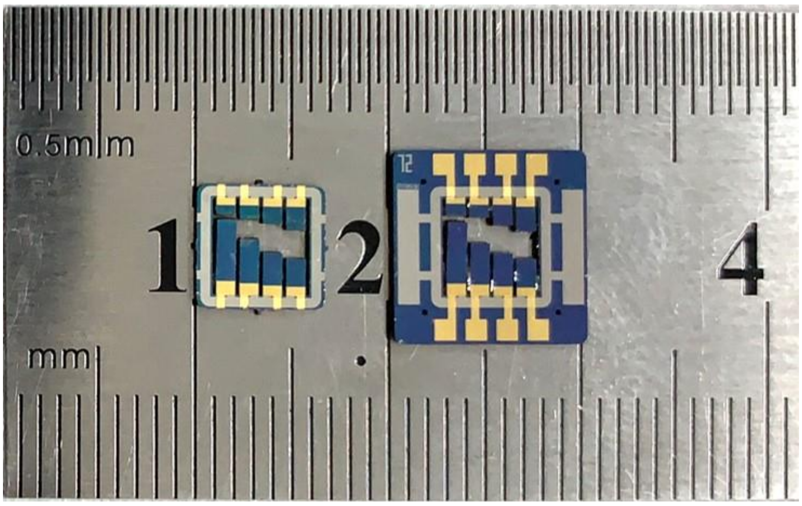

Figure 3.9. Transducer with and without outer test frame.

3.3. Summary

In this chapter, fabrication steps for the designed multi-channel thin film transducer were presented in detail. Each used material and its intended purpose were explained. Besides the applied process flow, alternative ways were described. By using this flow, the transducer was fabricated with a 92 % yield on a 4-inch wafer which contains 42 transducer dies.

CHAPTER 4

EXPERIMENTAL CHARACTERIZATION OF MULTI-CHANNEL ACOUSTIC TRANSDCER

4.1. Introduction

This chapter presents the experimental characterization of the multi-frequency acoustic transducer. The transducer is characterized by different types of excitations such as, electrical, electromechanical, and acoustic. Therefore, a systematical approach is required for proper characterization and progression during tests. In this chapter, systematical characterization methods are explained in the test methodology part. Then, auxiliary equipment used in tests is defined. After explaining general methods, each test result will be shown and compared with simulation results.

4.2. Test Methodology

Testing transducer under different excitations is required for comprehensive characterization and system level integration. These characterizations start during the fabrication and progress in a logical way. In this way, reasons for discrepancies between the design and the fabrication are eliminated. During these tests, auxiliary equipment is employed to increase the reliability of the results.

4.2.1. Test Systems

Tests start with measuring parameters of the transducer, which can be compared with design expectations and simulation results. They constitute electrical model and vibration characteristic of the transducer. The electrical model is defined by properties of used materials and dimensions of the layers. As a first step, this model is compared with measured electrical properties and the comparison shows the quality of the surface micromachining. The next test is about the electromechanical characterization of the transducer. In these tests, the aim is to inspect the output levels under certain acceleration values used in the COMSOL simulations. In the simulation, the transducer is excited with constant acceleration force while keeping the base constant, this setup correlates with shaker table tests. These comparison results show the condition of the bulk micromachining. Then, the agreement between the outputs of the designed and fabricated devices can be identified. After observing expected and reliable results, other characterization methods that cannot be simulated are applied to investigate the capabilities of the transducer for this special application. In further tests, the output characteristics of the transducer under sound pressure are measured. Finally, the sound detection and stimulation parts of the system are interconnected and tested. Summary of the tests can be seen in Table 4.1.

Table 4.1. *Applied test methods for characterization of acoustic transducer.*

Test Name	*Test Type*	*Input Excitation*	*Output Type*
Short-Capacitance Test	Electrical	Voltage	Capacitance & Resistance
LCR Test	Electrical	Voltage and Frequency	Resonance Characteristics, Capacitance and Resistance
Shaker Table	Mechanical	Acceleration and Frequency	Resonance Characteristics, Voltage
LDV Test	Acoustic and Mechanical	Sound Level and Frequency	Resonance Characteristics, Displacement and Voltage
Sound Test	Acoustic	Sound Record	Voltage Response of Each Channel
In-Vitro Test	System Integration	Sound Level and Frequency	Stimulation Signal
In-Vivo Test	System Integration	Sound Level and Frequency	ABR of Guinea Pig

4.2.2. Auxiliary Test Equipment

Each fabricated transducer is subjected to systematical tests. The transducer is connected to different auxiliary test equipment to carry out these tests. They provide electrical contacts and mimic the vibration of the hearing chain. Three main tools are used for this purpose: Transducer holder, parylene carrier, and artificial tympanic membrane.

4.2.2.1. Transducer Holder

Multichannel structure prolongs the process of making electrical contact for tests. For example, using a probe station for electrical connections to test the functionality of the channels takes a long time for a multichannel structure. Preparing wire bonds for initial tests also brings too much work. Therefore, a specific transducer holder was designed for connection and obtaining reliable test results. Figure 4.1 depicts designed holder.

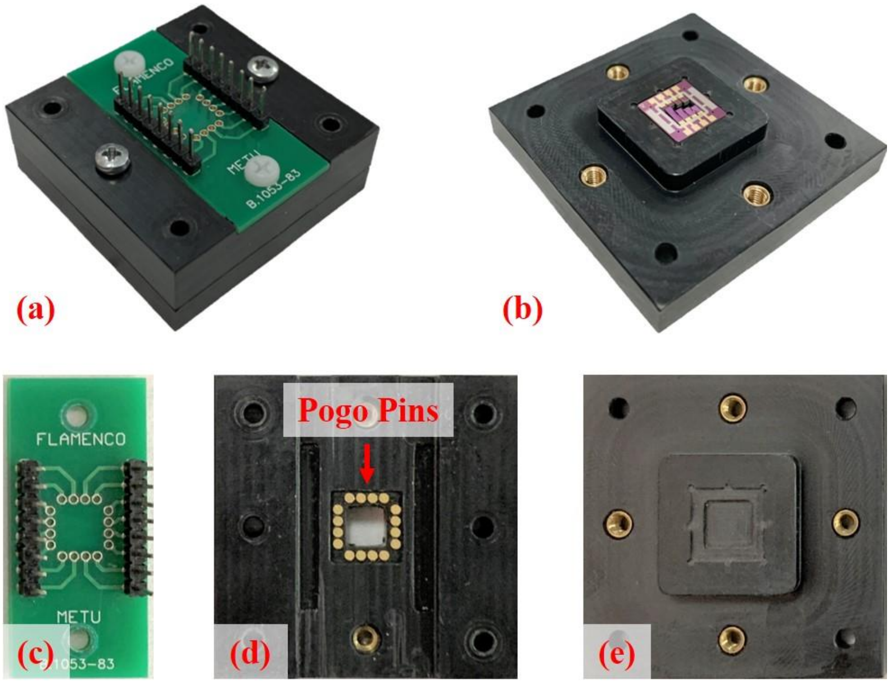

Figure 4.1. Transducer holder and its parts: packaged view (a), position of transducer (b), PCB (c), top part and pogo pins (d), and bottom part with double yards.

The holder provides an opportunity to make electrical connections with pogo pins which are spring-loaded connectors. While It was being designed, several problems were kept in mind. The bottom side of the holder includes a double yard where the first yard defines the position of the transducer, and the second yard prevents the collision of the beam to bottom. In addition, the top part of the holder contains the yard on the bottom side to provide smooth vibration to beams. This part incorporates holes for pogo pins that define their position. Finally, a printed circuit board (PCB) is used to transmit signals with headers and hold the pins stable at their position. Along with these, spring constants of the pins were taken into account for possible effects during the tests. The resonance frequency of the spring system was calculated for minimum value at it is around 8 kHz which is out of test range. These properties make the transducer holder suitable for tests.

The holder can be used for the short-capacitance tests, electrical resonance characterization test, and shaker table tests of the multichannel transducer. Moreover, the flexibility of the design and spring system enables us to use the holder for other structures and thinner transducers.

4.2.2.2. Artificial Tympanic Membrane

The transducer is planned to be implemented on the eardrum or ossicles. However, adding mass and position of the transducer have a significant effect on the performance. Therefore, the final performance of the transducer could be obtained after experiments on the cadaveric hearing system of humans. In the FLAMENCO project, a physical model of the tympanic membrane was designed and tested by Parinaz Ashrafi [61]. She also designed a membrane holder with a controlled stretching mechanism for the acoustic test. Holder and specifications can be seen in Figure 4.2.

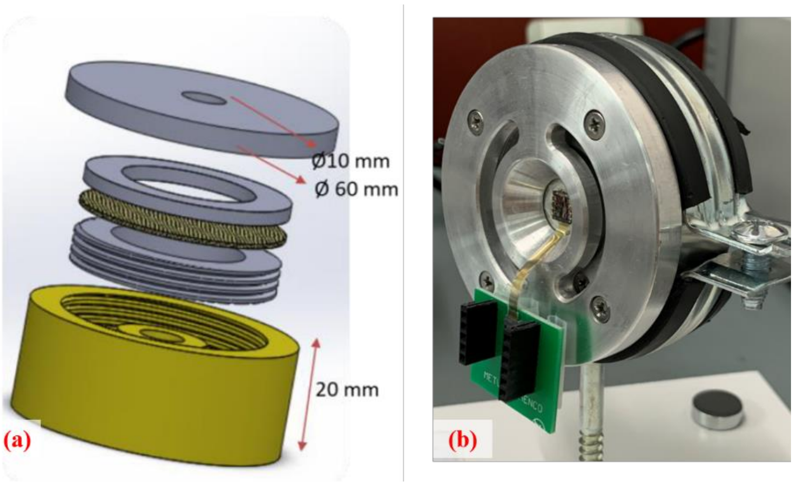

Figure 4.2. Artificial tympanic membrane holder for acoustic tests.

PDMS tympanic membrane was characterized by using Scanning Laser Doppler Vibrometer and acoustic holder. The first resonance frequency of the PDMS membrane is around 1kHz similar to the human tympanic membrane, also vibration magnitude is in the range of experimental results in the literature. Characteristic and the comparison with literature can be seen in Figure 4.3 [61].

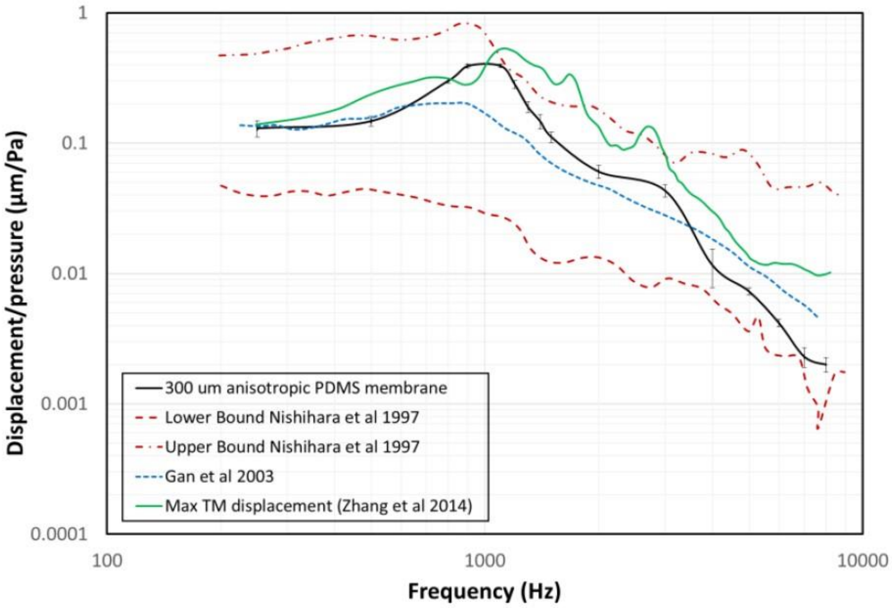

Figure 4.3. Vibration characteristic of PDMS membrane and its comparison with experimental results in literature [45], [61], [62].

As seen in Figure 4.3, PDMS membrane vibration characteristic is similar to experimental results in the literature. Therefore, the transducer is attached to the PDMS membrane to mimic the vibration of the hearing chain for acoustical characterization.

4.2.2.3. Parylene Carrier

In the FLAMENCO concept, transducers (sound detector and energy harvester) will be interconnected with interface circuits and battery by using a flexible and biocompatible package. The solution to this issue was proposed in our group [63]. In this aspect, transducers are packaged using Through Silicon Via (TSV) and parylene carrier system, which transmits signals to interface circuits and battery. For acoustic test on PDMS membrane, a modified version of the carrier was fabricated by Alper Kaan Soydan, which is shown in Figure 4.4. This version possesses larger pads for wire bonds. Thus, it enables the individual characterization of the transducer before packaging.

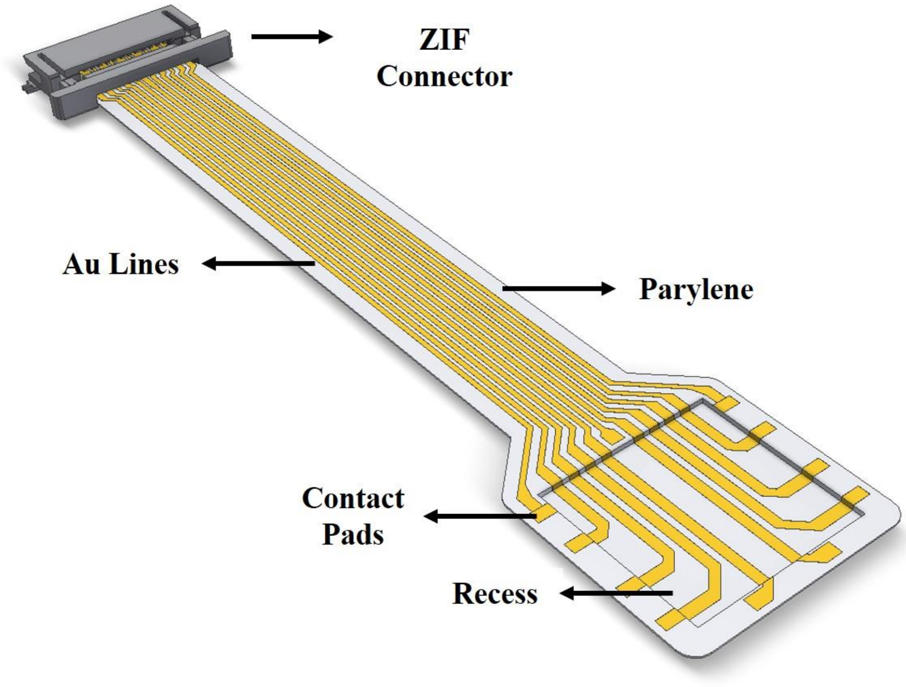

Figure 4.4. Parylene carrier for acoustical characterization of the transducer and integration of the system [63].

4.3. Transducer Characterization

4.3.1. Short-Capacitance Test

The first outcomes of the fabrication were detected by checking resistance and capacitance values between the top and bottom electrodes of each channel. This test was conducted via a handheld multimeter and microscope, as shown in Figure 4.5. Each channel has its own capacitance and resistance values depending on the design parameters. Deviations from this expectation or observing short circuits between the electrodes have resulted from the faults during the fabrication. Therefore, the results of this test show the quality of the fabrication and give the yield. These test results revealed that up to 92 % yield was obtained in this batch of the fabrication. Reasons for the faults were originated from defects in lithography processes for short circuits and broken channels while separating the wafers after tip mass formation.

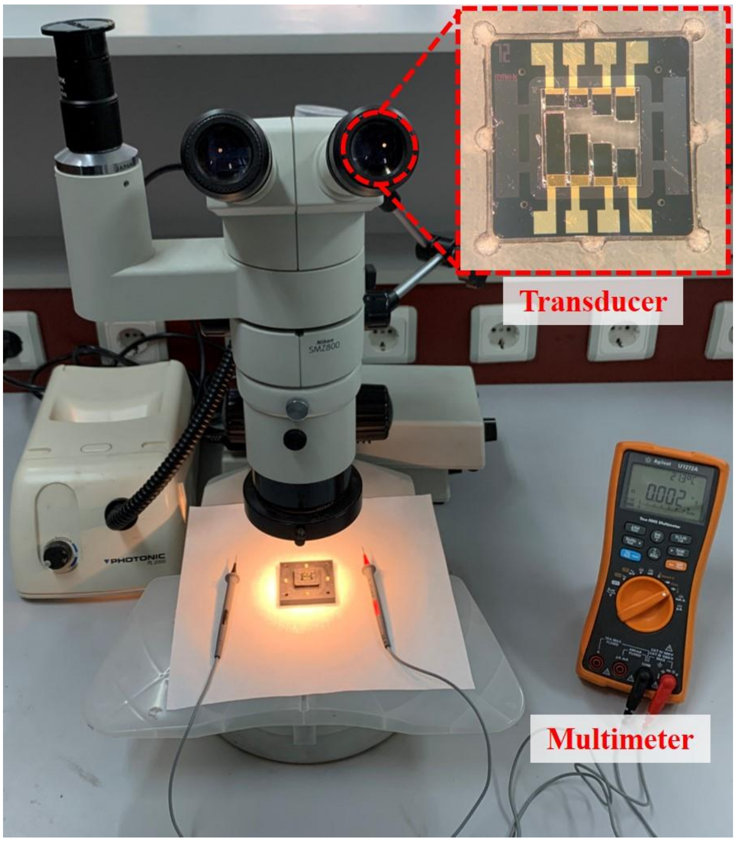

Figure 4.5. Short-capacitance test setup of the transducer.

4.3.2. Electrical Resonance Characterization

The electrical resonance characteristics of the piezoelectric transducer are observed using its resistance and capacitances in the frequency domain. These test results demonstrate the resonance frequency of the transducer. Figure 4.6 shows the test setup of the electrical resonance characterization.

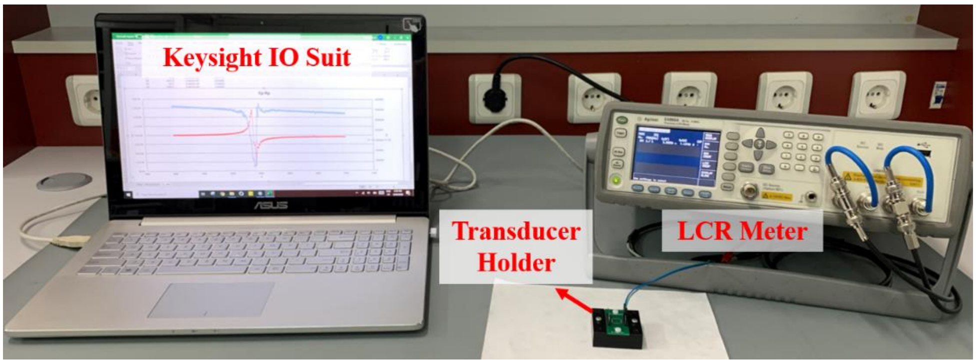

Figure 4.6. Electrical resonance characterization test setup of multi-channel transducer.

In this test, the LCR Meter (Agilent E4980) was employed to measure the electrical properties of the transducer. Configuration of the device was arranged in terms of parallel capacitance (CP) and parallel resistance (RP) model. Results were transferred thanks to Keysight IO Libraries Suite application and Excel Macro code extension provided by the same company. The results of the 2nd channel are shown in Figure 4.7.

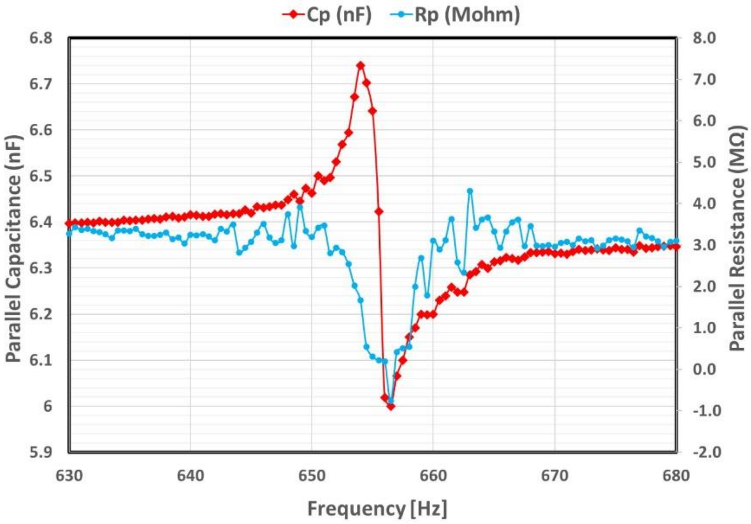

Figure 4.7. Electrical resonance characterization of the second channel obtained by LCR Meter.

4.3.3. Shaker Table Test

Mechanical vibration characteristic is one of the design characteristics of the transducer. This characteristic was obtained using the COMSOL module explained in chapter two. Measurements were taken during excitation of the transducer with a constant acceleration in the test setup. Figure 4.8 shows the experimental setup for mechanical characterization.

The setup consists of shaker table (B&K Type 4809), controller (VR 8500), amplifier (B&K Type 2718), accelerometer (B&K 4517-002), Data Acquisition Board (DAQ – NI cDAQ-9174), computer for interface programs, and spring-loaded holder. Vibration View program, controller, and amplifier define the excitation level of the shaker table. The accelerometer measures the acceleration level and gives feedback to the program to keep the excitation level constant. Electrical connections with channels are ensured via spring-loaded circuit and signals are measured by DAQ. LabView is used to visualize and save the voltage level and frequency.

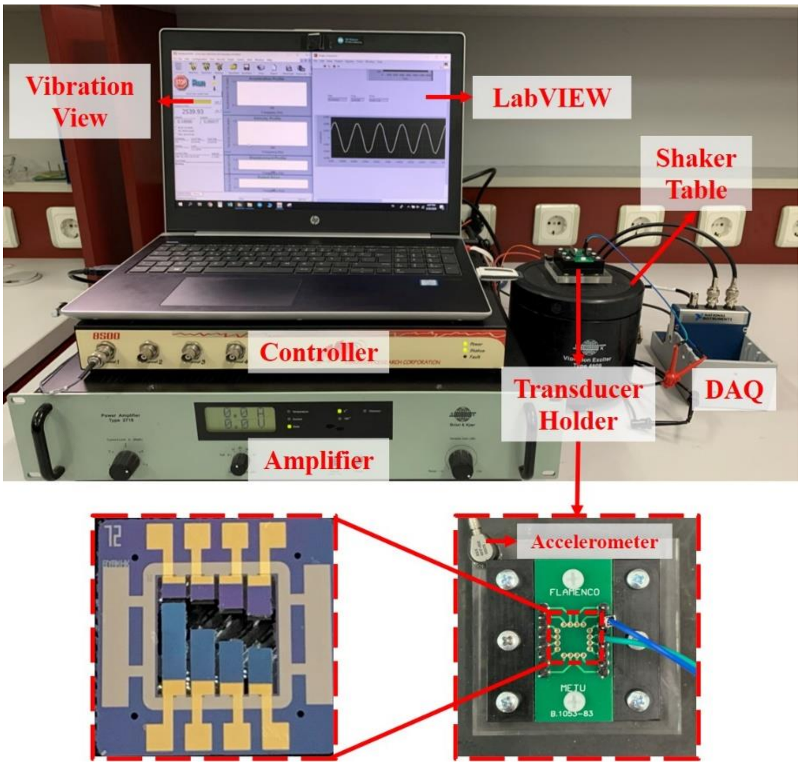

Figure 4.8. Mechanical characterization test setup of transducer.

This test was conducted under 0.1 g constant acceleration in simulation and on shaker tests. The results can be seen in Figure 4.9. This acceleration level corresponds to different sound excitation levels for tympanic membrane and ossicles in terms of sound pressure levels. These levels were available in the literature and they were collected from *in-vivo* tests. Therefore, excitation levels were not changed channel to channel.

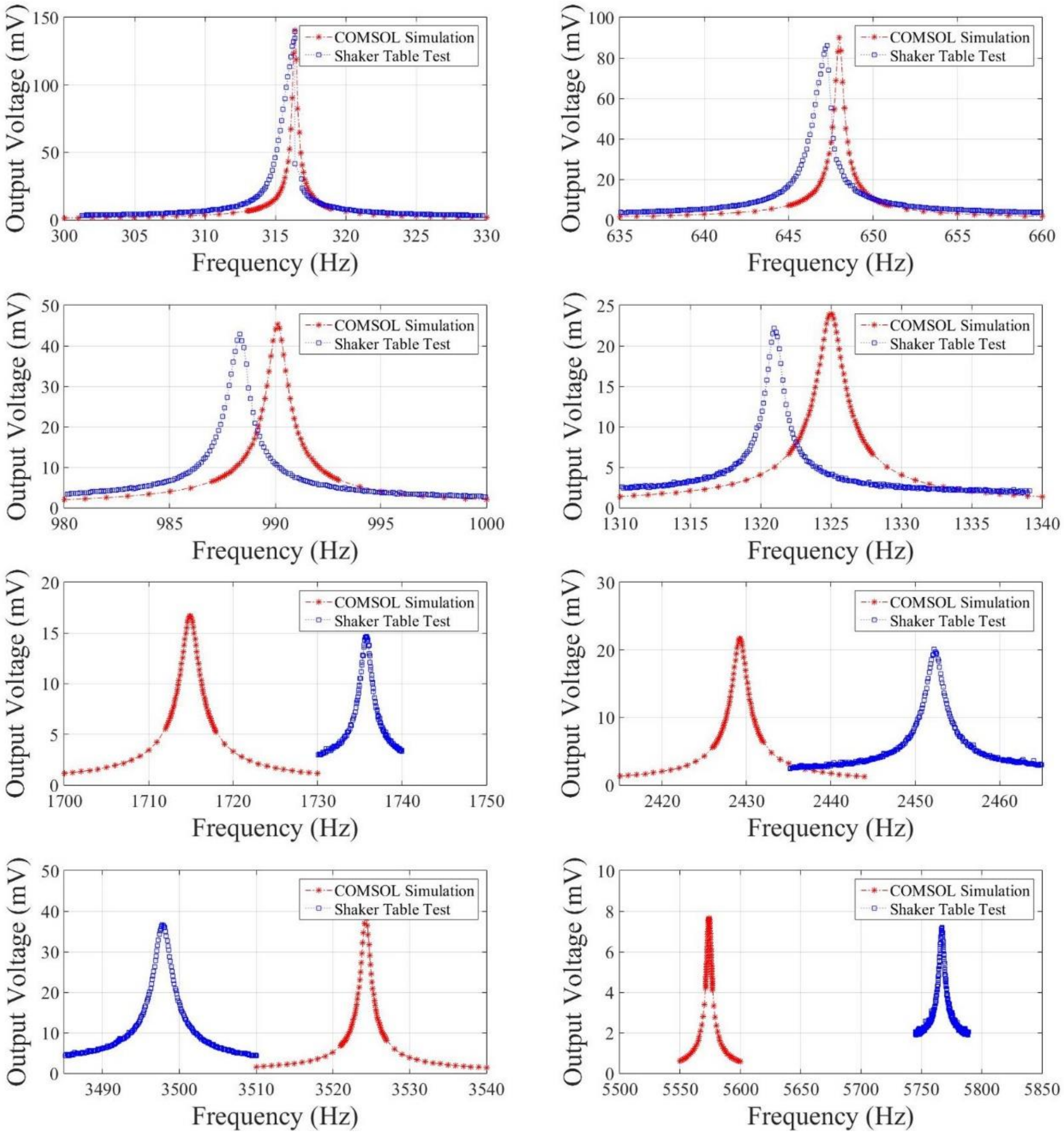

Figure 4.9. Output voltage characteristics of multi-channel acoustic transducer on shaker table test and simulation results under constant excitation 0.1g acceleration.

Test results show that fabricated transducer can generate up to 139.4 mVpp under 0.1 g acceleration at 316 Hz. Other channels` output levels vary between 7.18 mVpp and 86.15 mVpp and resonance frequencies distributed between 647.3 Hz to 5767.2 Hz. Table 4.2 presents the tabulated results of the simulation and mechanical characterization experiments.

Table 4.2. *Simulation and shaker table results of the multi-channel transducer under 0.1 g constant excitation.*

Channel Number	*Simulation*		*Experiment*	
	Frequency (Hz)	*Voltage (mV_{pp})*	*Frequency (Hz)*	*Voltage (mV_{pp})*
1	316.4	141.0	316.4	139.36
2	648.0	90.1	647.3	86.15
3	990.1	45.3	988.3	42.84
4	1325.0	23.9	1321.0	22.15
5	1714.9	16.7	1735.8	14.68
6	2429.2	21.6	2452.3	20.13
7	3534.3	38.8	3497.8	36.58
8	5574.0	7.6	5767.2	7.18

Experimental and simulation results are consistent with each other. Resonance frequencies are in 97 % and output voltages are in 89 % agreement as seen in the results.

Deviations in obtained results increase when number of channels goes up. For larger frequencies, residuals affect the channels more. Therefore, any small defect on the beam or particle disturbs the characteristic of the beam. These defects or particles were created mainly in the last step of the fabrication, tip mass formation. During the DRIE process, the active surface of the wafer (backside) gets heated and cooling gas flows under the Alumina wafer. Thermal conductivity of the alumina wafer and crystal bond is appropriate for this application. However, the photoresist layer between the process wafer and alumina wafer, which protects the device layer of the wafer, gets damage because of high temperature. Then, the crystal bond and photoresist layers interpenetrate each other. This mixture makes cleaning difficult and residuals of this step affect the characteristics of the shorter and lighter channels.

Even with these residuals, agreement on the simulation and test results of the fabricated devices shows that an established simulation module can be used for the next generations of the transducer and other similar applications.

Shaker table test results are the last designed characterization of the transducer. The remaining results are only expectations from combining the results with mechanical and vibration characteristics of the hearing chain.

4.3.4. Acoustical Characterization

Acoustical characterization of the transducer is critical for middle ear applications. Building a simulation model for the middle ear oscillations requires comprehensive study and expertise in programming; knowledge on middle ear dynamics, and vibration. Therefore, it is out of the scope of this thesis and project. FLAMENCO project comprises an artificial tympanic membrane that mimics the vibration characteristics of the hearing chain. Therefore, it is decided to use an artificial tympanic membrane before testing the transducers on the middle ear of cadavers.

Transducers that have demonstrated prospective mechanical and electrical characteristics were separated from their mechanical test frame to reduce the mass and size of the transducer. Then, tested in acoustical test setup which is shown in Figure 4.10. This setup includes Laser Doppler Vibrometer (Polytec NLV-2500 system), earphone (Etymotic Research ER-2), probe microphone (Etymotic Research ER-7C), Data Acquisition Board (DAQ – NI cDAQ-9174), audio amplifier (Denon PMA 520), laptop for programs, acoustic holder, artificial tympanic membrane, and parylene carrier.

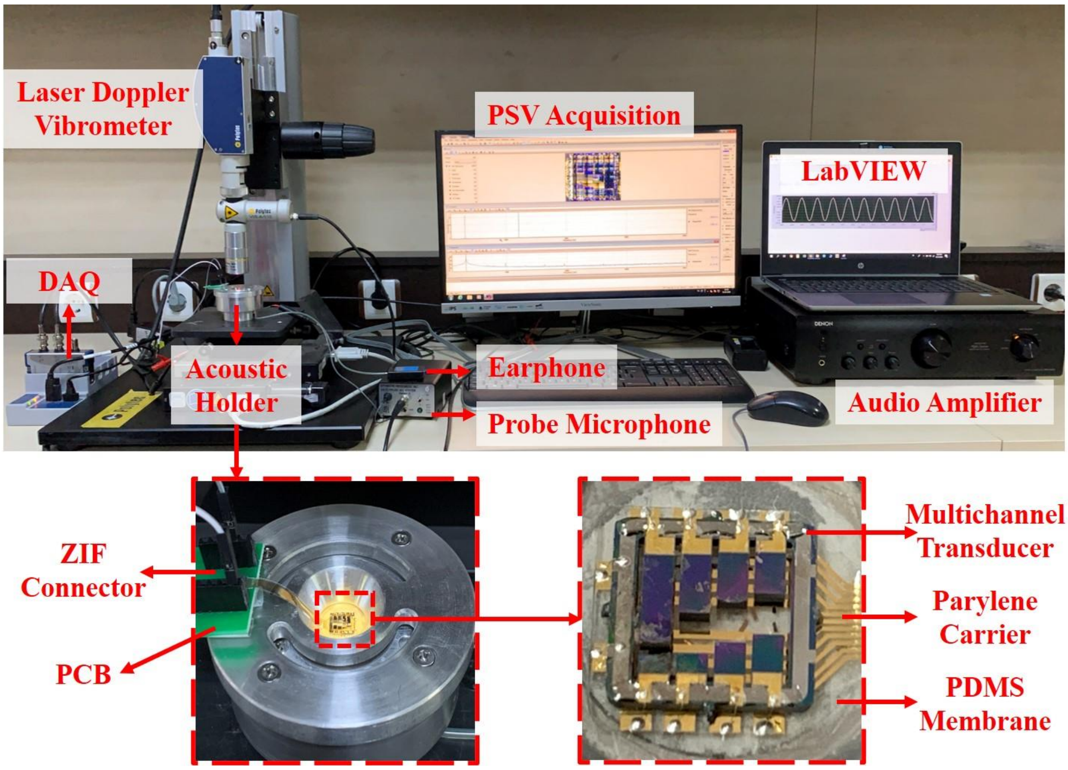

Figure 4.10. Acoustic test setup with Laser Doppler Vibrometer (LDV).

This setup is utilized to obtain responses of each channel of the transducer between 50 dB and 100 dB SPL in the hearing band. Measured qualities are output voltage and displacement of defined points of the transducer. In this setup, the PSV acquisition program generates signals via the LDV system, and this signal is amplified by using an audio amplifier. The amplified signal is turned into a sound signal by earphone and its level is measured by probe microphone. Sound signals excite the PDMS membrane on which transducer, mounted on parylene carrier with epoxy and wire bonds, is placed. Vibrating membrane activates the channels of the transducer which cover the equivalent frequencies. Generated output signals are measured by DAQ and saved using LabVIEW. In the meantime, the LDV meter evaluates the displacement and sensitivity of the specific points on beams. As a result of this test, output characteristics, sensitivities, and frequency bands of the channels under different sound pressure levels were obtained. Figure 4.11 reveals the output voltage characteristics of each channel.

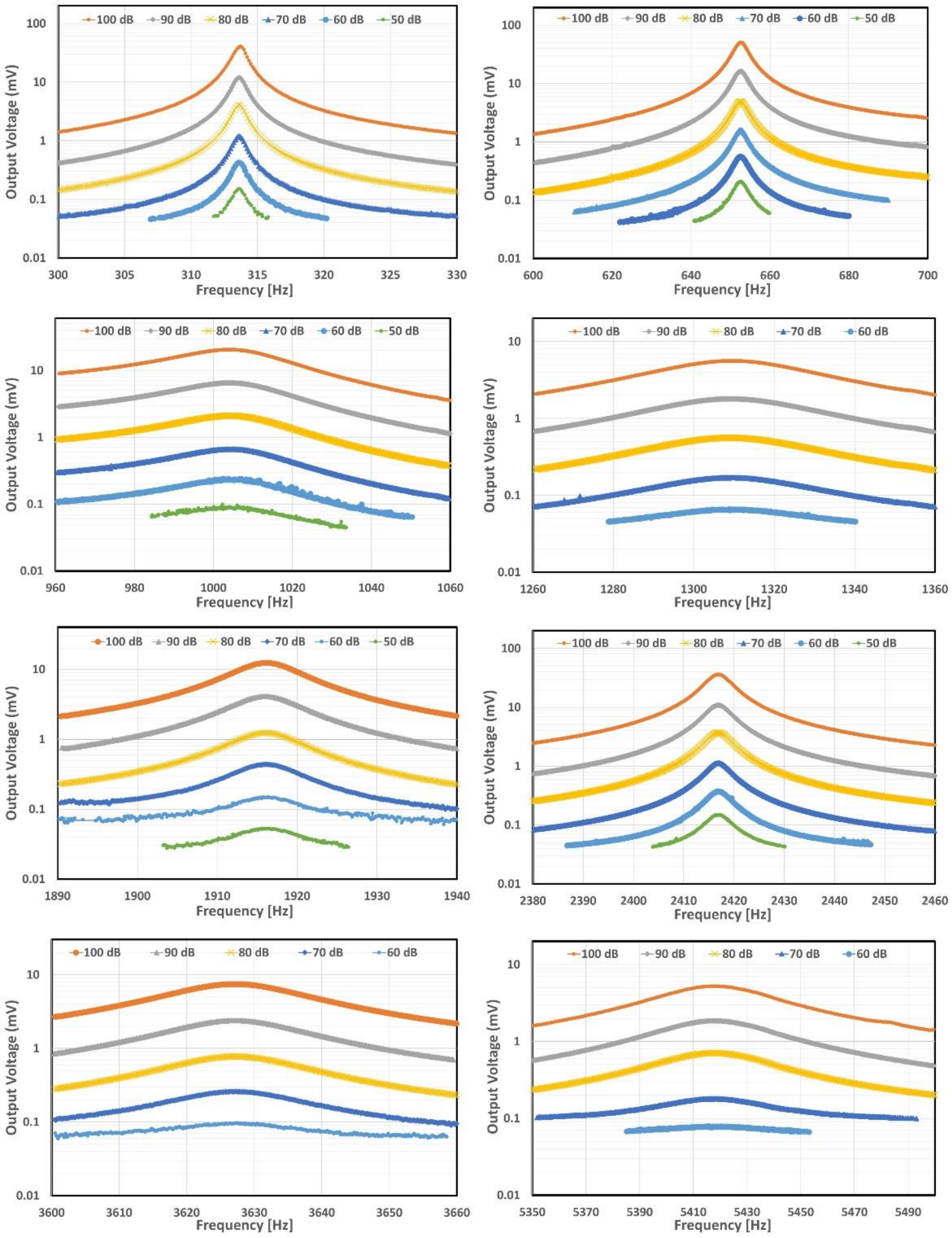

Figure 4.11. Output voltage characteristic of each channel under different sound pressure levels.

Probe microphone and LDV meter provide measuring sensitivity of the channels in terms of voltage and deflection with respect to applied pressure level in the acoustic holder. Table 4.3 shows the detailed output characteristics and sensitivities.

Table 4.3. *Acoustic test result of multi-channel acoustic transducer.*

Channel Number	*Frequency (Hz)*	*Output Voltage (mV_{PP})*						*Sensitivity*	
		100 dB	*90 dB*	*80 dB*	*70 dB*	*60 dB*	*50 dB*	$\frac{mV}{Pa}$	$\frac{\mu m}{Pa}$
1	313.7	40.73	11.95	4.09	1.20	0.43	0.15	20.04	32.05
2	652.6	50.69	16.27	4.92	1.60	0.56	0.21	25.79	13.65
3	1004.0	20.51	6.51	2.10	0.67	0.24	0.09	10.73	14.76
4	1309.5	5.62	1.80	0.56	0.17	0.07	-	2.93	1.44
5	1916.2	12.42	4.12	1.24	0.44	0.15	0.04	6.68	9.46
6	2416.9	36.28	10.84	3.71	1.13	0.38	0.15	18.14	3.51
7	3626.9	7.52	2.39	0.78	0.26	0.09	-	4.01	2.42
8	5417.5	5.24	1.86	0.57	0.18	0.07	-	2.95	1.84

Results show that channels of the transducer can sense the low dB SPL signals, and operate in a wide dynamic range (Note that 100 dB SPL is not the upper limit of the transducer, it is the limit of the test setup). Under 55 dB SPL excitation, all channels output voltage can be measured. However, at 50 dB SPL 4th, 7th and 8th channels` output cannot be measured. There are several reasons for discrepancies on these channels. Firstly, for measuring low amplitude sounds, a low noise amplifier is connected between the DAQ and transducer to eliminate the effect of the noise. This is because noise level of the DAQ is around 251 µVrms at the maximum sample rate. On the other hand, using an amplifier adds line noise to the system which also gets in the way of measurement. 4th channel output levels are lower than the expected. Its resonance frequency is close to the resonance frequency of the artificial tympanic membrane. Therefore, its vibration is coupled with membrane resonance which causes a reduction in the performance. Even with these problems, results indicate that the transducer is capable of filtering the signal into frequency bands in a hearing band while generating encouraging output voltage which are the critical parameters for FICI applications.

4.3.5. Speech Test

Shaker table test and acoustical tests defined the performance of the transducer. But filtering the sound mechanically for FICI application is a new research area and until now, none of the researchers have tested their transducer with the speech signal. However, the transducer could not sense the whole frequency spectrum in the hearing band at low sound levels. There are frequency gaps between the channels. Besides, the minimum input level of the interface circuit (100 µV) limits the frequency range, too. Results attained from the acoustical test at 70 dB SPL are shown in Figure 4.12.

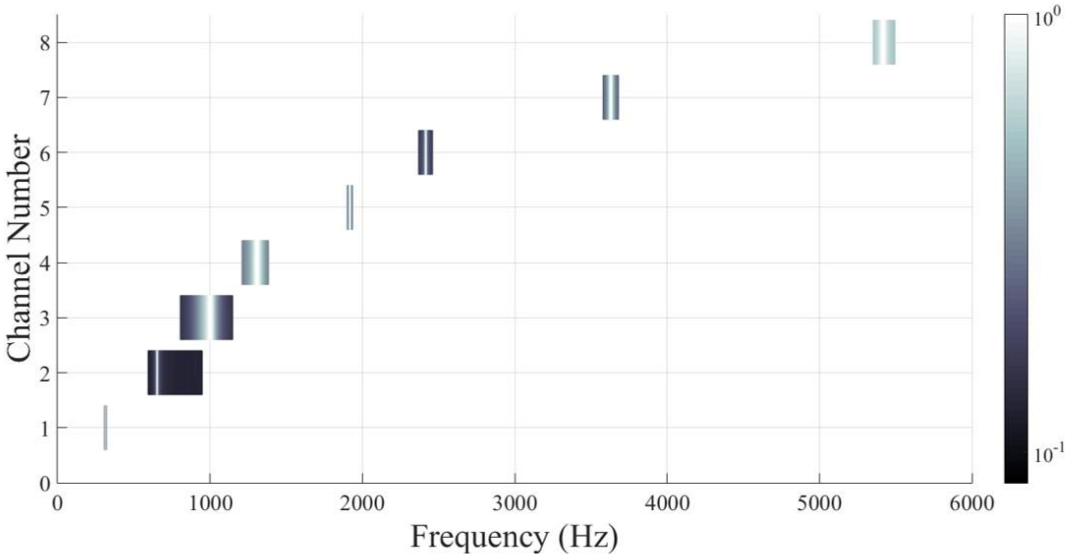

Figure 4.12. Covered frequency range by each channel, gray scale shows normalized output voltage.

These gaps are a problem for sensing pure single frequency signals, but speech and daily sounds consist of a range of frequencies. Therefore, to see the realistic performance of the transducer, a test sentence originally practiced to assess hearing quality of the cochlear implant patients, was used as input excitation. This setup can be seen in Figure 4.13.

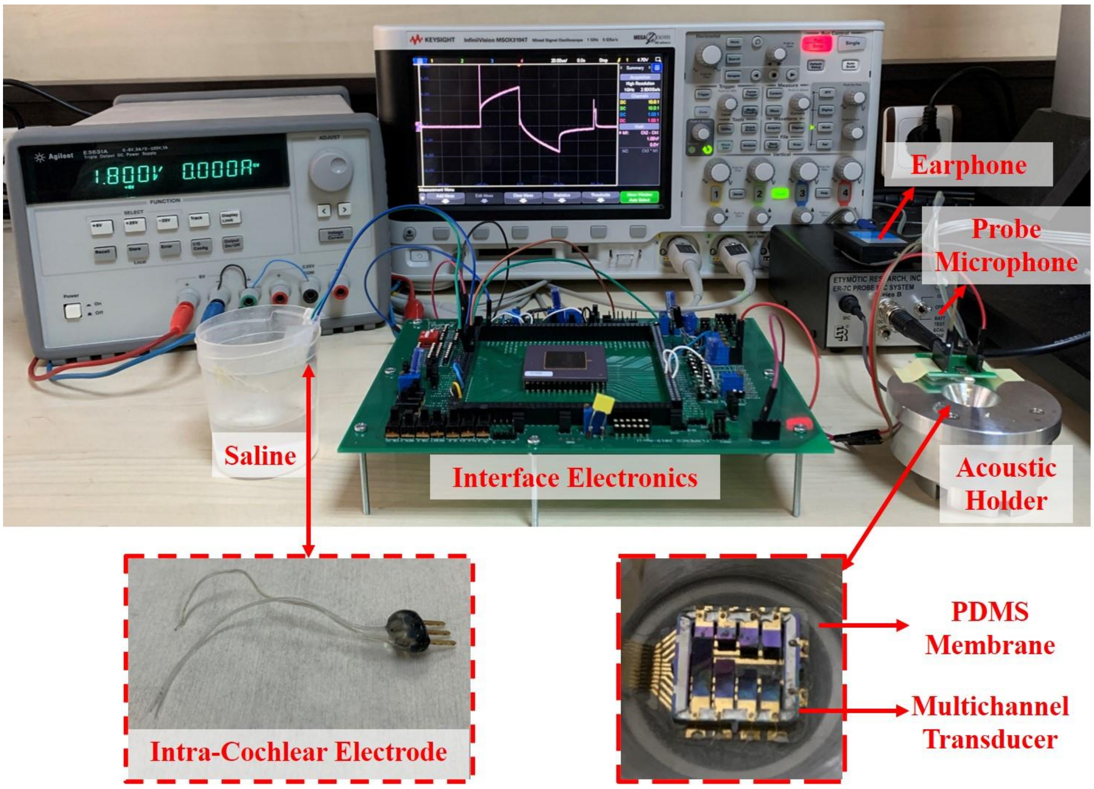

Figure 4.13. Speech test setup of acoustic transducer.

In this test, a generic sentence, “A white silk jacket goes with any shoes” was vocalized by Matlab. This sentence is used to test the hearing qualities of cochlear implant users [64]. In addition, control signals were added to the beginning of the sentence to eliminate phase differences while summing the signals. Control signals were pure sinusoidal signals whose frequencies were arranged for each channel in their band. This utilized speech record was played with 5 W speaker and its level was measured with a digital sound level meter (IEC 651 TYPE II). The sound level was arranged to give around 70 dB(A) SPL that is the average level of the home with TV or small office [65]. These sound signals excited the transducer on the artificial tympanic membrane. Output signals of each channel were amplified using LNA. DAQ measured and LabView recorded the output signals. Recorded signals were synchronized with the help of control signals and summed by using Matlab. Output responses can be seen in Figure 4.14.

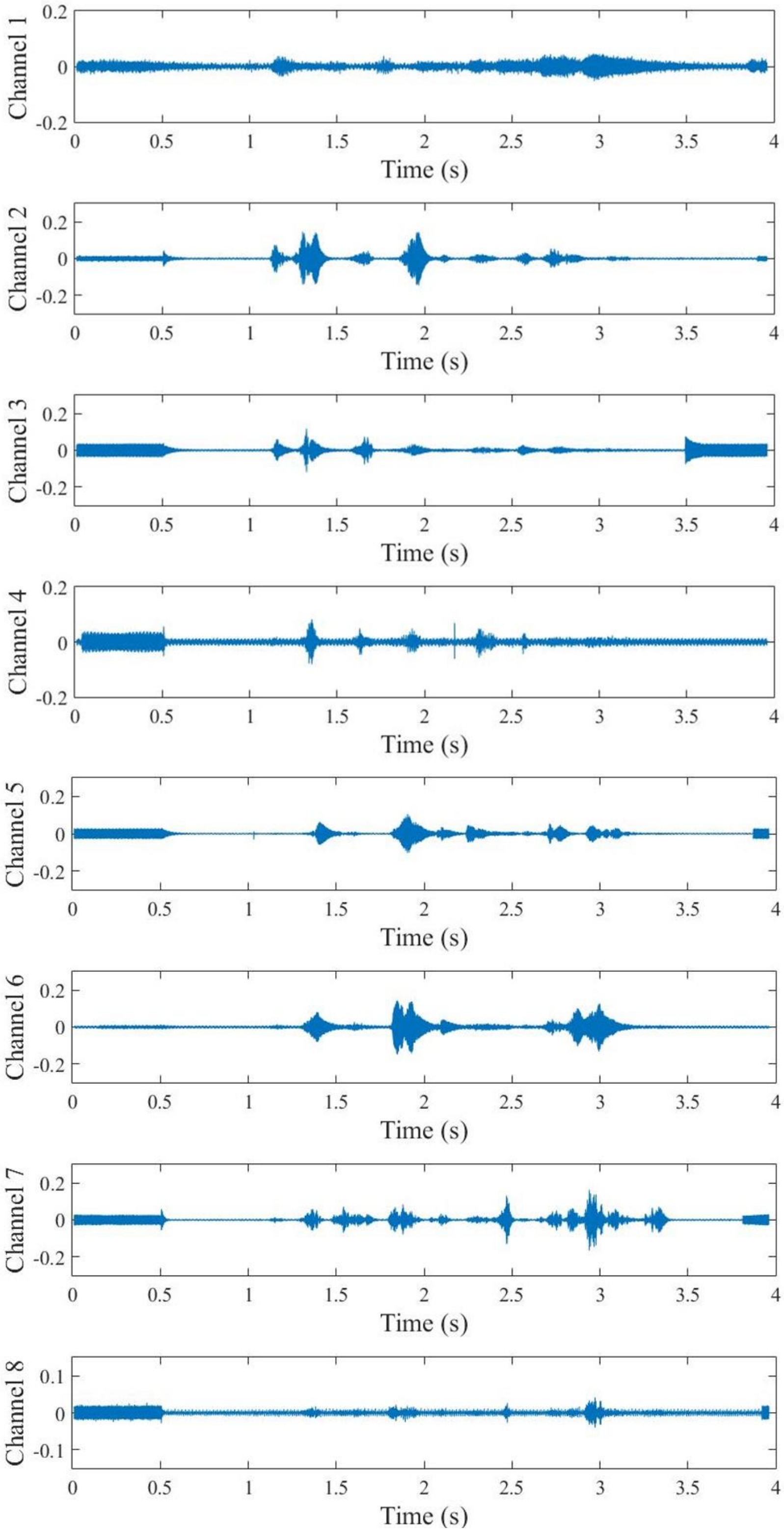

Figure 4.14. Recorded output responses of channels at 70 dB(A) SPL.

The output of the transducer includes the signals whose voltage levels are lower than 100 µV. Because of that, the system level covered frequency range at 70 dB SPL was modeled as Butterworth bandpass filters in Matlab, and speech signal was filtered to compare output results. Spectrograms of summed transducer output, Matlab filtered sound, and the original speech signal can be seen in Figure 4.15.

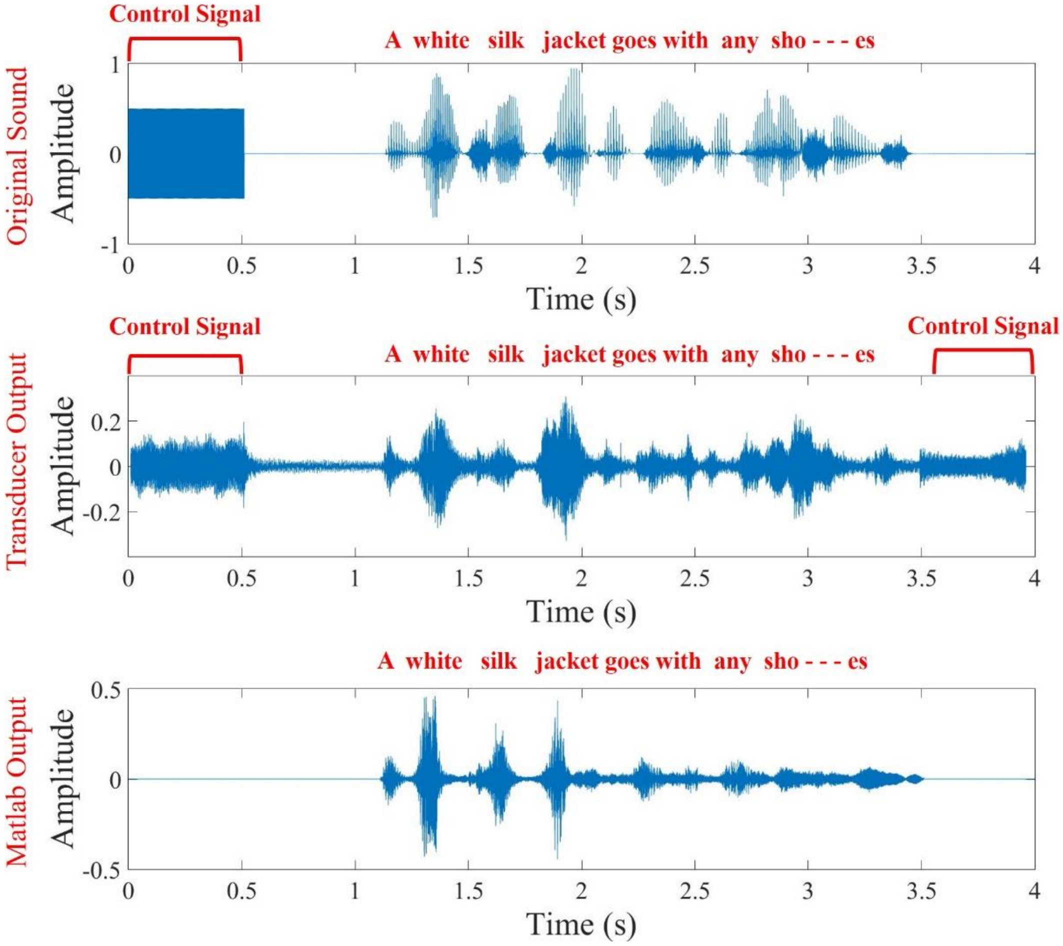

Figure 4.15. Spectrograms of speech signal, transducer output and filtered signal in Matlab.

Recovered sound signals were well-recognizable. As seen in the spectrograms, recovered speech sound also shows close characteristics to original sound and signal filtered by software filters. Discrepancies between the spectrograms are observed because software-generated input sound consists of clear sound which means the tone of the sound is constant. There are no sound shift and noise in the speech.

On the other hand, degrees of software filters were selected high to discriminate the output levels as above and below 100 µV, sharply. These high degree filters cause ringing in the sound which is not the case for Continuous Interleaved Sampling (CIS) stimulation method in cochlear implants. Briefly, the output of the channels stimulates the neurons one after another, not simultaneously. Therefore, there exists a seven times long duration required for the relaxation of each channel between stimulations cycles. This ringing effect causes noisy oscillation in software filtered signal.

The measured minimum output level of the transducer was around 40 µV in the test setup depicted in Figure 4.10. Therefore, channels cover wider frequency ranges without interface circuit. This wider range increase the sound perception, but the difference between output levels causes noisy oscillation on the spectrogram.

Results of the speech test proved the capabilities of the multi-channel acoustic transducer for cochlear implant applications. Test signal could be recovered by the transducer at daily domestic sound levels (70 dB SPL). Results are also endorsed using Matlab to prove the performance. Characterization of the stand-alone transducer was completed with this test. Results are discussed and compared with other transducers in the discussion section of the chapter.

4.4. Stimulation System Characterization of Fully Implantable Cochlear Implant

In Fully Implantable Cochlear Implant concept, outputs of the transducer are processed and turned to biphasic pulses to stimulate the neurons in the cochlea with interface electronics that operate in the CIS method. In the FLAMENCO project, several versions of interface circuits designed and tested by Hasan Uluşan and H. Andaç Yiğit [27]–[30]. Their main aims are to cover 60 dB dynamic range, sense 100 µV input signals and consume low power. Hasan Ulusan used an amplitude-modulated output system to stimulate the neurons with biphasic pulses and obtained a 60 dB dynamic range while consuming only 472 µW power [28]. H. Andaç Yiğit designed his interface circuit with pulse width modulation technique and covered 45 dB dynamic range while consuming 513 µW power for 8 channel stimulation [30]. The last versions of these interface circuits were combined with the multi-channel transducer for *in-vivo* and *in-vitro* tests.

4.4.1. In-Vitro Test

As the first step of system level tests, the multi-channel acoustic transducer, and pulse width modulated stimulation circuits were combined. In order to see the realistic performance of the system instead of connecting an ideal load to output, *in-vitro* test setup was constructed as seen in Figure 4.16.

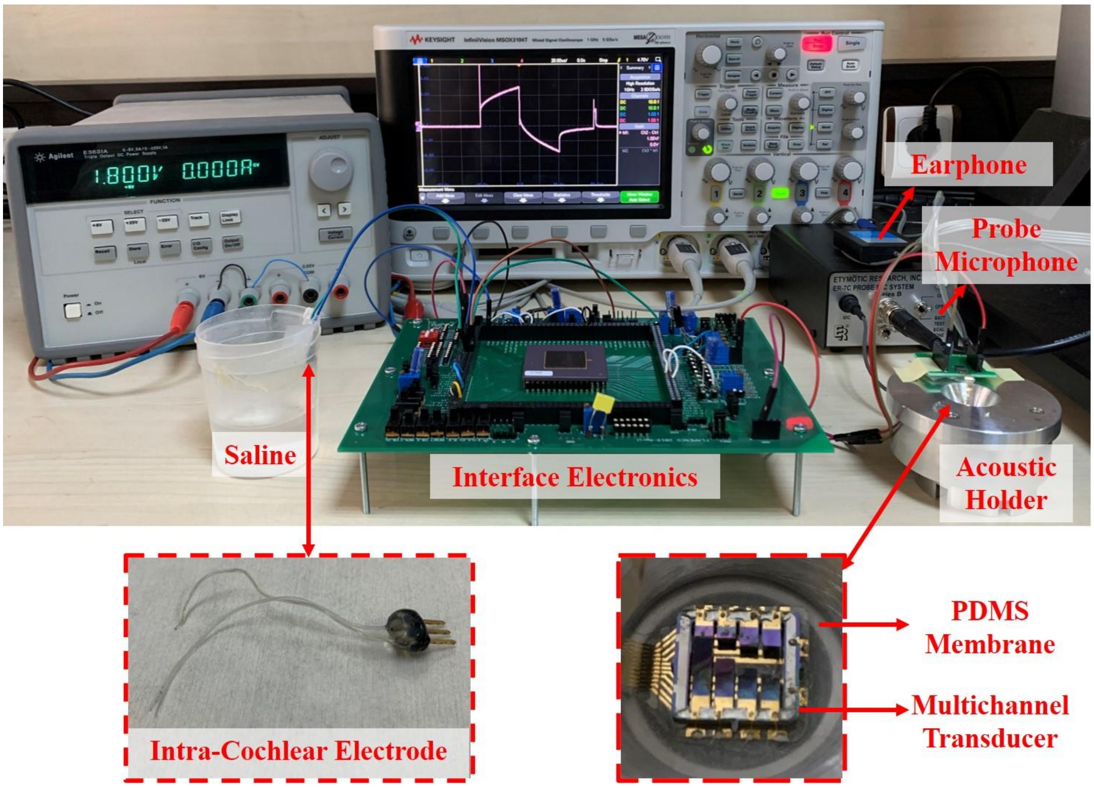

Figure 4.16. In-vitro test setup for stimulation system of FICI concept.

In this test, earphone (Etymotic Research ER-2), probe microphone (Etymotic Research ER-7C), and acoustic holder with PDMS membrane were used in order to excite transducer. Output of the transducer was connected to the interface circuit via parylene carrier and ZIF connector. Interface circuit works stand-alone and it uses only one supply, without any external chips or circuits. Finally, the produced stimulation signal was applied to a single channel animal electrode produced by MED-EL company which was placed in a saline solution as an artificial neural load (2.3 kΩ and 66 nF).

Single tone sinusoidal signal at 650 Hz was applied to the artificial tympanic membrane and the second channel of the transducer was connected to the interface circuit. Generated voltage differences between the electrodes and pulse widths of the generated current pulses under different sound level excitation are shown in Figure 4.17.

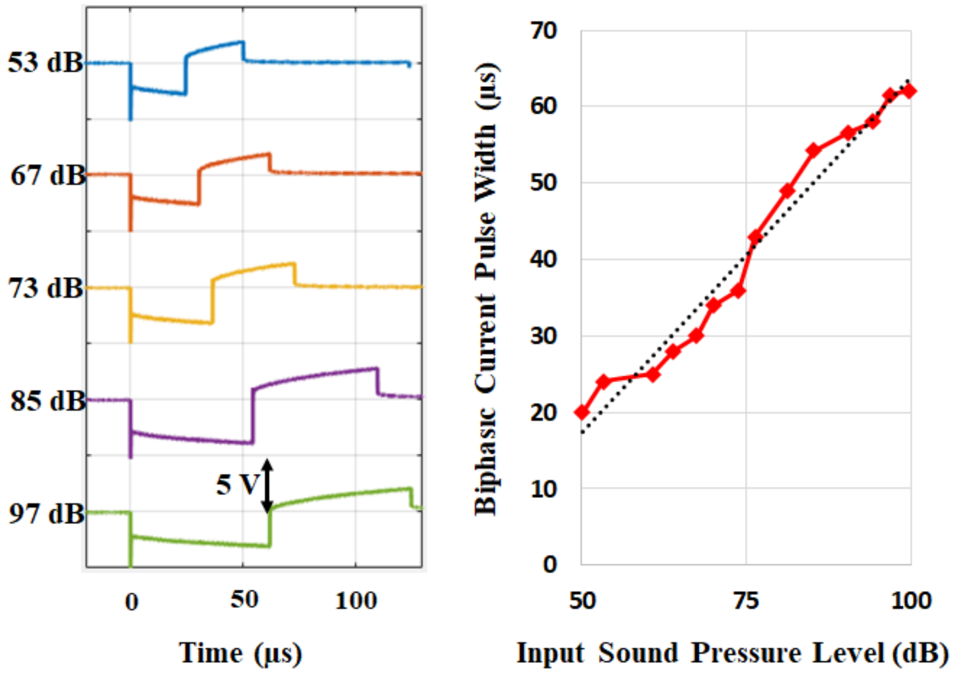

Figure 4.17. Voltage differences between the electrode when stimulation signal is applied to artificial neural load and pulse width change with respect to applied sound level.

Generated signals show that the system can work in a 50 dB dynamic range between 50 and 100 dB SPL. The system arranges the pulse widths according to incoming sound levels while consuming only 695 µW. These results demonstrate that the proposed system can achieve FICI requirements while applying produced signal to artificial neural load.

4.4.2. In-Vivo Test

In order to prove the functionality of the stimulation part of the FLAMENCO concept on a living guinea pig, multi-channel acoustic transducer and 2nd generation FICI Interface circuit designed by Hasan Uluşan [28] were interconnected in test setup shown in Figure 4.18. This setup was utilized to observe auditory brainstem response of the deafened guinea pig.

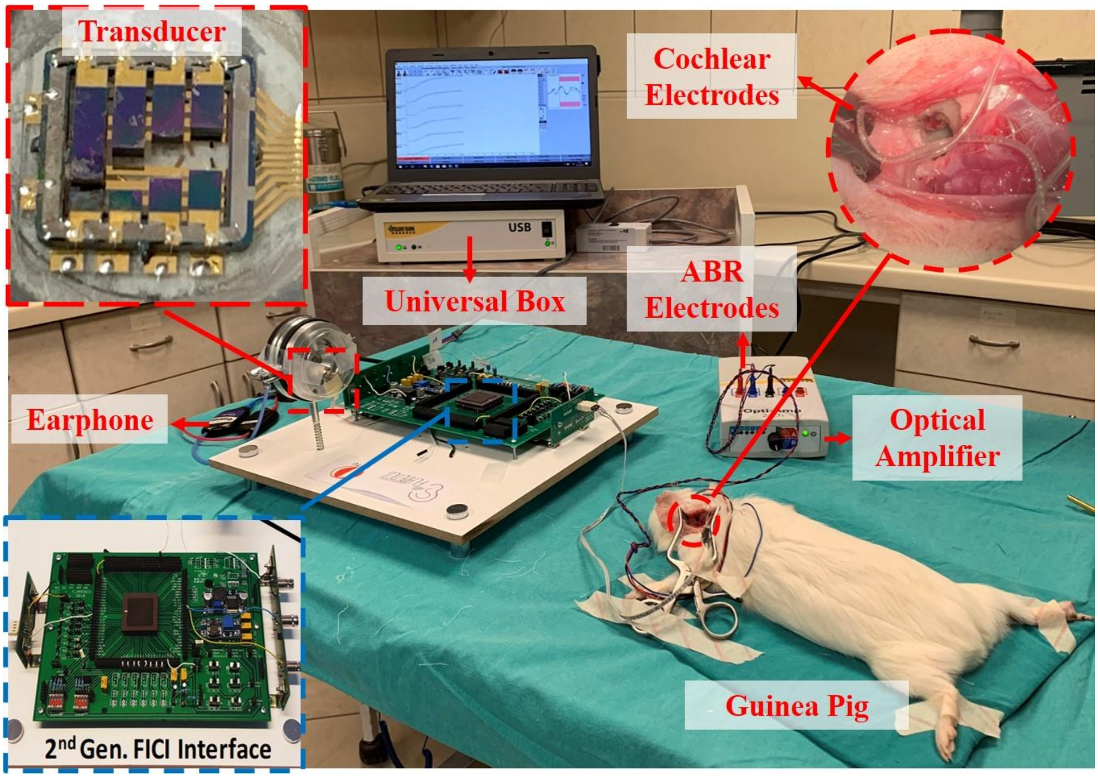

Figure 4.18. In-vivo test setup of stimulation part of the FICI concept.

The transducer is provoked by the sound signal via earphone and universal box. The output of the transducer is processed by 2nd generation interface circuit and turned into amplitude modulated biphasic pulses. Then, the cochlea of the guinea pig is stimulated by generated pulses via a single channel MED-EL cochlear electrode. Finally, the ABR system of Intelligent Hearing Systems measures the ABR response of the deafened animal.

In this test setup, 2nd channel of the transducer was excited, and stimulation circuit generated biphasic pulses. These pulses were used to excite the nerves in the cochlea via single channel MED-EL electrode. The system was initially operated with 115 dB SPL. Then, excitation level was gradually decreased to obtain the hearing threshold of the animal. Finally, the system could operate under 65 dB SPL, and system could work in 50 dB dynamic range. These measured ABR responses are shown in Figure 4.19.

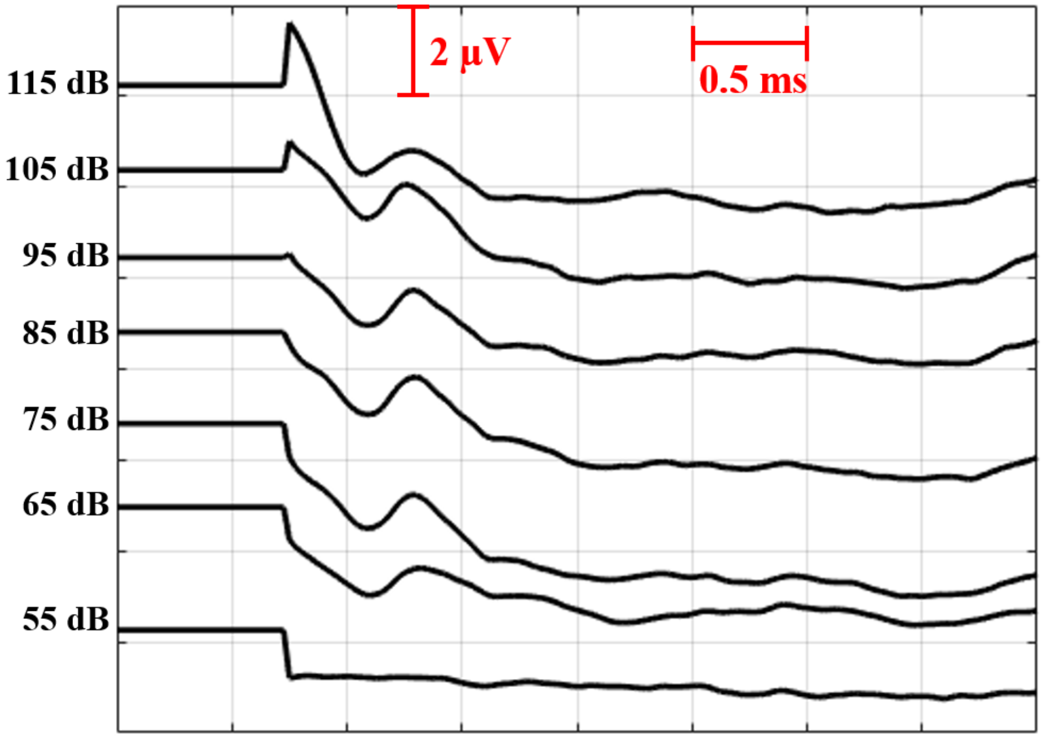

Figure 4.19. ABR responses of the deafened guinea pig while simulating by the multi-channel transducer and 2nd generation interface circuit.

4.5. Summary

MEMS-based multi-channel acoustic transducer examined under different excitations and it was characterized in various aspects. These aspects include testing electrical model parameter of the transducer, obtaining mechanical characteristic and comparing with simulation results, acoustical characterization on the artificial tympanic membrane, speech test to see the performance to daily sounds, and system level tests with interface circuits. In this section, test results are compared with different acoustic transducers existing in the literature.

After the functionality test of channels with the short capacitance test, first characterization method was the electrical characterization with the LCR meter. This device measured equivalent circuit parameters of the piezoelectric model as parallel resistance and parallel capacitance. Test results showed the quality of the surface micromachining because these equivalent circuit parameters depend on used piezoelectric material and its dimensions. During measurements, the LCR meter excites the transducer, so the transducer works as an actuator and gives the resonance frequencies of channels. Bulk micromachining quality was obtained by comparing resonance frequencies with expected results. There were small differences between the expected and obtained resonance frequencies. There are several reasons for these discrepancies. Firstly, a 15 µm error margin was defined between layers during mask drawing. This margin alters the resonance frequencies. Residuals on the cantilevers are another reason of discrepancy. Especially, cantilevers with short beam length and small tip masses were affected more from these residuals and layout margins. All functional channels pass this test with small deviations because of explained reasons.

Resonance frequencies of the channels were obtained by operating them in actuator mode by LCR meter. Then, the transducer was excited with a constant acceleration and excitation frequency was swept around resonance frequency on the shaker table. This was a critical test for the design because in simulations, the same excitation type was applied to the transducer. Therefore, this test results showed attribution of the used model and built module in COMSOL Multiphysics. Resonance frequencies of the channels were distributed in the audible range (250 – 5500Hz) and could generate up to 139.4 mV_{pp} under 0.1 g acceleration at 316 Hz during shaker table test. Other channels` output levels vary between 7.18 mV_{pp} and 86.15 mV_{pp} and resonance frequencies are distributed between 647.3 Hz to 5767.2 Hz. These test results are in good agreement with post-simulation results on resonance frequencies (97 %) and output voltages (89 %), as seen in Table 4.2. This output voltage range was expected while designing the channel characteristics. Vibration characteristic of the hearing mechanism changes with applied frequency under the same pressure level as shown in *in-vivo* test [18]. There was a small deviation between post-simulation results and simulation results while designing the channels. These differences occurred because of the error margin of mask layout. Up to 15 µm error could change the resonance frequency and output voltage of the transducer. Change in the damping of the structure due to the errors and stress distribution also caused a small deviation from design.

Acoustic characteristics of the multi-channel transducer were figured out from *in-vivo* test results of umbo displacement in the literature. Acceleration levels were extrapolated from pressure levels which correspond to different levels with respect to applied frequency. Parameters of the structure were defined using this *in-vitro* test results as a base for acoustical characteristics. Meanwhile, in the concept of the FLAMENCO project, the artificial tympanic membrane was designed and fabricated by Parinaz Ashrafi [61]. This structure mimics the tympanic membrane and shows similar vibration characteristics as shown in Figure 4.3. Therefore, to establish a test environment similar to the middle ear, the transducer was placed on this membrane with proper connections via parylene carrier, and sound was transmitted via acoustical holder whose dimensions are analogous to the ear canal. In this utilized test environment, the transducer could generate 50.7 mV under 100 dB SPL excitation. These test results proved the capabilities of the transducer for the FICI application. However, discrepancies arose due to membrane characteristics at specific frequency ranges. Near the first resonance frequency of the membrane, the 4th channel was coupled with its vibration and generated a lower output voltage than expected. At some frequency levels, output voltage could not be measured due to line noise in the test environment at low pressures.

In the literature, different methods and materials were used for implantable acoustic sensors. Relevant studies are compared in Table 4.4. They were characterized by different methods and cover different frequency ranges. These parameters are shown in the table.

Table 4.4 *Acoustical transducer in literature for fully implantable cochlear implant applications.*

Study	*Channel Number*	*Frequency Range*	*Excitation*	*Output Level(mV)*	*Dimension (mm^3)*
[23]	1	1325 Hz	100 dB	~40	5×5×0.5
[34]	16	300-700 Hz	1 g	9.6	32×32×0.55
[38]	10	10-37 kHz	112.4 dB	3.55	~6.5×6.5×0.35
[39]	8	2.9-12.6 kHz	101.7 dB	4.06	2.5×2.5×0.6
This Study	8	250-5500 Hz	0.1 g 100 dB	139.4 50.7	5×5×0.6

As seen from the comparison table, the transducer presented in this study provides the most suitable option for the cochlear implant applications. The highest output voltage is generated even though higher excitation levels are applied to others. In [39], the occupied volume is lower than this study but, the presented study does not cover the lower part of the hearing band and generates much smaller output voltage (~20 dB difference). In order to reach the lower frequencies, the lengths of the cantilever beams are needed to be increased. The main reason for occupying a 5 × 5 mm2 area is the first channel (300 Hz) in this study. Therefore, in terms of dimensions and frequency range, this study leads the literature.

None of the transducers that were implemented for the FICI applications have been tested with the daily sounds to the best of my knowledge. For the first time, the presented transducer was excited with the test sentence which is used to measure the hearing quality of the cochlear implant users at daily sound levels. The recovered signal was well-recognizable and spectrograms of the signals show a similar pattern in the time domain. Furthermore, these results were supported by filtering recorded sound in Matlab and applying the measured frequency ranges of channels. Its spectrogram also gave a similar pattern with the original sound and the recovered output.

In the FLAMENCO concept, the transducer was connected to the stimulation interface circuits after completing the stand-alone characterizations. This system was tested in *in-vivo* and *in-vitro* environments. *In-vitro* test results showed that the transducer and the pulse width modulated interface circuit designed by H. Andaç Yiğit can work in a 50 dB dynamic range between 50 and 100 dB while consuming only 695 µW power without any external device or circuits.

CHAPTER 5

WIDE-BAND BEAM STRUCTURE

5.1. Introduction

In previous chapters, the multi-channel acoustic transducer was presented with its detailed design, fabrication, and test methods. In characterizations, the feasibility of the transducer was proved. Acoustical and speech test results showed that this structure can be used as a middle ear implantable transducer. It can recover test sentence, which used for the hearing test of cochlear implant users, at daily sound level 70 dB SPL.

However, further modifications are needed to improve filtered sound quality since there are gaps between the frequency bands of channels, especially at low sound levels. They cause a problem for detecting single tone sound signals such as a whistle. Therefore, bandwidths of the channels must be expanded to cover the whole audible frequency range. This problem can be solved with different aspects:

- Decreasing the minimum input level of the stimulation circuit improves the covered bands because the transducer can generate 40 μV output voltage while the minimum input level requirement of the circuit is 100 μV. There is ~8 dB difference between the signal levels which reduces the covered band due to filter characteristic. On the other hand, the bottleneck on this approach is power consumption of the stimulation circuit. Reducing the input level of the circuit or using a low noise amplifier as the input level will increase power consumption.
- Vibration level of the eardrum can be increased with surgical operations. Zurcher et al. removed incus from the hearing chain [20] and reported the difference which is shown in Figure 2.12. Extrapolated data from the graph

shows ~15 dB improvement in this method. However, long term effects are not known. It presents only test results just after the incus removal.

- The output voltage of the same structure can be improved. This can be feasible with two methods. The first one is boosting the stress on the piezoelectric layer by increasing the mass at the tip of the cantilever beam while the latter method makes use of a vacuum package to eliminate air drag damping. However, increasing stress levels make the structure more fragile. So, limits must be defined properly. The structure must be durable for external impacts.
- The structure can be modified to cover wider bands with the same limitations. Different methods have been used in order to widen the bands of the mechanical structures.

These methods may be used for covering all the acoustic band with eliminating their drawbacks or finding a solution for them. In this chapter, a possible solution for this problem is proposed with a structure.

In the next section, used methods to widen band in the literature are presented. Then, the proposed structure is explained with simulation results, and a road map to reach the final structure is given.

5.2. Bandwidth Extension Methods

Bandwidth issue has not been studied on implantable sensors, yet. Therefore, wide-band harvesters are also included, in this part. In the literature, there are different methods to widen the band of the sensors and vibration energy harvesters. These methods mainly use two approaches. The first method is introducing a nonlinearity on the structure by using a magnet or nonlinear structure. The second method is adding new modes which are close to the first mode to get a wider band.

Tang et al. [66] reported a nonlinear method with a magnet to improve the bandwidth of the structure. Using a magnet is not suitable due to MRI incompatibility. However, the logic behind the structure can be used for different approaches. In this structure, the first stage pickups vibration and excites second stage with electromagnetic effect.

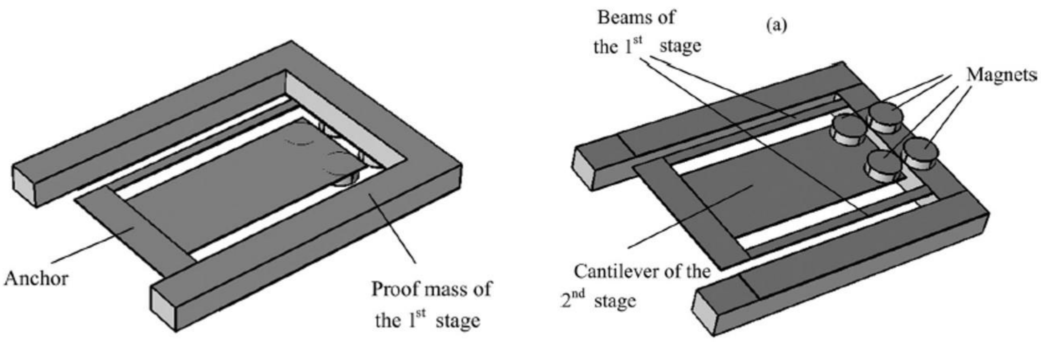

Figure 5.1. Nonlinear two stage structure [66].

Hajati et al. [67], [68] proposed two structures. Figure 5.2 shows the structures. At first, MEMS-scale pie-shaped structure was introduced to broaden the frequency range. The second one is the doubly clamped beam. Both structures are based upon the same logic. Symmetries in both structures prevent rotational and lateral motion of the proof mass other than their vertical motion. Therefore, the stretching force causes an inevitable increase in the beam length. This results in additional nonlinear stiffness that acts like negative feedback which proves wide band. However, to obtain broadband with these structures, heavy proof masses are required. For example, the PZT layer of the structure (b) covers 4×4 mm2 for a single beam where proof mass is 180 mg. The footprint of the doubly clamped system is also not feasible for multi-channel applications. Therefore, this approach is not feasible for middle ear implantable acoustic transducer.

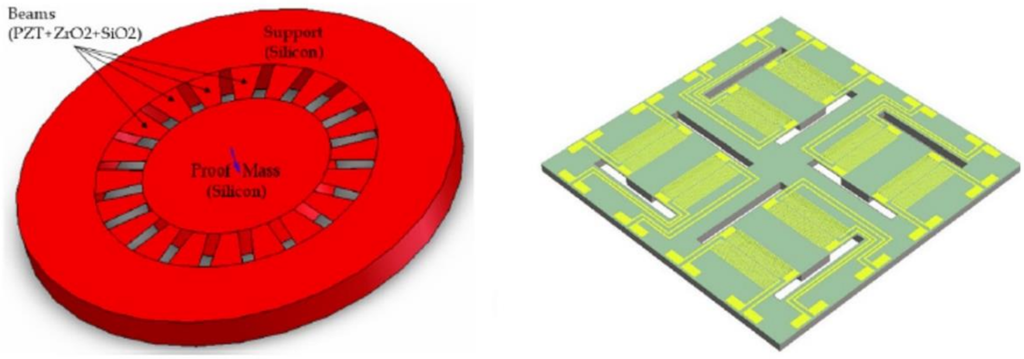

(a) **(b)**

Figure 5.2. Nonlinear geometric structures a) [67] *and b)* [68].

Wang et al. [69] presented a back to back cantilever array structure to obtain wideband. Figure 5.3 shows the structure. In this structure, six cantilevers have the same parameters excluding holes on the masses. These holes change resonance frequencies of channels. By this way, bandwidth of the structure increases with the number of used cantilevers. In this study, they also vacuum packaged this structure with three wafer bonding process. However, this approach is not practical due to the mass and area limitation of the middle ear implantable transducer. Resonance filter characteristics of the structure still have high-quality factor and independent characteristics.

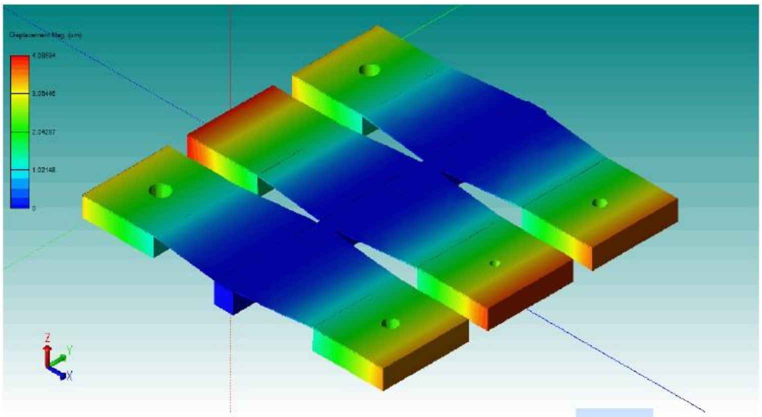

Figure 5.3. Wideband back-to-back cantilever structure [70].

Zhang et al. [70] designed a multimodal MEMS structure by using meandering beams. Figure 5.4 shows the illustration of the structure. The meandering structure decreases the resonance frequency. Adding mass at specific points also introduces new modes to the structure. Nevertheless, resonances of the modes are too far from each other.

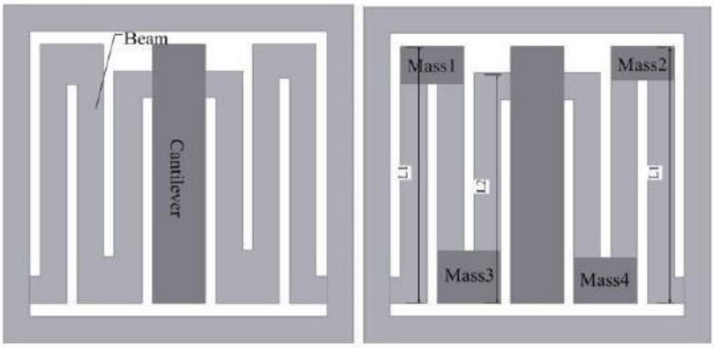

Figure 5.4. Top and bottom view of multimodal meandering beam structure [70].

5.3. Parylene Bridge Structure

Main methods to obtain wideband to sense the vibrations were shown in the previous section. These methods are not suitable for middle ear implantable acoustic devices. Nonlinear structures have a mass and area problem. Resonance frequencies of multimodal structures are far from each other or their quality factors are still high while they are connected electrically.

In order to broaden the covered bands by each filter, thin silicon beams have connected each other with elastic (parylene) bridges as shown in Figure 5.5. The aim of this structure is to use different modes of the structure. They have connected each other with parylene to vibrate in harmony while interacting with each other. Tip masses of the beams have small differences compared to each other; therefore, their resonance modes are placed closer. They are also connected electrically in series with alternating polarities to get rid of phase differences between the channels.

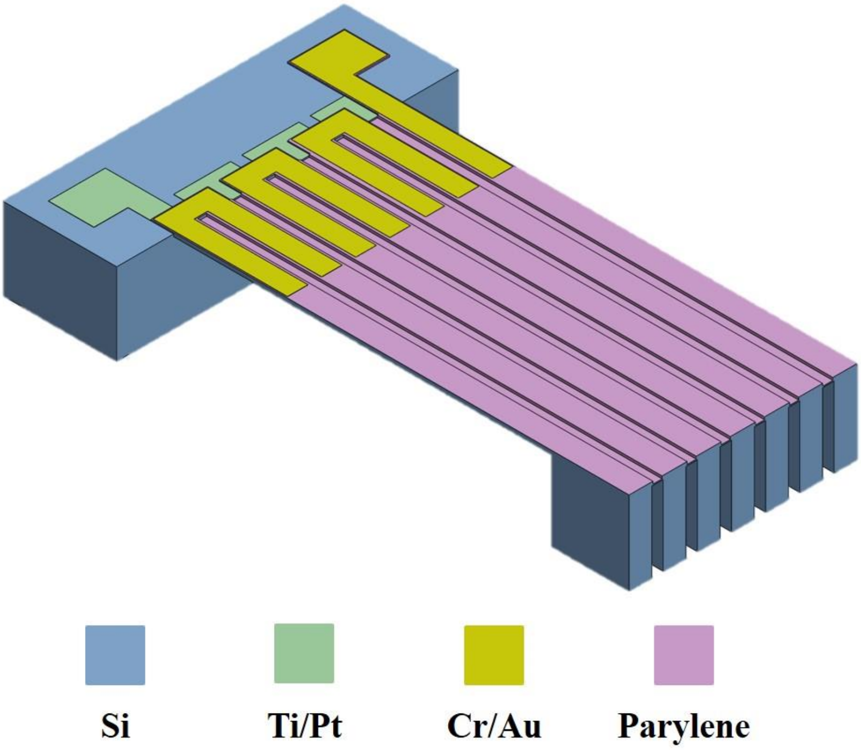

Figure 5.5. Proposed structure to widen covered band namely, parylene bridge.

5.3.1. Finite Element Analysis

Parylene bridge structure was implemented with its initial version to COMSOL Multiphysics to obtain output characteristics. In this version, three cantilever beams connected to each other with parylene bridges as seen in Figure 5.6. Increasing beam number prolongs required computational time and design process. Therefore, to see the feasibility of the structure, this version was created.

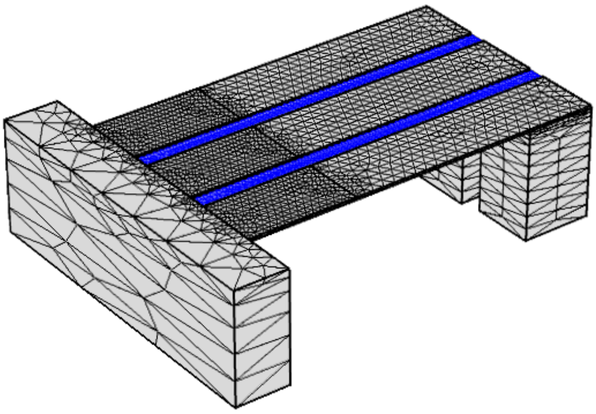

Figure 5.6. Parylene bridge structure with three cantilever beams, blue parts indicate parylene.

The total mass and dimensions of this structure and standard cantilever beam are the same except for the width of the parylene bridges. Therefore, they can be compared without defining any figure of merit. Figure 5.7 shows output characteristics.

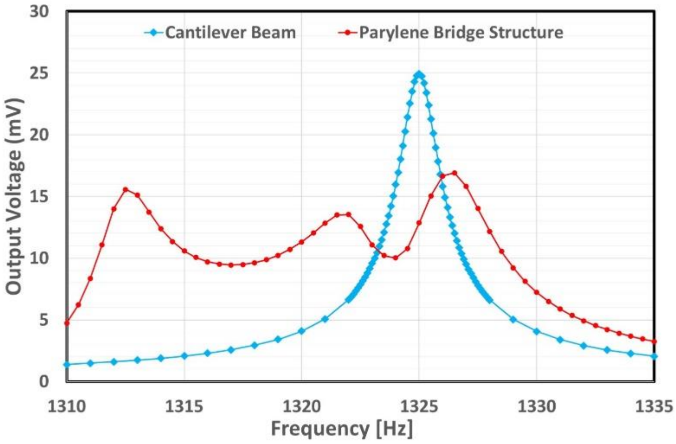

Figure 5.7. Comparison of output characteristics of parylene bridge structure and cantilever beam with same total mass and dimensions.

The graph shows the band of the structure was increased while losing output voltage slightly. This reduction can be prevented by applying a vacuum package or increasing stress on the piezoelectric layer by increasing mass. Therefore, the approach can be employed in implantable transducers after proving the feasibility of the structure with a fabricated device. There are some critical points in the model i.e. damping constants of the defined materials which could affect the characteristic after fabrication.

5.3.2. Fabrication Methodology

This structure can be fabricated in a MEMS fabrication process similar to the multi-channel acoustic transducer. The same fabrication methods can be applied on SOI wafer in a different order. Figure 5.8 shows the planned fabrication flow for the parylene bridge structure. Different than the multi-channel transducer, beam formation is applied before parylene deposition and buried oxide layer is removed with a wet etch process to protect parylene bridges.

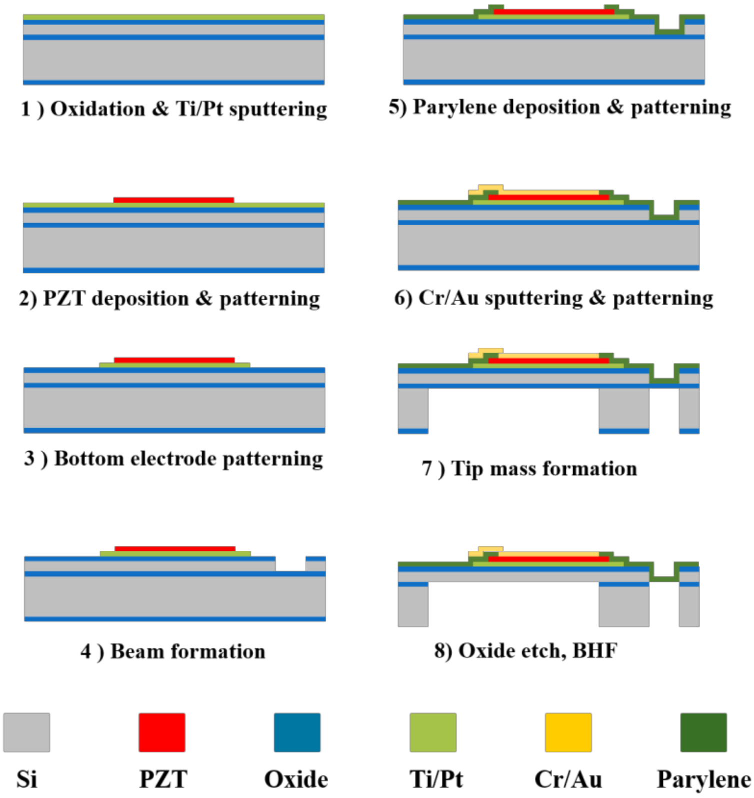

Figure 5.8. Planned fabrication flow of the parylene bridge structure.

5.4. Summary

Sound detecting quality of the multi-channel transducer can be increased with several methods: Reducing the input level of the interface circuit, changing the anatomy of the ear during implantation, and increasing the stress on the PZT. These methods cannot be used independently due to the restriction of middle ear implantable transducer. Therefore, in this chapter, a new structure was proposed to increase covered band by channels of the cochlear implant. The structure improves the covered frequency band while it has the same dimensions and mass as cantilever beam structure. It can be fabricated utilizing MEMS processes. Furthermore, this approach can be applied with more beams depends on the fabrication process restriction.

CHAPTER 6

CONCLUSION AND FUTURE WORK

This thesis presents a multi-channel MEMS transducer. This structure can mimic the operation of the cochlea by filtering the sound mechanically with piezoelectric cantilever beams distributed within the audible frequency range. This transducer is well suited to be implantable on the eardrum or ossicles in the middle ear cavity. With the help of this property, the natural vibration of the hearing mechanism can be used to sense the incoming sound without any external source or excitation. Therefore, it can be used to overcome the bottlenecks of FICIs in terms of acoustic sensing. In the concept of this thesis, modeling, fabrication, and experimental characterization of a multi-channel acoustic MEMS transducer were presented. Furthermore, a transducer structure is proposed to improve the sensing quality of the transducer by expanding the covered frequency range. This chapter highlights the overview of the research and suggests the future works in this area.

6.1. Achieved Research Tasks

During this research, following tasks were achieved to obtain implantable transducer.

- Bottlenecks of the fully implantable cochlear implants have been investigated and possible solutions were searched in the literature in terms of acoustic sensing of the sound.

- Limitations on the middle ear implantable transducer are determined and an array of cantilever beams is chosen to overcome the restrictions. This structure can be utilized for implantable devices.

- The structure was utilized considering properties of the natural hearing mechanism. Output voltages of the channels were defined to cover wide dynamic range while generating minimum output voltage level of stimulation circuits at low sound pressure levels to increase the hearing quality.

- The multi-channel piezoelectric structure was modeled using Finite Element Model. This study was carried out inside COMSOL Multiphysics environment.

- Utilized output characteristics have been obtained with an established FEM model in COMSOL and parameters of the structure have been calculated on this model. The transducer was well suited to be implanted in the middle ear cavity with an active volume of 5×5×0.6 mm^3 and 4.8 mg, excluding the test frame whose dimensions are below the limitations (9×10 mm^2 and 25 mg) for a system (including packaging).

- 6-mask fabrication method was improved via several MEMS fabrication techniques. The yield of the fabrication was 92 % inside a 4-inch SOI wafer which includes 42 transducers.

- Fabricated transducer was tested in a systematic test flow to understand reasons behind problems which could have been occurred after patterning the top electrode of the piezoelectric structure.

- Auxiliary test equipment was developed with group members to test transducer in a similar environment where it would be placed. Also, special holders were designed for mechanical and acoustical tests to improve the accuracy and repeatability of the tests.

- Electrical model parameters and quality of surface and bulk micromachining were investigated in LCR tests.

- The electromechanical test was applied to the transducer to see its characteristic under constant acceleration. Experiments show that the transducer can generate up to 139.36 mV_{pp} under 0.1 g excitation which is the highest output voltage in the literature to the best of my knowledge.

- Electromechanical test results were consistent with the established FEM model on the frequency (97%) and output voltage (89%) values.

- Placement and voltage levels showed that each channel works in the audible frequency range (250-5500 Hz).

- The transducer was placed on an artificial tympanic membrane to measure the acoustic characteristics of the transducer under different sound pressure levels. The transducer can generate up to 50.7 mV_{pp} under 100 dB SPL.

- For the first time in the literature, the acoustical transducer was excited with speech sound at a daily sound level and recovered by using software. Spectrograms of the signals show close patterns and recovered sound can be understood.

- In order to support speech test results, the covered frequency spectrum by each channel was implemented as a filter characteristic in Matlab. Speech sound was filtered with these filters and spectrograms showed a close pattern between original sound and transducer output.

- Beside stand-alone tests, *in-vitro* tests have been conducted with stimulation circuits. The system containing multi-channel transducer can work in 50 dB dynamic range.

- Transducer and 2nd generation stimulation circuit have been tested on the deafened guinea pig. These tests still ongoing and out of scope of this thesis.

Finally, a beam type which uses an elastic connection between the cantilevers was proposed to improve the filtering quality of the channels by widening the frequency bands of the channels.

6.2. Future Work

The human ear is a magnificent sensor with its frequency resolution and dynamic range. Therefore, fully implantable cochlear implant concepts have a long way to reach the natural hearing standards. This thesis revealed the capability of mechanical filtering of the sound with the piezoelectric effect. There are many opportunities for this application. Some of them are discussed below.

- The transducer model can be tested on a middle ear model in finite element analysis. This study will give a chance to optimize all parameters of the structure.

- In order to see more realistic results of this study, the transducer can be tested on the ear of a human cadaver. Optimum location of the transducer also can be defined in this study.

- System level *in-vitro* tests must be completed to declare capabilities of a fully implantable system which includes low power stimulation circuit and multi-channel acoustic transducer.

- The proposed wide bandwidth structure must be fabricated to see the capabilities of the structure. Then, the multi-channel structure of this beam can be used for FICI applications.

- Frequency bands of the beams can be increased at low sound pressure levels using different topologies and newly developed materials with higher coupling constants.

REFERENCES

[1] World Health Organization, “Deafness and hearing loss.” [Online]. Available: https://www.who.int/news-room/fact-sheets/detail/deafness-and-hearing-loss. [Accessed: 27-Jun-2020]

[2] F. G. Zeng *et al.*, “Cochlear Implants: System Design, Integration, and Evaluation,” *IEEE Reviews in Biomedical Engineering.*, vol. 1, no. dc, pp. 115–142, 2008.

[3] B. S. Wilson and M. F. Dorman, “Cochlear implants: A remarkable past and a brilliant future,” *Hearing Research*, vol. 242, no. 1–2, pp. 3–21, 2008.

[4] W. R. Drennan and J. T. Rubinstein, “Music perception in cochlear implant users and its relationship with psychophysical capabilities,” *Journal of Rehabilitation Research and Development*, vol. 45, no. 5. NIH Public Access, pp. 779–790, 2008.

[5] M. K. Cosetti and S. B. Waltzman, “Cochlear implants: current status and future potential,” *Expert Review of Medical Devices*, vol. 8, no. 3, pp. 389–401, May 2011.

[6] M. Bartholomew, *Essentials of Anatomy &Physiology*, 4th ed. Pearson, 2007.

[7] L. E. H. Fred H. Bess, *Audiology : The Fundamentals* , 4th ed. Lippincott William & Wilkins 2008.

[8] R. Häusler *et al.*, “A novel implantable hearing system with direct acoustic cochlear stimulation,” *Audiology Neurotology.*, vol. 13, pp. 247–256, 2008.

[9] D. S. Haynes *et al.*, “Middle Ear Implantable Hearing Devices: An Overview,” *Trends in Amplification.*, vol. 13, no. 3, 2009.

[10] B. S. Wilson and M. F. Dorman, “Cochlear implants: Current designs and future possibilities,” *Journal of Rehabilitation Research and Development*, vol. 45, no. 5, pp. 695–730, 2008.

[11] K. Wong *et al.*, “Auditory Brainstem Implants: Recent Progress and Future Perspectives,” *Frontiers in Neuroscience,* 2019.

[12] M. Yip *et al.*, “A fully-implantable cochlear implant SoC with piezoelectric middle-ear sensor and arbitrary waveform neural stimulation,” *IEEE Journal*

of Solid-State Circuits, vol. 50, no. 1, pp. 214–229, 2015.

[13] F. G. Zeng *et al.*, “Development and evaluation of the Nurotron 26-electrode cochlear implant system,” *Hearing Research*, vol. 322. Elsevier B.V., pp. 188–199, 2015.

[14] I. Hochmair *et al.*, “MED-EL Cochlear Implants: State of the Art and a Glimpse Into the Future The MAESTRO CI System,” *Trends in Amplification.*, vol. 10, no. 4, 2006.

[15] F. B. Simmons, “Electrical Stimulation of the Auditory Nerve in Man,” *Archives of Otolaryngology* ., vol. 84, no. 1, pp. 2–54, Jul. 1966.

[16] H. Külah, “A Fully-Implantable MEMS-Based Autonomous Cochlear Implant | FLAMENCO Project | H2020 | CORDIS | European Commission.” [Online]. Available: https://cordis.europa.eu/project/id/682756. [Accessed: 26-Jun-2020].

[17] C. Zhao *et al.*, “Modeling, fabrication, and testing of a MEMS multichannel aln transducer for a completely implantable cochelar implant,” *TRANSDUCERS 2017 - 19th International Conference of Solid-State Sensors, Actuators Microsystems*, pp. 16–19, 2017.

[18] D. J. Young *et al.*, “MEMS Capacitive Accelerometer-Based Middle Ear Microphone,” *IEEE Transactions on Biomedical Engineering.*, vol. 59, no. 12, pp. 3283–3292, Dec. 2012.

[19] W. H. Ko *et al.*, “Studies of MEMS acoustic sensors as implantable microphones for totally implantable hearing-aid systems,” *IEEE Transactions on Biomedical Circuits and Systems.*, vol. 3, no. 5, pp. 277–285, 2009.

[20] M. A. Zurcher *et al.*, “Effect of incus removal on middle ear acoustic sensor for a fully implantable cochlear prosthesis,” *Annual International Conference of the IEEE Engineering in Medicine and Biology - Proceedings*, pp. 539–542, 2006.

[21] FLAMENCO, “A Fully-Implantable MEMS-Based Autonomous Cochlear Implant.” [Online]. Available: https://flamenco.metu.edu.tr/. [Accessed: 26-Jun-2020].

[22] M. B. Yuksel *et al.*,“Multi-channel thin film piezoelectric acoustic transducer for cochlear implant applications,” *2019 IEEE Sensors*, Montreal, QC, Canada, pp. 1–4, 2019.

[23] B. İlik *et al.*,"Thin film piezoelectric acoustic transducer for fully implantable cochlear implants," *Sensors Actuators, A Phys.*, vol. 280, pp. 38–46, 2018.

[24] B. İlik *et al.*, "Thin Film PZT Acoustic Sensor for Fully Implantable Cochlear Implants," *Proceedings of Eurosensors Conference 2017*, vol. 1, no. 10, p. 366, 2017.

[25] A. Koyuncuoğlu *et al.*, "Bulk PZT Cantilever Based MEMS Acoustic Transducer for Cochlear Implant Applications," *Proceedings of Eurosensors Conference 2017*, vol. 1, no. 10, p. 584, 2017.

[26] L. Beker *et al.*, "Stimulating auditory nerve with MEMS harvesters for fully implantable and self-powered cochlear implants," in *2013 Transducers & Eurosensors XXVII: The 17th International Conference on Solid-State Sensors, Actuators and Microsystems (TRANSDUCERS & EUROSENSORS XXVII)*, 2013, pp. 1663–1666.

[27] H. Ulusan *et al.*, "Fully Implantable Cochlear Implant Interface Electronics With 51.2-μW Front-End Circuit," *IEEE Transactions on Very Large Scale Integration (VLSI) Systems*, pp. 1–9, 2019.

[28] H. Uluşan *et al.*, "A Sub-500 μW Interface Electronics for Bionic Ears," *IEEE Access*, pp. 132140–132152, 2019.

[29] H. A. Yigit *et al.*, "Charge Balance Circuit for Constant Current Neural Stimulation with Less than 8 nC Residual Charge," *2019 IEEE International Symposium on Circuits and Systems (ISCAS)*, 2019.

[30] H. A. Yiğit *et al.*, "A Pulse-Width Modulated Cochlear Implant Interface Electronics with 513 μW Power Consumption," in *EEE/ACM International Symposium on Low Power Electronics and Design (ISLPED)*, pp. 2–6, 2019.

[31] S. Chamanian *et al.*, "An adaptable interface circuit for low power MEMS piezoelectric energy harvesters with multi-stage energy extraction," in *2017 IEEE Biomedical Circuits and Systems Conference, BioCAS 2017 - Proceedings*, vol. 2018-January, pp. 1–4, 2018.

[32] S. Chamanian *et al.*, "A self-adapting synchronized-switch interface circuit for piezoelectric energy harvesters," *IEEE Transactions Power Electronics*, vol. 35, no. 1, pp. 901–912, 2020.

[33] B. Çiftci *et al.*, "Low-Cost Fully Autonomous Piezoelectric Energy Harvesting Interface Circuit with up to 6.14x Power Capacity Gain," in *Proceedings of the*

Custom Integrated Circuits Conference, 2019.

[34] P. Udvardi and J. Ferencz, “Spiral-Shaped Piezoelectric MEMS Cantilever Array for Fully Implantable Hearing Systems.” *Micromachines,* vol. 9, 2017.

[35] C. Zhao *et al.*, “Voltage readout from a piezoelectric intracochlear acoustic transducer implanted in a living guinea pig,” *Scientific Reports.*, vol. 9, no. 1, pp. 1–11, 2019.

[36] X. H. Jia *et al.*, “A new floating piezoelectric microphone for the implantable middle ear microphone in experimental studies,” *Acta Otolaryngologica*, vol. 136, no. 12, pp. 1248–1254, 2016.

[37] N. Gao *et al.*, “The frequency response of a floating piezoelectric microphone for the implantable middle ear microphone,” *Laryngoscope*, vol. 123, no. 6, pp. 1506–1513, Jun. 2013.

[38] J. Jang *et al.*, “MEMS piezoelectric artificial basilar membrane with passive frequency selectivity for short pulse width signal modulation,” *Sensors Actuators, A Physical*, vol. 203, pp. 6–10, 2013.

[39] J. Jang *et al.*, “A microelectromechanical system artificial basilar membrane based on a piezoelectric cantilever array and its characterization using an animal model,” *Scientific Reports*, vol. 5, no. January, pp. 1–13, 2015.

[40] Z. Djinović *et al.*, “In-vitro and in-vivo measurement of the animal’s middle ear acoustical response by partially implantable fiber-optic sensing system,” *Biosensors and Bioelectronics*, vol. 103, no. December, pp. 176–181, 2018.

[41] A. J. Maniglia *et al.*, “Bioelectronic microphone options for a totally implantable hearing device for partial and total hearing loss,” *Otolaryngologic Clinics of North America*, vol. 34, no. 2, pp. 469–483, Apr. 2001.

[42] D. J. Carpenter *et al.*, “Disagreement in middle ear volume estimation between tympanometry and three-dimensional volume reconstruction in the context of tympanic membrane perforation,” *Journal of Otology*, vol. 12, no. 2, pp. 74–79, 2017.

[43] S. A. Gelfand, *Hearing : an introduction to psychological and physiological acoustics*. Marcel Dekker, 2004.

[44] Earth`s Lab., “Anatomy - Middle Ear.” [Online]. Available: https://www.earthslab.com/anatomy/middle-ear/. [Accessed: 28-Jun-2020].

[45] S. Nishihara *et al.*, "Effect of Changes in Mass on Middle Ear Function," *Otolaryngology–Head and Neck Surgery* , vol. 109, no. 5, pp. 899–910, 1993.

[46] Y. Suzuki *et al.*, "Equal-loudness-level contours for pure tones ," *The Journal of the Acoustical Society of America* , vol. 116, p. 918, 2004.

[47] B. S. Wilson, "Engineering Design of Cochlear Implants," Springer, New York, NY, 2004, pp. 14–52.

[48] K. Arora, "Cochlear Implant Stimulation Rates and Speech Perception," in *Modern Speech Recognition Approaches with Case Studies*, InTech, 2012.

[49] N. B. H. Croghan *et al.*, "Re-examining the relationship between number of cochlear implant channels and maximal speech intelligibility," *The Journal of the Acoustical Society of America*, vol. 142, p. 537, 2017.

[50] L. M. Friesen *et al.*, "Speech recognition in noise as a function of the number of spectral channels: Comparison of acoustic hearing and cochlear implants," *The Journal of the Acoustical Society of America*, vol. 110, no. 2, pp. 1150–1163, Aug. 2001.

[51] C. Garnham *et al.*, "Speech understanding in noise with a Med-El COMBI 40+ cochlear implant using reduced channel sets," *Ear and Hearing*, vol. 23, no. 6, pp. 540–552, 2002.

[52] Y. Q. Fu *et al.*, "Advances in piezoelectric thin films for acoustic biosensors , acoustofluidics and lab-on-chip applications," *Progress in Material Science*, vol. 89, pp. 31–91, 2017.

[53] M. Jambunathan *et al.*,, "Pulsed Laser Deposited-PZT based MEMS Energy Harvesting Devices," *Proceedings of ISAF-ECAPD-PFM,* pp. 10–13, 2012.

[54] M. D. Nguyen *et al.*,"Film-thickness and composition dependence of epitaxial thin-film PZT-based mass-sensors," *Sensors Actuators A Physical*, vol. 199, pp. 98–105, 2013.

[55] M. Renaud, "Piezoelectric Energy Harvesters for Wireless Sensor Networks," KU Leuven, 2009.

[56] J. H. Lin *et al.*, "Modeling and simulation of piezoelectric MEMS energy harvesting device," *Integrated Ferroelectrics*, vol. 95, no.1, pp. 128–141, 2007.

[57] A. M. Flynn and S. R. Sanders, "Fundamental limits on energy transfer and circuit considerations for piezoelectric transformers," *IEEE Transactions on*

Power Electronics, vol. 17, no. 1, pp. 8–14, 2002.

[58] A. Erturk and Daniel J. Inman, *Piezoelectric Energy Harvesting*, Wiley, 2011.

[59] Z. Bi *et al.*„ "Characterization of PZT Ferroelectric Thin Films by RF-magnetron Sputtering," *Journal of Physics Conference Series*, 2007.

[60] N. Majid *et al.*, "The parylene-aluminum multilayer interconnection system for wafer scale integration and wafer scale hybrid packaging," *Journal of Electronic Materials*, vol. 18, no. 2, pp. 301–311, 1989.

[61] P. Ashrafi *et al.*, "A synthetic tympanic membrane for middle ear acoustic sensor tests of a fully implantable cochlear prothesis," in *The 8th International Symposium on Middle-Ear Mechanics in Research and Otology*, 2018.

[62] R. Z. Gan and Q. Sun, "Three-Dimensional Finite Element Modeling of Human Ear for Sound Transmission," *Annals of Biomedical Engineering,* 2004.

[63] A. K. Soydan, "System Integration of Mems Devices on Flexible Substrate," Middle East Technical University, 2019.

[64] H. G. Mueller, "Signia Expert Series: Speech-in-Noise Testing for Selection and Fitting of Hearing Aids: Worth the Effort?," *Audiology Online*, 2016.

[65] C. Díaz and A. Pedrero, "Sound exposure during daily activities," *Applied Acoustics*, vol. 67, no. 3, pp. 271–283, 2006.

[66] Q. Tang and X. Li, "Two-stage wideband energy harvester driven by multimode coupled vibration," *IEEE/ASME Transactions on Mechatronics*, vol. 20, no. 1, pp. 115–121, 2015.

[67] A. Hajati and S. G. Kim, "Wide-bandwidth MEMS-scale piezoelectric energy harvester" *PowerMEMS*, 2009.

[68] A. Hajati and S. G. Kim, "Ultra-wide bandwidth piezoelectric energy harvesting," *Applied Physics Letters*, vol. 99, no. 8, pp. 2009–2012, 2011.

[69] N. Wang *et al.*, "AlN wideband energy harvesters with wafer-level vacuum packaging utilizing three-wafer bonding," *Proceedings of the IEEE International Conference on Micro Electro Mechanical Systems*, 2017.

[70] Q. Zhang *et al.*, "Multimodal Design of a Novel MEMS structure for Piezoelectric Energy Harvester," in *Proceedings of the 12th IEEE International Conference on Nano/Micro Engineering and Molecular Systems*, 2017.